Selective Ablation for Patterning Organic Electronics

Selectieve ablatie voor patroondefinitie van organische elektronica

Sanjeev Naithani

Promotor: prof. dr. ir. G. Van Steenberge
Proefschrift ingediend tot het behalen van de graad van
Doctor in de Ingenieurswetenschappen: Elektrotechniek

Vakgroep Elektronica en Informatiesystemen
Voorzitter: prof. dr. ir. R. Van de Walle
Faculteit Ingenieurswetenschappen en Architectuur
Academiejaar 2014 - 2015

UNIVERSITEIT
GENT

ISBN 978-90-8578-788-4
NUR 959
Wettelijk depot: D/2015/10.500/32

Ghent University
Faculty of Engineering and Architecture
Department of Electronics and Information Systems

Promoter:

Prof. dr. ir. Geert Van Steenberge
Center for Microsystems Technology (CMST),
Technologiepark 914A, B-9052 Gent, Belgium
Tel.: +32-9-264.5560, Fax.: +32-9-264.5374

Examination Committee:

Prof. dr. ir. Rik Van de Walle – *Chairman*
Dean, Faculty of Engineering and Architecture,
Ghent University, Belgium

Prof. dr. ir. Erwin Bosman – *Secretary*
Department of Electronics and Information Systems,
Ghent University, Belgium

Prof. dr. rer. nat. Andreas Dietzel
Institute of Microtechnology,
University of Technology, Braunschweig, Germany

Dr. ir. Yves Hernandez
Applied Photonics Department,
Multitel ASBL, Mons, Belgium

Dr. Rajesh Mandamparambil
Additive Manufacturing,
TNO, Eindhoven, The Netherlands

Prof. dr. ir. Peter Van Daele
Department of Information Technology,
Ghent University, Belgium

Prof. dr. ir. Herbert De Smet
Department of Electronics and Information Systems,
Ghent University, Belgium

A dissertation submitted in partial fulfillment of the requirements for
the degree of Doctor of Electrical Engineering
Academic Year 2014–2015

To

My mother

Smt.(late) Sarojini Naithani

&

father

Dr. Laxmi Prasad Naithani

Acknowledgements

This dissertation has been the culmination of consistent support and guidance from many people for past four years and I must take this opportunity to thank them for helping me in different ways throughout the process. First and foremost, I was fortunate to work at CMST under the supervision of my promotor Geert Van Steenberge. It would not have been possible to complete this dissertation without his insightful and encouraging suggestions. He taught me the various aspects of conducting research. Besides his technical guidance and professional expertise, he has always been very kind and helpful. My sincere thanks to Jan Vanfleteren for being helpful when needed. I am also thankful to CMST management for providing a friendly, positive and cordial work environment.

I am extremely thankful to the reading committee: Erwin Bosman, Peter Van Daele, Andreas Dietzel and Yves Hernandez, for their valuable time in reading this thesis and providing me critical suggestions to improve it. I am grateful to Rajesh Mandamparambil and Henri Fledderus (Holst Center, The Netherlands) for valuable discussions and support during our collaborative work in the TP6 program. I am also thankful to Prof. Luc Van Vaeck and Yannick Vercammen (University of Antwerp) for the TOF-SIMS measurements.

Special thanks to Steven Van Put, with whom I have conducted most of the experimental work during past four years. His detailed knowledge of the workbench has been very helpful in resolving experimental issues and successfully completing the experiments. Having an electronics background, it was difficult in the beginning for me to understand the chemistry behind organic electronics. All credit goes to David Schaubroeck for explaining and answering my queries about chemistry. Thanks to David again for his support in the SEM measurements.

I am extremely thankful to the following people – Filip Vermeiren for conducting the RIE experiments; Peter Geerinck for performing PEDOT:PSS oxygen plasma treatment experiments, PMMA sample preparation and dicing of quartz substrates; Kristof for providing valuable help with Tencor measurements; Steven Vervusft for Dektek measurements and polycarbonate samples; Jeroen for helping me with the rotary stage and newport stages assembled with mid-IR ablation set-up; Bram for helping in OSA measurements; Filip Thielemans for preparing the metal safety sheets and an off-set block for mounting the PPLN heating oven, John George and Manoj Purohit at LCP group for helping me in the measurement of absorption spectrum with UV-vis instrument.

I would like to thank all the partners in the EU-FP7 improv project, especially to Arnaud Grisard (Thales Research and Technology, France), Yves Hernandez (Multitel, Belgium) and Karsten Walzer (Heliatek, Germany), for the critical and valuable discussions during our project work. I am also thankful to our optical team members: Erwin, Bram, Jeroen, Sandeep, Pankaj, Kamal, Nuria, Ahmed, Paolo, Andres and Nivesh; it was interesting to share and discuss the recent experimental results in our team meetings.

I would like to thank my office-mates Sheila, Rik, Jeroen, Thomas, David, Amir, Sandeep, Nuria, Patricia and Nivesh from my current office and Tom, Jendrich and Benoit from my previous office for providing a wonderful working atmosphere. I am very much thankful to Shiela, Peter, Filip and Steven, for driving to Astrid and UZ, during lunch times, which ensured my good health during these four years.

I am thankful to my friends: Amir, Jeroen, Rik, Pankaj, Jendrich and Bram for helping me with writing the PhD dissertation. I would like to thank our secretary Katrien Vanneste for helping me all these four years of my PhD. I thank Peter Sebrechts for his valuable assistance with computer programs. It was fun being a member of CMST football team. I thank Thomas, Steven, Geert, Erwin, Bram, Frederick, Amir, David, Dominique, Ahmed and Sandeep for all the time we enjoyed playing football and sharing light moments.

Another sporting thanks to my cricket friends: Samir, Ananth, Sukumar, Manan, Sandeep, Pankaj, Abhishek, Shailesh, Amit, Ark, Ashok and Chetan for providing refreshing moments out of gadgets. Special thanks to my friend Unmesh Menon, for his valuable support from Berlin till Gent.

I would like to thank Wim and Veronique, for providing me a peaceful and nice apartment during these four years of my stay in Gent.

Last but not least, I am highly thankful to my parents, Bhai and Bhabhi Ji, Didi and Jija Ji, and younger brother, for their full support and motivation throughout this period.

Sanjeev Naithani,
Gent

Table of Contents

1 General Introduction **1**

1.1 Organic Electronics 1
1.1.1 Organic field effect transistor 2
1.1.2 Organic light emitting diode 3
1.1.3 Organic photovoltaic cell 5
1.2 Organic Electronics Materials 7
1.2.1 Small molecules 7
1.2.2 Conducting polymers 7
1.3 Patterning Technologies 8
1.4 Problem Statement and Objectives 10
1.5 Research Trajectory and Dissertation Structure 13
1.6 Research Context and Related Projects 14
1.7 Research Dissemination 15
1.7.1 Journal papers 15
1.7.2 International conference proceedings 16

2 Fundamentals of Polymer Ablation **21**

2.1 Introduction 21
2.2 Ablation Principles 22
2.2.1 Fluence 22
2.2.2 Absorption coefficient 24
2.2.3 Ablation rate 24
2.2.4 Selective ablation 27
2.3 Laser Parameters 29
2.3.1 Wavelength selection 29
2.3.2 High pulse power 30
2.3.3 Short pulse length 31
2.3.4 Beam optics and delivery 34
2.4 Material Parameters 36
2.5 Ablation Mechanisms 37

2.6 Conclusions 39

3 Barrier Influence on Thin Film Patterning 45
3.1 Introduction 45
3.2 Ablation Set-up 49
3.3 Why a Multilayer Barrier? 50
3.4 Thin Film Patterning 51
3.4.1 Thin films absorption spectra 52
3.4.2 Barriers absorption spectra 53
3.4.3 Thin films selective ablation 54
3.5 Barrier Influence on Patterning 61
3.6 Conclusions 63

4 Flexible OLED Fabrication 67
4.1 Introduction 67
4.2 Organic Light Emitting Diodes 69
4.2.1 General principle 69
4.2.2 Life time and efficiency 71
4.3 Silicon Nitride Barrier Threshold 72
4.4 Thin Films Ablation Thresholds 74
4.5 Flexible OLED Fabrication 76
4.6 Conclusions 80

5 Monolayer Investigation: TOFSIMS 83
5.1 Introduction 83
5.2 Materials and Methods 85
5.2.1 Sample preparation 85
5.2.2 Ablation parameters 86
5.2.3 Non-contact optical profiler 86
5.2.4 Scanning electron microscopy 87
5.2.5 Plasma cleaning 87
5.2.6 TOF-SIMS equipment 87
5.3 PEDOT:PSS Area Patterning 88
5.4 TOF-SIMS Investigations and Analysis 88
5.5 Conclusions 99

6 Ultra-short Laser Pulses for Thin Film Patterning 103
6.1 Introduction 103
6.2 Picosecond Ablation Set-up 106
6.3 Methodology 107

6.3.1 Sample preparation . . . 107
6.3.2 Absorption characteristics . . . 108
6.3.3 Analysis . . . 108
6.4 PEDOT:PSS Thin Films . . . 108
6.5 Plexcore Thin Films . . . 117
6.6 Silicon Nitride Thin Films . . . 121
6.7 Conclusions . . . 122

7 Mid-infrared Ablation 127
7.1 Introduction . . . 127
7.2 Poly(methyl methacrylate):PMMA . . . 129
7.3 Tunable Mid-IR Ablation Set-up . . . 129
7.4 Methodology . . . 131
7.4.1 Sample preparation . . . 131
7.4.2 Infrared spectral characterization . . . 132
7.4.3 Analysis . . . 132
7.5 Results and Discussion . . . 132
7.5.1 Bulk sheets . . . 132
7.5.2 Thin films patterning . . . 135
7.6 Conclusions . . . 138

8 Thin Film Resonant Mid-IR Patterning 143
8.1 Introduction . . . 143
8.2 Organic Photovoltaics . . . 145
8.3 Methodology . . . 147
8.3.1 Sample preparation . . . 147
8.3.2 Mid-infrared absorption spectra . . . 148
8.3.3 Ablation set-up . . . 148
8.3.4 Analysis . . . 153
8.4 PEDOT:PSS mid-IR selective patterning . . . 153
8.5 Thin films patterning on PET foil . . . 156
8.6 BPAPF, αNPB and HDR014 mid-IR nanosecond patterning . . . 161
8.7 Investigations at higher mid-IR wavelengths . . . 164
8.8 Conclusions . . . 170

9 Conclusions and Future Work 173
9.1 Main Contributions . . . 173
9.1.1 Multilayered barrier optimization . . . 173
9.1.2 Demonstration of a laser patterned flexible device 174

9.1.3 Proposing TOF-SIMS for monolayer investigation 174
9.1.4 Ultrafast patterning 174
9.1.5 Proof-of-concept RIA 175
9.1.6 RIA for OPV layer patterning 175
9.2 Outlook and Future Work 175

List of Figures

1.1 Paper like display, fabrication of thin film transistor (TFT) arrays on flexible plastic substrate, a low cost and "roll-to-roll" manufacturing process [18]. 3
1.2 Demonstration of a 4.1" prototype flexible display from Sony: Ultra-thin OLED screen could continue to play video while being rolled around a pen [25]. 5
1.3 Material developments in photovoltaics from 1st generation to 3rd generation, adopted from Heliatek [29]. 6
1.4 Overview of some applications of organic solar cells, picture adopted from SNe Research [30]. 6
1.5 Examples of small molecules. 8
1.6 Examples of conducting polymers. 8
1.7 Comparison of various patterning and printing technologies for organic electronics devices [32]. 9
1.8 A comparison of photolithography versus laser patterning processing steps. 9
1.9 Integration of laser patterning for roll-to-roll(R2R) production of electronics devices, picture adopted from Coherent, Inc. [33]. 11

2.1 Schematic plot of the three fluence ranges which are typically observed for polymers. At low fluence range (blue line), there is incubation effect observed, medium fluence range (green line) efficient decomposition of polymer and at high fluence range (red line) the incident laser light is screened by solid, liquid, and gaseous ablation products and the laser produced plasma [13]. 23
2.2 Schematic diagram of laser-induced ablation on the samples (top) and corresponding Gaussian fluence profile along x-axis (bottom), D indicates the diameter of the ablated area [19]. 25

2.3 Schematic of a spatially Gaussian beam profile. F_0 and F_{th} denote the maximum laser fluence and the ablation threshold fluence, respectively. The distance $2W_0$ represents the $1/e^2$-Gaussian beam diameter [19]. 25
2.4 Plot of ablation depth vs. number of pulses, which is used to determine the ablation rate at a given fluence. The typical feature of incubation, i.e. ablation starts only after certain number of pulses, is shown for the low fluence curve [13]. 26
2.5 Schematic diagram to represent Beer-Lambert law for absorption of light in a medium. 27
2.6 Schematic to represent selective ablation of "Polymer B" on "Polymer A" with a laser. 28
2.7 Generation of a Q-switched pulse, a technique for obtaining energetic pulses from laser by modulating the losses in the resonator cavity, picture adapted from [35]. 31
2.8 Mode locked or phase locked pulses in a resonator cavity, a technique to obtain ultrashort duration (ps/fs) pulses. E - field, I - Intensity, L - the length of cavity and c is the velocity of light [39]. 33
2.9 Dependence of self organized structures on the state of polarization after ablation [40]. 35
2.10 Laser drilling methods for via drilling or microfabrication [41]. 36

3.1 Ultrafast laser patterning of ITO thin film on a glass substrate for OLED application, picture adopted from Park et al. [5]. 47
3.2 Laser assisted patterning process for organic electronics, the thickness of thin polymer films is 100 nm, picture adopted from [16]. 48
3.3 Nanosecond ablation set-up. 50
3.4 Samples prepared with thin organic films on a multilayered barrier and flexible PEN substrate: (a) illustrates the general concept and (b) to (d) describe specific sample structure. 52
3.5 The UV absorption spectra of PEDOT:PSS and LEP thin organic films. 53
3.6 The absorption spectra of different kinds of Silicon Nitrides used in multilayered barrier foils. 54

3.7 Ablation plots for least absorbing (a) and most absorbing (b), Silicon Nitrides barrier foils. 55
3.8 A comparison of PEDOT:PSS ablation on SiN(1) and SiN(4) barrier foils for identical ablation parameters. . 57
3.9 A comparison of PEDOT:PSS ablation on SiN(1) and SiN(4) barriers, (a) Clean removal on SiN (1) (b) Damage on barrier SiN(4); for identical ablation parameters: Fluence 125 mJ/cm^2, 2 Pulses. 58
3.10 Ablation plots for LEP on least absorbing and most absorbing Silicon Nitrides barrier foils. 59
3.11 A comparison of LEP ablation on SiN(1) and SiN(4) barrier foils for identical ablation parameters. 60
3.12 A line patterning comparison of LEP ablation on SiN(1) and SiN(4) barrier foils for at 75 mJ/cm^2 and 5 pulses. 60
3.13 Ablation plots for LEP and PEDOT:PSS on (a) SiN(1) barrier (b) SiN(4) barrier. 62

4.1 A simple schematic diagram of the OLED layered structure. 70
4.2 Model of energy band diagram for organic semiconductor material and operation of OLED [19]. 71
4.3 A multilayered barrier used for the fabrication of flexible OLED. 73
4.4 Silicon Nitride barrier threshold at 248 nm wavelength. 73
4.5 Onset of ablation for the PEDOT:PSS and LEP thin films on an optimized multilayered barrier. 75
4.6 The optical microscopic images at the onset of ablation for thin organic films (a) PEDOT:PSS and (b) LEP. . 75
4.7 The selective removal of thin organic films from barrier with single pulse (a) PEDOT:PSS and (b) LEP. . . . 76
4.8 PEDOT:PSS thin film line patterning on barrier (a) Optical microscopic image and (b) Wyko depth profile. 77
4.9 LEP thin film line patterning on barrier (a) Optical microscopic image and (b) Wyko depth profile. 77
4.10 Schematic of a flexible OLED layered structure and various selective ablation steps for patterning: (A) To ablate PEDOT:PSS on a barrier (B) To ablate PEDOT:PSS on bus bar (C) To ablate LEP on the barrier (D) To ablate LEP on the bus bar. 78
4.11 Process flow for the laser patterned flexible OLED device. 79

4.12 A functional flexible OLED device incorporating PEDOT:PSS and LEP selective ablation using excimer laser, demonstration under environmental conditions. . 80

5.1 Schematic diagram of TOF-SIMS, indicating the primary gun bombardment on sample and detection of secondary ions [14]. 85
5.2 The PEDOT:PSS thin film on a multilayered barrier, sample prepared for TOF-SIMS analysis. 86
5.3 Area patterning of PEDOT:PSS on barrier foil with different pulses. On the left top corner in all images there is a square mark, which is a reference mark during experiments. 89
5.4 Depth profile of the laser ablated area using a non-contact optical profiler. 90
5.5 SEM micrographs of (a) the laser ablated area with 5 shots per location, shows the presence of debris particles (b) ablated crater with 7 shots per location, with few tiny sub-micron particles (c) selective removal of PEDOT:PSS with 10 shots per location, yielding a clean debris free ablated area. (d) bare Silicon Nitride surface, included for the purpose of comparison. 90
5.6 Chemical structure of PEDOT:PSS. 91
5.7 Positive ion mass spectrum recorded by TOF-S-SIMS from a pure PEDOT:PSS layer. 92
5.8 Tentative structural assignment of the positive and negative ions of major diagnostic interest detected from a pure PEDOT:PSS layer by S-SIMS. 93
5.9 Negative ion mass spectrum recorded by TOF-S-SIMS from a pure PEDOT:PSS layer. 94
5.10 Positive ion mass spectrum recorded by TOF-S-SIMS from the crater after laser ablation (10 pulses). 95
5.11 Negative ion mass spectrum recorded by TOF-S-SIMS from the crater after laser ablation (10 pulses). 95
5.12 Positive ion mass spectrum recorded by TOF-S-SIMS from the crater after laser ablation (10 pulses) and subsequent RIE treatment (1 minute). 97
5.13 Negative ion mass spectrum recorded by TOF-S-SIMS from the crater after laser ablation (10 pulses) and subsequent RIE treatment (1 minute). 98

6.1 Ultrafast laser system used for thin film patterning equipped with automated software and controlling units. 106
6.2 Ultrafast (ps/fs) laser heads, power supplies and chiller. 107
6.3 PEDOT:PSS thin films absorption spectrum obtained with LAMBDA 35 UV/Vis System on a quartz substrate. 109
6.4 Selective patterning of PEDOT:PSS thin films with picosecond pulses. The spot diameter in (a) is 9 µm and in the part (b) is 17 µm. 109
6.5 Multiple static pulse experiment; the diameter of spot: (a) 17 µm with 2 pulses (b) 20 µm with 5 pulses. . . . 110
6.6 Selective line patterning of the PEDOT:PSS thin films with picosecond pulses. 111
6.7 The PEDOT:PSS ablation on glass with 532 nm picosecond pulses, indicating onset of the ablation and selective removal with single pulse. 111
6.8 The Wyko NT3300 depth measurement after PEDOT:PSS thin film removal with 532 nm picosecond pulses. . . . 112
6.9 Comparison of the line patterns with different pulse overlaps at 532 nm picosecond pulses. 113
6.10 Onset of the ablation and single pulse removal of the PEDOT:PSS thin film on a glass substrate, with 1064 nm picosecond pulses. 113
6.11 Selective ablation of PEDOT:PSS on a quartz substrate, with 1064 nm wavelength at 1000 kHz. 115
6.12 (a) Line pattern traces with 1064 nm wavelength at 1000 kHz picosecond pulses. (b) A line pattern design for the isolation of area to measure conductivity / resistance. 116
6.13 Comparison of ablation thresholds of PEDOT:PSS thin film at 355 nm, 532 nm and 1064 nm wavelengths; picosecond pulses. 117
6.14 Plexcore thin film absorption spectrum obtained with LAMBDA 35 UV/Vis System on a quartz substrate. . 118
6.15 Plexcore thin film selective ablation with 355 nm wavelength at 200 kHz picosecond pulses, spot diameter in (b) is 15 µm. 119
6.16 Plexcore thin film patterning with 355 nm wavelength at 200 kHz picosecond pulses. 119

6.17 SEM micrographs of Plexcore thin film ablation (a) Single pulse (b) Line patterning. 120
6.18 Selective patterning of Plexcore thin film on glass substrate with 532 nm wavelength at 300 kHz picosecond pulses. 120
6.19 Selective patterning of Plexcore thin film on glass substrate with 1064 nm wavelength at 1000 kHz picosecond pulses. 121
6.20 Comparison of ablation thresholds of Plexcore thin film at 355 nm, 532 nm and 1064 nm wavelengths with picosecond pulses. 122
6.21 Silicon Nitride thin film patterning on ITO substrate with 1064 nm picosecond pulses. 123

7.1 Chemical structure of PMMA:$(C_5O_2H_8)$n. 129
7.2 Schematic diagram of the mid-IR ablation set-up consisting of six sub-divisions: (A) pump laser (B) attenuator / isolator (C) OPO / wavelength conversion unit (D) filtering section (E) beam delivery unit (F) motorized sample stage. 130
7.3 Photograph of the bench-top mid-IR tunable high power nanosecond ablation set-up (schematic is illustrated in Figure 7.2). 131
7.4 Mid-infrared absorption spectrum of PMMA indicating a highest peak of absorption at 3.39 µm, a lower peak at 3.34 µm and minimum absorption at 3.20 µm. 133
7.5 SEM micrographs of PMMA mid-IR ablation at three wavelengths (a) 3.20 µm (b) 3.34 µm and (c) 3.39 µm. . 134
7.6 Ablation depth plots for PMMA at three different wavelengths: 3.20 µm, 3.34 µm and 3.39 µm. 135
7.7 Ablation rate plots for PMMA at three different mid-IR wavelengths of absorption: 3.20 µm, 3.34 µm and 3.39 µm. 136
7.8 Cross-section profile of an ablated structure indicating a spot size of 17.1 µm at full-width-half-maximum (FWHM). 137

7.9 Optical microscopic images: (a) and (c), of RIA patterned 650 nm and 1300 nm thin films of PMMA on a glass substrate. On the right: (b) and (d) are the corresponding depth profiles, indicating the removal of 648 nm and 1298 nm of PMMA thin films. 137
7.10 SEM micrographs of the patterned PMMA thin films (a) 650 nm (b) 1300 nm. The micrographs are taken with 45 degree tilt and 1000 magnification. 139

8.1 A typical and general schematic layered structure of organic photovoltaics (OPV) consisting of different organic thin films. 146
8.2 Mid-IR nanosecond ablation set up: 149
8.3 PPLN crystal output wavelengths and temperature relationship. (Datasheet: Covesion Ltd, UK) 151
8.4 Measurement of signal wavelength through an Optical Spectrum Analyzer (OSA), the measured wavelength in this case is 1512.16 nm. 152
8.5 Picosecond tunable mid-IR resonant ablation set-up. . 152
8.6 Transmission / absorption spectra of PEDOT:PSS and PET in mid-IR wavelength region. 154
8.7 Patterning of the PEDOT:PSS thin film with mid-IR nanosecond laser at 3.40 µm wavelength: (a) optical microscopic image (b) SEM micrograph. 155
8.8 Depth profile measurement after mid-IR nanosecond laser patterning of PEDOT:PSS at 3.40 µm wavelength. 156
8.9 SEM micrographs and wyko optical depth profiles, for identical experimental laser settings (ns, 80 mW, 40 mm/s, 2 µJ), except the wavelengths. 157
8.10 SEM micrograph after mid-IR picosecond laser selective patterning (3.03 µm, 90 mm/s, pulse energy ≈8 µJ) of 210 nm PEDOT:PSS on PET foil and beam profile of the mid-IR source used for this experiment. 158
8.11 SEM micrograph and corresponding EDX elemental maps after picosecond laser ablation (3.03 µm, 100 mm/s, 3 µJ) of 140 nm PEDOT:PSS on PET foil, spot diameter in the focal plane is 12 µm. 159
8.12 Absorption spectra of DCV4T-Et2 and HDR014 in the mid-IR region. 160

8.13 SEM micrographs (a) DCV4T-Et2 on PET at 3.31 µm, ps, 1 mm/s, 3.2 µJ and (b) HDR014 on PET at 3.37 µm, ps, 10 mm/s, 2.5 µJ. 161
8.14 Mid-IR absorption spectra of BPAPF and αNPB. . . . 162
8.15 Mid-IR patterning of BPAPF thin film (3.30 µm, ns, 170 mW, 20 kHz). 163
8.16 Mid-IR patterning of αNPB thin film (160 mW, ns, 20 kHz , 3.30 µm). 164
8.17 Mid-IR patterning of HDR014 thin film (160 mW, ns, 20 kHz , 3.37 µm) 165
8.18 EDS spectra of HDR014 patterning on glass substrate with 160 mW, ns, 20 kHz , 3.37 µm. 166
8.19 Higher absorption bands for αNPB at higher mid-IR wavelengths compared to 3 µm range. 167
8.20 Higher absorption bands for DCV4T-Et2 (HDG075) at higher mid-IR wavelengths compared to 3 µm range. 167
8.21 Mid-IR nanosecond laser set-up tunable around 4.50 µm at Thales Research and Technology, France. 168
8.22 Patterning investigations of HDR014 thin film at higher wavelengths, track width 12 µm. 169

List of Tables

1.1 Historical developments in Organic Electronics 2

2.1 Nanosecond laser systems available at CMST. 30
2.2 Ultrafast laser systems available at CMST. 30
2.3 Material properties relevant to laser ablation. 36
2.4 Examples of typical laser wavelength regimes and corresponding photons energy [41]. 37
2.5 Polymer chemical bonds and corresponding energies [41]. 37
2.6 Ablation regimes based on the energy transfer rate into material [41] 39

3.1 Damage thresholds (values in mJ/cm^2) with 2 pulses. 63

4.1 Layer composition, thicknesses and deposition methods of the OLED stack 79

List of Acronyms

A

AMOLED	Active Matrix Organic Light Emitting Diode
Alq3	Tris(8-hydroxyquinolinato)aluminium
ATR-IR	Attenuated Total Reflectance Infrared Spectroscopy

B

BPAPF	9,9-bis[4-(N,N-bis-biphenyl-4-yl-amino)phenyl]-9H-fluorene
BCP	Bathocuproine

C

CPA	Chirped Pulse Amplification
CMST	Centre for Microsystems Technology
cd	Candela
CWL	Centre Wavelength

D

DCV4T-Et2	2,2'-[(3,3"'-diethyl [2,2': 5': 2": 5", 2"'-quaterthiophene]-5,5"'-diyl) dimethylidyne] bis-Propanedinitrile
DC	Direct Current

E

EDX	Energy Dispersive X-ray spectroscopy
e-paper	Electronic-paper
EL	Electroluminescence
eV	Electron Volt
EA	Electron Affinity
ETL	Electron Transport Layer

F

FET	Field Effect Transistor
FDC	Flexible Display Center
fs	Femtosecond
FWHM	Full Width Half Maximum
FEL	Free Electron Laser

G

Ge	Germanium
GaAs	Gallium Arsenide

H

HOMO	Highest Occupied Molecular Orbital
HDMI	High Definition Multimedia Interface

HIL	Hole Injection Layer

I

IR	Infra-Red
IMPROV	Innovative Mid-infrared high Power source for Resonant ablation of Organic based photo-Voltaic devices
ITO	Indium Tin Oxide
IP	Ionization Potential

L

LED	Light Emitting Diode
LUMO	Lowest Unoccupied Molecular Orbital
LCD	Liquid Crystal Display
LEP	Light Emitting Polymer
Laser	Light amplification by stimulated emission of radiation
LDW	Laser Direct Write
lm	Lumen

M

MOSFET	Metal Oxide Semiconductor Field Effect Transistor
Maser	Microwave amplification by stimulated emission of radiation

N

NPB	N,N'-diphenyl-N,N'-bis(1-naphthyl)-1,1' biphenyl-4,4"-diamine
Nd:YAG	Neodymium-doped Yttrium Aluminum Garnet
Nd:YLF	Neodymium-doped Yttrium Lithium Fluoride
ns	Nanosecond
NA	Numerical Aperture

O

OLED	Organic Light Emitting Diode
OSC	Organic Solar Cell
OPV	Organic Photovoltaics
OTR	Oxygen Transmission Rate
OPO	Optical Parametric Oscillator
OPA	Optical Parametric Amplifier
OEFT	Organic Field Effect Transistor
OSA	Optical Spectrum Analyzer

P

PDA	Personal Digital Assistant
PEDOT:PSS	Poly 3,4 ethylenedioxythiophene: polystyrene sulfonate
PET	Polyethylene terephthalate
PEN	Polyethylene naphthalate
PMMA	PolyMethyl Methacrylate
PPLN	Periodically-Poled Lithium Niobate
PECVD	Plasma Enhanced Chemical Vapor Deposition
POLED	Polymer Organic Light Emitting Diode
PMOLED	Passive Matrix Organic Light Emitting Diode
PPV	Poly(p-phenylene vinylene)

ps	Picosecond
PRF	Pulse Repetition Frequency
PDP	Plasma Display Panel
PDMS	Polydimethylsiloxane
Plexcore	Poly(thiophene-3-[2[(2-methoxyethoxy)ethoxy]-2,5-diyl
PANI	Polyaniline
PS	PolyStyrene
P3HT	Poly(3-hexylthiophene)
PCBM	Phenyl-C61-butyric acid methyl ester

Q

OPM	Quasi-Phase Matching
QCM	Quartz Crystal Microbalance

R

R-2-R	Roll-to-Roll
RIA	Resonant Infrared Ablation
RIE	Reactive Ion Etching

S

SEM	Scanning Electron Microscope
Si	Silicon
SMOLED	Small Molecule Organic Light Emitting Diode

T

TFT	Thin Film Transistor

TOF-SIMS	Time of Flight Secondary Ion Mass Spectrometry
TCO	Thin-film Conducting Oxide

U

UV	Ultra-Violet
UHV	Ultra High Vacuum
USB	Universal Serial Bus
UTCP	Ultra Thin Chip Package

W

WVTR	Water Vapor Transmission Rate

Samenvatting

De elektronica markt evolueert meer en meer naar compactere en lichtere devices. In elk aspect van ons dagelijks leven worden deze devices gebruikt en verbruikt. Het wordt moeilijk om ons een wereld voor te stellen zonder GSM, e-mail, computer of televisie. De recente ontwikkelingen in de elektronica richten zich niet alleen op miniaturizatie maar ook op lichtere en flexibele devices. Klassieke elektronica worden gefabriceerd met anorganische materialen zoals silicium en germanium. De ontwikkeling van flexibele elektronica vereist het gebruik van flexibele materialen zoals elektrisch geleidende polymeren of lichtgevende polymeren. Deze applicaties worden geklassificeerd als organische elektronica of flexibele elektronica, waarbij de werkingsprincipes vergelijkbaar zijn met deze van anorganische elektronica, met dien verstande dat de energie bandgap gedefinieerd wordt door het energieverschil tussen de LUMO (lowest unoccupied molecular orbital) en de HOMO (highest occupied molecular orbital). Doordat deze devices uit een opeenstapeling van dunne films van (geleidende) polymeren bestaan, verlaagt dit het gewicht en verhoogt dit de mechanische flexibiliteit.

Het onderzoek naar organische elektronica kwam in een stroomversnelling aan het eind van de jaren tachtig wanneer de eerste OLED (organic light emitting device) ontwikkeld werd. Sindsdien is de OLED technologie verder ontwikkeld en wordt deze beeldschermtechnologie gebruikt in toestellen zoals televisieschermen, computerschermen, schermen van GSMs. De OLED-displays zijn veel lichter, met bredere kijkhoeken, betere helderheid, een snellere responstijd en bieden ook perspectief wat betreft een lagere kost. Deze voordelen maakt OLEDs geschikt om de Liquid Crystal Displays (LCDs) in televisie of computer schermen te vervangen. Naast OLED, zijn ook organische zonnecellen (OSC) of organische fotovoltasche cellen (OPVs) van groot maatschappelijk belang, en veel wetenschappelijk onderzoek is besteed aan hun ontwikkeling. Organische zonnecellen heb-

ben een brede waaier van toepassingen, maar de meest fascinerende eigenschap is hun mechanische flexibiliteit, waardoor we ze kunnen integreren in apparaten zoals auto's, ramen en textiel, om maar een paar voorbeelden te geven. In het algemeen is organische elektronica opgebouwd uit een opeenstapeling van zeer dunne lagen met een dikte van enkele honderden nanometer. De belangrijkste aspecten bij de productie zijn de depositie en de patroondefinitie van dergelijke hoog kwalitatieve dunne lagen. Deze lagen kunnen aangebracht worden via opdamping, of via coating en printing uit een oplossing. Hierbij zijn de homogeniteit en masker selectiviteit cruciale eigenschappen/-parameters bij de selectie van de depositiemethodes. Dunne films in OLED of OPV worden doorgaans gedeponeerd via methodes zoals screen printing, gravure coating of lithografie, waarbij iedere methode zijn voor- en nadelen heeft. Hierbij zijn, afhankelijk van de applicatie, resolutie en feature size meestal de doorslaggevende factoren.

In dit proefschrift wordt selectieve laser ablatie onderzocht als methode voor patroondefinitie van dunne lagen bij de productie van organische elektronica, met nadruk op dunne lagen gebruikt voor de opbouw van OLED of OPV. Laser ablatie wordt gekenmerkt door enkele uitzonderlijke eigenschappen die voordelig kunnen zijn voor het patterneringsproces: snellere uitvoering (minder uit te voeren stappen), geen gebruik van nat-chemische methodes, weinig impact op het milieu door minimale productie van afvalstoffen en potentiële integratie in een roll-to-roll productie proces. Twee grote doelstellingen worden naar voor geschoven in dit werk. Ten eerste is er de selectieve verwijdering van dunne organische lagen die deel uitmaken van een OLED opbouw, met als finale demonstrator een OLED vervaardigd op een flexibel substraat. Hierbij is de grootste uitdaging om de onderliggende lagen (organisch of anorganisch) niet te beschadigen tijdens ablatie. De tweede grote doelstelling bestaat erin om een laser met een golflengte in het infrarood gebied aan te wenden voor de selectieve ablatie van dunne organische lagen in een OPV cel. Bij deze techniek wordt het principe van resonante infrarood ablatie (RIA) gebruikt. Bij deze RIA techniek wordt de golflengte van de laser aangepast aan de energie nodig voor een moleculaire vibrationele transitie van het te ableren organisch materiaal.

Het eerste deel van deze thesis handelt over selectieve patternering van dunne organische films die relevant zijn voor de productie van een OLED op flexibele drager. Dit werk werd uitgevoerd in sa-

menwerking met het Holst Centre in Nederland. De eerste opdracht in dit onderzoek bestond uit het optimalizeren van de barriere laag in functie van de patternering via laser ablatie. Een barriere laag die beter bestand is tegen penetratie van zuurstof en water is nodig voor de verlenging van de levensduur van OLED en OPV devices. Om dit doel te bereiken werden verschillende barriere multilagen ontworpen gebaseerd op hun optische absorptie eigenschappen, om zo schade in de barriere laag tijdens laser ablatie van een bovenliggende laag te vermijden. Deze barriere multilagen bestaan uit alternerende lagen van organische en anorganische dunne films die een aanzienlijke vertraging van de zuurstof en vochtpenetratie vertonen. De invloed van de optische absorptie van deze verschillende barriere multilagen op de laserablatie van bovenliggende organische dunne films (248 nm UV eximeer laser) werd onderzocht. De dunne organische films die onderworpen waren aan dit onderzoek zijn: lichtemitterende polymeren, zoals LEP, en elektrisch geleidende polymeren zoals PEDOT:PSS (Poly3,4ethylenedioxythiophene: polystyrene sulfonaat). Gebaseerd op de resultaten werd n type barriere multilaag geselecteerd voor de vervaardiging van een functionele flexibele OLED. De functionaliteit van deze laser gepatroniseerde OLED werd aangetoond onder standaard omgevingscondities, dus niet in een gecontroleerde stikstofomgeving. De hermetische sluiting van de OLED is vooral kwetsbaar aan de overgang tussen de barriere multilaag en de encapsulatie laag er bovenop. Tussen beide lagen mogen er geen restanten meer aanwezig zijn van de tussenliggende (geableerde) organische film. Op die manier kan de penetratie van vocht langs de zijkant fors gereduceerd worden. Zelfs een resterende monolaag van de organische dunne film kan voor een vochtbrug zorgen, wat catastrofaal is voor de levensduur van de OLED. Om dit te onderzoeken werden de geableerde regios geanalyzeerd met TOF-S-SIMS (Time of flight static secondary ion mass spectroscopie). Deze techniek analyzeert de bovenste monolaag van het oppervlak. Verschillende geableerde zones al dan niet behandeld met een zuurstof plasma of een reactief ionen plasma, werden onderzocht, samen met zuiver PEDOT:PSS en zuivere barriere lagen als referentie. De conclusie van dit onderzoek was dat RIE nabehandeling nodig is om alle residuele componenten van de ablatie te verwijderen. Tot slot werd er nog een ultrasnelle pico seconde laser gebruikt voor dezelfde ablatie doelstellingen. Drie golflengtes (355 nm, 532 nm en 1064 nm) werden gebruikt om dunne lagen van

PEDOT:PSS en Plexcore (een commerciële organische conductieve inkt op basis van PEDOT derivaten) selectief te verwijderen. De ablatie drempel werd bepaald en de invloed van de golflengte werd bestudeerd.

Het tweede gedeelte van dit eindwerk bestaat uit de selectieve ablatie van OPV lagen met behulp van een laser met golflengtes in het mid-infrarood (mid-IR) gebied. Dit werk kadert in het Europees project IMPROV. In de eerste fase werd het principe van resonante infrarood ablatie aangetoond voor een relatief eenvoudig polymeer zijnde polymethylmethacrylaat (PMMA). Daarna werden gaten transport lagen en absorberende materialen uit een OPV stack gepatterneerd via RIA met infrarood nano seconde en pico seconde laser pulsen. De nanoseconde experimentele opstelling is gebaseerd op een commerciële laser met een golflengte van 1064 nm, die een resonerende optische parametrische oscillator (OPO) pompt, gebouwd rond een periodiek polig lithiumniobaat kristal met verschillende quasi-phase matching periodes. De laser levert meer dan 0.30 W aan infrarood vermogen (met een golflengte rond 3 µm), wat bij een puls frequentie van 20 Hz overeenkomt met een puls energie van 15 µJ . De picoseconde laser opstelling is gebaseerd op optische parametrische versterking (OPA) op een soortgelijk kristal, waardoor een directe vergelijking tussen beide pulslengte regimes mogelijk was. De golflengte van de mid-infrarood laser kan afgesteld worden op een golflengte waarbij het te ableren materiaal absorbeert door een moleculaire vibrationele transitie. De infrarood absorptie van typische organische materialen werd hiertoe bepaald met behulp van IR spectroscopie. In het bijzonder werden de infrarood gebieden bestudeerd die overeenkomen met het golflengte gebied dat kan geadresseerd worden door de infrarood laser. Drie verschillende functionele materialen van een organische zonnecel werden in beschouwing genomen: planarizatie laag (PEDOT:PSS), twee gaten transport lagen die alternerend gebruikt worden in OSCs (BPAPF en α-NPB); en hoog efficiënt absorberende materialen (HDR014 van Heliatek en DCV4T-Et2). BPAPF en α-NPB worden doorgaans gebruikt als gaten transport lagen in organische zonnecellen en OLEDs. Het ablatieproces van deze dunne film materialen werd succesvol aangetoond voor selectieve patternering en de invloed van de laser parameters werd besproken.

De resultaten van dit eindwerk zijn nuttig in de verdere ontwikkeling en optimalizatie van laser ablatie technieken voor het selectief

verwijderen van dunne organische lagen. Daarnaast werd een breed gamma aan golflengtes (UV tot IR) aangewend voor verscheidene substraten van glas tot flexibele barriere folies in dit onderzoek. Deze onderzoeksresultaten kunnen leiden tot een robust industrieel proces voor de patternering van dunne lagen tijdens de roll-to-roll productie van OLED en OPV.

Summary

Electronics world is becoming compact and lighter, each and every day. Indeed, electronics devices are used in every aspect of life in our day-to-day activities and it is hard to imagine the world without mobile phones, electronic mail, computer or television. The recent trends in electronics are not only limited to the miniaturization but also in the development of lighter and flexible devices. The conventional electronics devices are fabricated with inorganic materials such as Silicon or Germanium. However, in order to achieve the flexibility, the device needs to be fabricated in a flexible package with organic materials such as conducting polymers or small molecules. The field of electronics and material science, in which the devices are fabricated with conducting organic materials, is referred to as organic electronics. Organic electronics devices work in a similar manner as of their inorganic part, however the energy band gap of organic materials is defined as the energy difference between Lowest Unoccupied Molecular Orbitals (LUMO) and Highest Occupied Molecular Orbital (HOMO). As these devices consist of various thin films of conducting polymers or small molecules, making them lighter in weight and flexible in nature, therefore organic electronics is also known as plastic electronics.

The research on organic electronics boomed around late 1980s, when the first working Organic Light Emitting Diode (OLED) was demonstrated. Since the time of its invention, the OLED technology has been very well established and its applications are very common in daily life such as in television screens, computer monitor displays, portable devices like mobile phones. The OLED displays are lightweight, having wider viewing angles, better brightness, faster response time and lower costs in future. These advantages made OLEDs suitable to replace the Liquid Crystal Displays (LCDs) in television or computer screen. In addition to OLED, the Organic Solar Cells (OSCs) or Organic Photovoltaics (OPVs) have been of prime

importance and a lot of scientific research work has been devoted in their development. Organic solar cells have wide range of applications, but the most fascinating feature is their flexibly to embed into devices like cars, windows and cloths, to name a few. In general, the organic electronics devices (OLED and OPV) are made of very thin organic films of thicknesses about 100s of nanometer. Most important aspect in the fabrication of these devices is the processing and patterning method, either solution processed or vacuum evaporated or printed. Layer homogeneity and mask selectivity are very crucial step in the process selection for patterning of thin films. The OLED or OPV thin films are generally processed by deposition methods such as screen printing, gravure coating or lithography. These printing methods have their merits and demerits as well, it depends particularly on the application, resolution or feature size needed.

In this dissertation, we propose selective laser ablation as an alternative patterning technology for organic electronics. This work is mainly focused on the patterning of thin organic films used in OLED or OPV stack. The drive for using laser patterning as an alternative method is due to its exceptional advantages, for instance: faster processing (fewer processing steps), no wet-chemicals, no environmental pollution due to chemical waste and possibility to integrate with roll-to-roll (R2R) production. There are two main objectives in this work, first is to selectively pattern the thin organic films, which are a part of OLED stack and then demonstrate a fully functional OLED on a flexible substrate. It is a challenging task to selectively pattern one thin organic film on a polymeric substrate or another thin organic film, without damaging the underneath layer. The second objective is to apply Resonant Infrared Ablation (RIA) technique, for selective patterning of thin organic films used in the OPV stack. This is a noble approach to use RIA for patterning application in organic electronics, where the laser wavelength is tuned to the molecular vibrational transition of the organic material (film) to be ablated.

The first part of this PhD work, which has been conducted in collaboration with Holst Center (The Netherlands), the focus is on selective patterning of thin organic films which are relevant to the fabrication of an OLED device. The primary task was to optimize the barrier foil in terms of laser patterning. In fact, a barrier foil with better tolerance against water or oxygen permeation into an OLED or OPV stack is necessary, as this penetration will lead to shortening the

life time of the device. For this purpose, five different kinds of multilayered barrier foils are designed based on their absorption properties. The proposed multilayered barrier, consisting of different inorganic and organic thin films combination, which plays a vital role in slowing down the Water Vapor Transmission Rate (WVTR) and Oxygen Transmission Rate (OTR) into the stack. The influence of barrier optical absorption on laser patterning, has been investigated using ultraviolet (248 nm) excimer laser for thin organic films of Light Emitting Polymer (LEP) and Poly 3,4 ethylenedioxythiophene: polystyrene sulfonate (PEDOT:PSS). Hence, an optimized multilayered barrier foil is selected for further investigation. Afterward, the thin films of an OLED stack are selectively patterned and structured on the multilayered flexible barrier foil, using excimer laser. A laser patterned fully functional flexible OLED device has been demonstrated in environmental conditions. Since the sealing of the barrier (bottom layer) to encapsulation (top layer) is highly responsible for the protection of OLED device, hence it is important that there is no organics left after selective laser processing. Even a monolayer of left-over organics is enough to degrade the sealing of barrier-encapsulation layers, which will in turn lead to ingress of oxygen or moisture into the fabricated OLED stack. In order to investigate the surface of the laser patterned regions, Time Of Flight Secondary Ion Mass Spectrometry (TOF-SIMS) technique is used, it provides the chemical composition of the surface even if there is a monolayer organics left after laser processing. The TOF-SIMS spectra are measured for a variety of samples: laser patterned areas without any contamination or change on the surface, laser patterned areas with Reactive Ion Etching (RIE) treatment, laser patterned with O_2 plasma treatment, the pure (un-ablated) PEDOT:PSS surface and pure Silicon Nitride surface. The conclusion of this analysis is that a post RIS treatment is necessary to remove all residues from the thin organic film ablation. Alternatively, the selective thin films patterning has been performed with ultrafast laser system. Picosecond laser pulses are used to selectively pattern PEDOT:PSS and Plexcore (an organic conducting ink from Plextronics) thin films with 355 nm, 532 nm and 1064 nm wavelengths. Eventually, the thin films ablation thresholds are determined and influence of wavelength on patterning is compared.

In the second part of this PhD work, which has been carried out in the framework of European Project "IMPROV", the major focus

is on selective patterning of OPV layers using a mid-infrared (mid-IR) wavelengths. First, the proof-of-concept for resonant infrared ablation (RIA) has been demonstrated for PolyMethyl Methacrylate (PMMA), as a sample material. Next, hole transport materials and absorber materials of an OPV stack, are patterned using RIA technique employing nanosecond and picosecond laser pulses. The nanosecond experimental set-up is based on a commercial laser at 1064 nm, pumping a singly resonant Optical Parametric Oscillator (OPO) built around a Periodically-Poled Lithium Niobate (PPLN) crystal with several Quasi-Phase Matching (QPM) periods. The laser delivers more than 0.30 W of mid-IR power (at the wavelength of around 3 µm) at 20 Hz , corresponding to 15 µJ pulses. The picosecond laser set-up is based on Optical Parametric Amplification (OPA) in a similar crystal, allowing for a direct comparison between both pulse length regimes. The wavelength of the mid-infrared laser can be tuned to one of the molecular vibrational transitions of the organic material to be ablated. For that reason, the IR absorption spectra of the organic materials used in a typical organic photovoltaic device were characterized in the wavelength region that can be reached by the laser setups. Focus was on three types of materials prototypical for organic solar cells: as a planarization layer (the polymer PEDOT:PSS); as hole transport layer two typical materials that can be used alternatively in OSCs (BPAPF and α-NPB); and as typical high-efficiency absorber materials (like Heliatek's HDR014 and DCV4T-Et2). BPAPF and α- NPB are widely used as hole transport materials in organic solar cells and organic light-emitting diodes. In a nutshell, the ablation process has been successfully demonstrated for selective thin film patterning, and the influence of the various laser parameters is discussed.

This dissertation work is useful in developing and optimizing the laser process for patterning thin films. Furthermore, a broad range of wavelengths (from ultraviolet to infrared), and different substrates (rigid glass to flexible barrier foil) have been investigated in this study. All these investigations could lead to a robust industrial process for patterning OLED or OPV in R2R manner.

1
General Introduction

This chapter is an overview of the complete dissertation including the motivation of work and recent technological developments. First of all, the basic concepts of organic electronics, its applications and future prospective are presented. In the second part, the patterning technologies for organic electronics devices are introduced and the motivation for laser patterning has been justified. At the end, the chapter provides the sketch of this dissertation, its trajectory and related research projects involved in this work.

1.1 Organic Electronics

Organic electronics is based on the organic materials such as conducting polymers or small molecules. On the otherhand, the conventional electronics uses inorganic or semiconductor materials. Organic electronics has low production costs at high volume compared to its inorganic part. The devices which have been mostly researched in organic electronics are organic field effect transistors (OFETs), organic light emitting diodes (OLEDs) and organic photovoltaics (OPVs). The earlier reports on these devices were on organic electroluminescent diodes[1, 2] and organic thin film transistors (OTFTs) [3–5] based on either small organic molecules or conjugated polymers. The history and progress in the organic electronics field is illustrated in Table 1.1

Table 1.1: Historical developments in Organic Electronics

Year	Development
1940s	Studies of organic semiconductor materials [6]
1950s	Discovery of semi-conducting charge-transfer complexes
1950s	First observation of electroluminescence in organic material [7, 8]
1960	Development of ohmic dark-injecting electrode contacts [9, 10]
1963	Tetraiodopyrrole showed conductivity [11]
1972	Higher conductivity in charge-transfer complexes
1977	Polyacetylene used to produce conducting materials [12]
1987	1st OLED by C W Tang and S Van Slyke [1]
1987	1st OFET by Koezuka and co-workers [13]
1990s	Thin and plastic substrate, plastic electronics
2000	Noble prize for discovery of conducting polymer [14]
2010s	Flexible displays and roll-to-roll production

1.1.1 Organic field effect transistor

Organic thin field effect transistors are a particular kind of field effect transistors (FETs) which use the organic thin film material as its channel. OTFTs based on conjugated polymers or small molecules have been envisioned as a viable alternative to more traditional, mainstream thin film transistors (TFTs) based on inorganic materials[6]. Due to the relatively low mobility of organic semiconductors, OTFTs can not compete the performance of field-effect transistors based on single-crystalline inorganic semiconductors such as Silicon (Si), Germanium (Ge) or Gallium Arsenide (GaAs), which have charge carrier mobilities of three or more orders of magnitude higher[15]. The FETs are broadly divided into three categories based on their architecture (source, gate, drain, channel configuration): Metal Oxide Semiconductor FET (MOSFET), Metal Semiconductor FET (MESFET) and Thin Film Transistors (TFTs). The OFETs are based on the architecture of the Thin Film Transistor [16], however the channel is made of organic small molecules or conjugated polymers. A complete overview of the development of the Organic Thin Film Transistor (OTFTs) is provided by Dimitrakopoulos et.al [6] and Klauk [17] in review articles. At the moment the research efforts are being on flexible displays, which can be produced roll-to-roll (R2R). The researchers at HP Labs and the Flexible Display Center (FDC) at

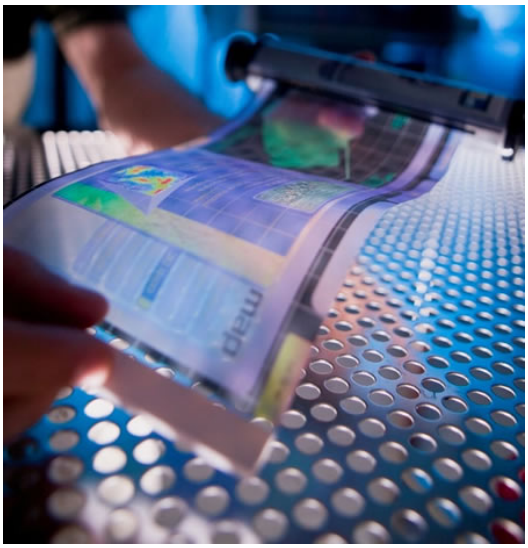

Figure 1.1: Paper like display, fabrication of thin film transistor (TFT) arrays on flexible plastic substrate, a low cost and "roll-to-roll" manufacturing process [18].

Arizona State University, US created the flexible displays by using self-aligned imprint lithography (SAIL) technology, invented by HP Labs, which enables the fabrication of thin film transistor (TFT) arrays on flexible plastic as shown in Figure 1.1. The HP lab claims this manufacturing process as a low cost and "roll-to-roll". The potential applications for the new flexible displays, according to HP and the FDC, are in electronic paper (e-paper) and future electronic devices that could use the extra battery life, such as smart-phones and notebook computers.

1.1.2 Organic light emitting diode

In early 1950s at Nancy University (France), Andre Bernanose group were the first to observe electroluminescence (EL) in organic materials operated with alternating current (AC) [7, 8]. They proposed that the electroluminescence mechanism is due to either excitation of dye molecules or excitation of electrons. In 1960, Martin Pope and co-workers at New York University developed the ohmic injecting electrodes for organic crystals[9, 10, 18]. They emphasized the necessity of energetic requirements such as work function,

for hole or electron injecting electrode contacts. The concept of high work function of anode and low work function of cathode electrode is still applied in recent production of organic electronics devices. In 1963, the same group of Martin reported the first direct current (DC) operated organic light emitting diode based on single crystal of antracene [19]. The AC electroluminescence based on polymer was reported shortly later in the year 1967[20]. C. W. Tang and S. A. Van Slyke in the year 1987 reported the bright green thin film small molecule OLEDs (SMOLEDs) based on tris(8-hydroxyquinoline)Aluminum (Alq_3) that were deposited by thermal vacuum evaporation and yielded an external efficiency of about 1 %[1]. This was the first demonstration of the working OLED. In 1990, Burroughes at al. reported yellow - green polymer LEDs (PLEDs) based on poly(p-phenylene vinylene) (PPV) that were fabricated by spin coating a precursor polymer onto the transparent conducting anode and converting the precursor to PPV by heating it[2]. Since the invention of OLEDs, there has been tremendous development in terms of life time and efficiency. These developments led to improve the performance of white light OLEDs for general lighting applications[21, 22].

A general organic light emitting diode consists of two electrodes (anode, cathode) and an emissive layer of the light emitting organic material either small molecule or conducting polymer. The emission of light from an OLED can be either top, bottom or both sided; depending on the type of electrodes (anode, cathode) either transparent or opaque. The OLED displays can be addressed with active or passive schemes, hence on the basis of operation they are divided in two types: Active Matrix OLED (AMOLED) and Passive Matrix OLED (PMOLED). The active matrix OLEDs use the thin film transistors (TFTs) to switch the pixels "ON" and "OFF".

Nowadays, OLED technology has been matured and it has commercial applications in displays such as in mobile phones, digital cameras, portable digital media players and car radios. Some prototypes have been made of flexible and rollable displays which use OLEDs' unique characteristics. Moreover, there are applications of OLED displays in flexible signs and lighting purposes. Some of the advantages of OLEDs include the lower costs in future, flexible and light-weight plastic substrates, wider viewing angle, improved brightness and faster response time. On the other hand, the limitations of OLEDs are shorter life span compared to liquid crystal displays (LCDs), lower efficiency for blue OLEDs and water damage (mois-

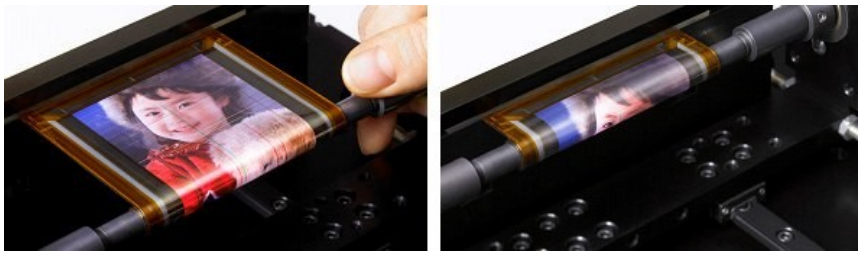

Figure 1.2: Demonstration of a 4.1" prototype flexible display from Sony: Ultra-thin OLED screen could continue to play video while being rolled around a pen [25].

ture, oxygen) to organic materials. In the year 2007, SONY announced the first OLED TV "XEL-1", it was just 3 mm thin, and has 960 x 540 resolution. It has an amazing 1,000,000:1 contrast ratio (much better than Plasma or LCD Televisions), a terrestrial digital tuner, speakers, HDMI, USB and Ethernet jacks [23]. That was just the first version of OLED TV, since then there has been much improvements in the size and other features. In recent developments, the most fascinating feature is flexible production, to produce roll-to-roll. A demonstration of flexible OLED display is shown in Figure 1.2 manufactured by Sony [24]. The other prime companies who have the major applications of OLED displays are LG and Samsung.

1.1.3 Organic photovoltaic cell

Organic Photovoltaic (OPV) Cell or Organic Solar Cell (OSC) is a device of prime importance these days. It works on the principle of photovoltaic effect, the organic materials are used for absorption of sun light such as conducting polymers or small molecules. Thin film of organic material is placed in between two electrodes; a high work function anode such as Indium Tin Oxide (ITO) and low work function cathode like Aluminium (Al), Magnesium (Mg) or Calcium (Ca). Organic photovoltaic solar cells can be made of single layer, bi-layer or multilayer structure. In order to improve the efficiency of OPV different architectures have been proposed such as planar hetero-junction, bulk hetero-junction or graded hetero-junction [25–27].

The material transitions and developments for photovoltaics are shown in the Figure 1.3. Flexible organic solar cell has a wide range of applications in day to day life, few applications are illustrated in

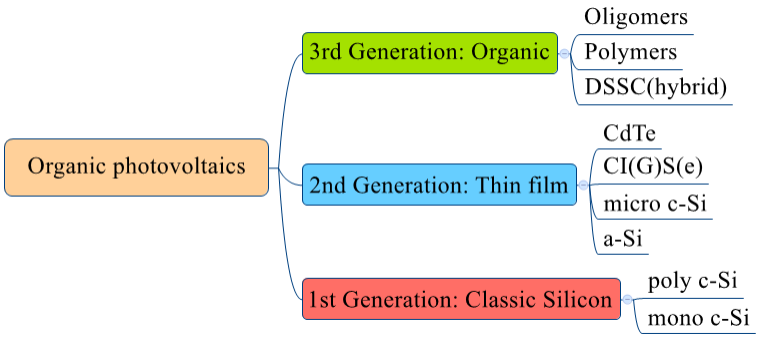

Figure 1.3: Material developments in photovoltaics from 1st generation to 3rd generation, adopted from Heliatek [29].

Figure 1.4: Overview of some applications of organic solar cells, picture adopted from SNe Research [30].

the Figure 1.4.

1.2 Organic Electronics Materials

Organic electronics is based on two kinds of carbon based materials, namely small molecules and conducting polymers. These luminescent organic molecules are π conjugated compounds, i.e. materials in which single (C−C) and double (C=C) or single and triple (C≡C) bonds alternate throughout the molecule or polymer backbone [28]. The organic molecules are conducting due to the delocalization of π electrons because of the conjugation property. These materials are sometimes referred as organic semiconductors as their conductivity lies in between the insulators and conductors. The Lowest Unoccupied Molecular Orbital (LUMO) and Highest Occupied Molecular Orbital (HOMO) of the organic materials, are analogous to the "conduction band" and "valence band" of the inorganic semiconductors respectively. The energy band gap between the highest occupied molecular π orbital (HOMO) and the lowest unoccupied molecular π^* orbital (LUMO) is about 1.4 eV to 3.5 eV. In the organic electronics devices, the materials are usually used in the form of thin films of thicknesses ranging from approximately 50 nm to 150 nm.

1.2.1 Small molecules

A small molecule is a low molecular weight organic material with the size in the order of nanometer. They have the conjugation property, which is useful for the charge carriers transportation in the organic electronics devices. The examples of the small molecules which are common in organic electronics purposes are organometallic chelates (Alq_3), pentacene, antracene and rubrene. Chemical structures of few small molecules are shown in Figure 1.5.

1.2.2 Conducting polymers

The other organic materials useful for organic electronics application are the polymers with conjugation properties which makes them suitable for conducting. The conducting polymers frequently used for organic electronics device fabrication are polyacetylene, polypyrrole, polyaniline, and their copolymers. Poly(p-phenylene vinylene) (PPV) and its derivatives are used for electroluminescent semiconducting

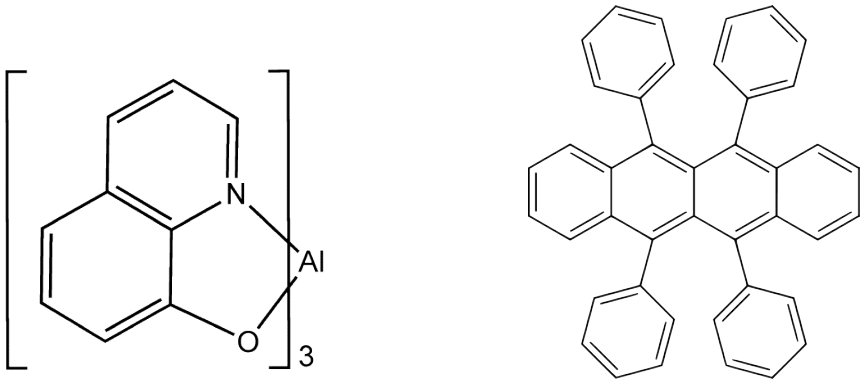

(a) Alq_3 (b) Rubrene

Figure 1.5: Examples of small molecules.

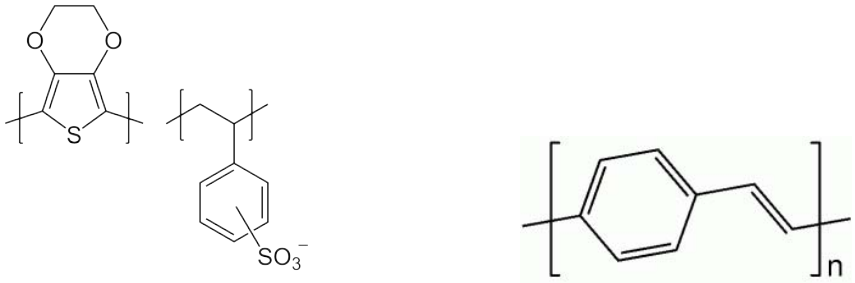

(a) PEDOT:PSS (b) PPV

Figure 1.6: Examples of conducting polymers.

polymers. The chemical structures of widely used conducting polymer materials such as Poly(3,4-ethylenedioxythiophene) Polystyrene sulfonate (PEDOT:PSS) and PPV are shown in Figure 1.6.

1.3 Patterning Technologies

There are many printing technologies which can be used for the printing of organic electronics devices. A comparison of the throughput and feature sizes that can be achieved by different patterning technologies is shown in the Figure 1.7.

It is very clear from this picture that laser ablation has high resolution feature sizes, below $<10\,\mu m$. The photolithograpy is very well

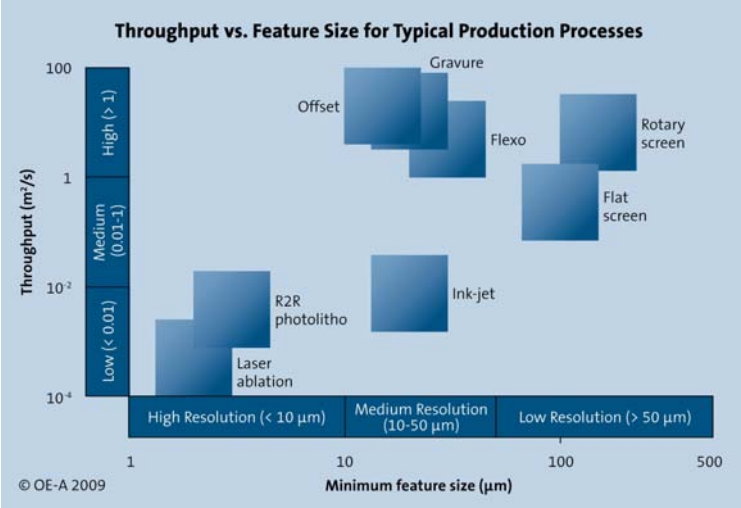

Figure 1.7: Comparison of various patterning and printing technologies for organic electronics devices [32].

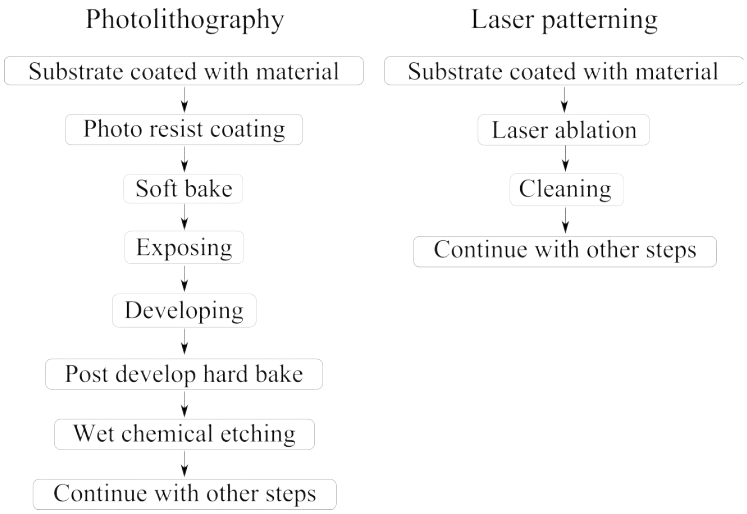

Figure 1.8: A comparison of photolithography versus laser patterning processing steps.

established technology, however laser patterning is highly competitive especially for roll-to-roll production. There are several advantages of laser patterning over conventional lithographic technology as shown in the flow chart in Figure 1.8. Some of the advantages of laser technology compared to other patterning techniques are listed:

- **Non-contact processing**: In laser patterning there is no direct contact of the material, the photons interaction do not create any mechanical impact or stress on material, and there are no material handling issues.
- **No wet-chemicals**: There are no wet hazardous chemicals used for patterning, means there is no wastage of handling, hence it is an environmental friendly technique. Laser patterning is an emerging alternative to the wet-chemical-etching processes.
- **Selective patterning**: With proper power density adjustment (fluence control) and laser wavelength selection, it is possible to selectively remove one layer from another layer. The structuring is possible without a mask and at well defined areas of interest.
- **Less complexity and faster processing**: There are many steps and complexities in photolithographic technique, however laser structuring is quicker and less steps to perform.
- **Parameters flexibility**: Most of the industrial laser systems are equipped with advanced softwares to control the parameters, hence the change in parameters can be easily done when required.
- **Roll-2-Roll integration**: The other important aspect of laser patterning is its feasibility to integrate with future roll-to-roll device production, as shown in Figure 1.9.

1.4 Problem Statement and Objectives

Selective patterning of thin organic films for organic electronics applications is a challenging task, especially when the film thicknesses are around 100 nm or 200 nm. Organic electronic devices such as OLEDs or OPVs consist of a multilayered stack of thin organic material films. The problems of patterning and the objectives to achieve are:

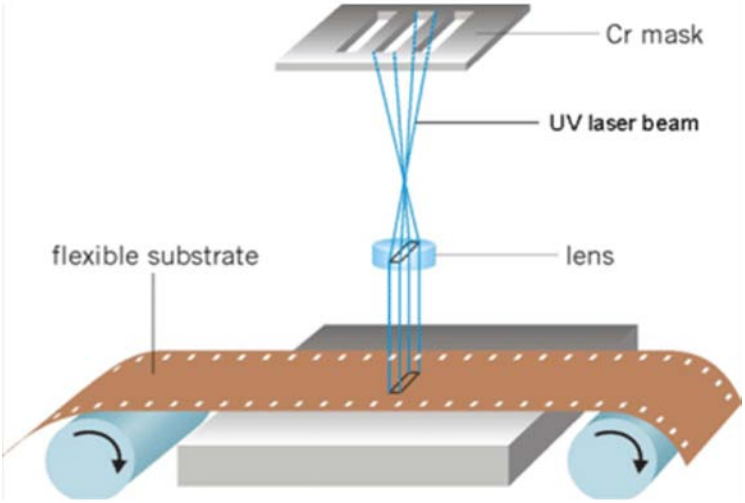

Figure 1.9: Integration of laser patterning for roll-to-roll(R2R) production of electronics devices, picture adopted from Coherent, Inc. [33].

- **Problem 1**: The thickness of the films used in these devices (OLED / OPV) is very low (10s or 100s of nanometers), in such a case the power density adjustment is critical. There is always a probability of either damaging the underneath layer or leaving a remaining layer or monolayers. This kind of uncertainty (damage or left over polymer) leads to penetration of moisture or oxygen into the OLED or OPV stack, which eventually damages the device i.e. shortens its life time. Therefore, a very precise and fine tuning of power density is needed.

- **Problem 2**: As most of the thin film materials used in these stacks are organic layers, they all have similar absorption characteristics, therefore it is highly challenging to find a suitable wavelength of laser (which is available also) at which one layer absorption is high whereas another layer hardly absorbs. For flexible production, the substrate is usually Poly ethylene terephthalate (PET) or Polyethylene naphthalate (PEN), means a polymer material. Therefore, in such a multilayered thin film polymer stack, the selectivity is very difficult to achieve.

To address these problems, the following objectives are kept into consideration:

- **Objective 1**: To develop the selective ablation processes for the patterning of an OLED stack using different laser systems with different wavelengths or pulse lengths. The selective patterning of thin films on a flexible substrate such as PET or PEN is targeted. To demonstrate a laser patterned OLED device on a flexible substrate.

- **Objective 2**: To investigate the mid-IR wavelengths for the structuring of the OPV layers by utilizing the Resonant Infrared Ablation (RIA) technique. The idea is to prove the concept of RIA first, for bulk polymers and thin films. Later, the processes are developed for thin film patterning using a high power mid-IR tunable source based on Periodically Poled Lithium Niobate (PPLN) crystal and an Optical Parametric Oscillator (OPO).

1.5 Research Trajectory and Dissertation Structure

Nowadays, the electronics world is moving toward the e-paper, washable, flexible and stretchable electronics devices. The Center for Microsystems Technology (CMST) at UGent is working on various research domains such as flexible and stretchable electronics, UTCP technology, polymer photonics, smart power systems and display systems. The trajectory of this research work is to develop processes for patterning and structuring of flexible organic electronics devices using laser technology. This task needed a joint venture of organic electronics and laser technology. The organic electronics devices have been fabricated and demonstrated using printing technologies, hence this work is noble as well as challenging to carry out. Laser structuring and patterning is visualized as a pioneering technology for organic electronics, especially when it is integrated with future roll-2-roll production. There has been a lot of work in which the laser was used for patterning thin films on a rigid glass substrate, however laser patterned flexible organic devices were hardly mentioned. The drive for this work was to integrate the laser process for roll-to-roll production of OLED / OPV, which has been not explored much. As mentioned earlier in this chapter, laser patterning has many advantages for high volume production of flexible devices.

This dissertation is broadly divided into two categories, one part focused on the OLED patterning and another is dedicated to the OPV layer structuring. There are three chapters focused on OLED patterning related work (Chapter 3, Chapter 4, Chapter 5), one chapter is common for both OLED and OPV related work (Chapter 6), one chapter is the proof-of-principle of using RIA for patterning (Chapter 7), and one chapter is dedicated to OPV thin film patterning (Chapter 8). If we summarize, Chapter 1 is the "General Introduction" of the research work, showing the motivation for flexible devices and predicting the future world of electronics as the "Organic Electronics". The chapter also describes the benefits of laser patterning over other printing or patterning technologies. In Chapter 2, the basic fundamentals of polymer laser ablation are explained, which is a pre-requisite knowledge for the understanding of laser patterning and results in the following chapters. The ablation mechanisms are explained briefly, with sufficient references to follow if needed. The Chapter 3 begins with the experimental work and focuses on how the substrate can influence the laser patterning of thin films. Various flex-

ible barrier substrates with different absorption properties are used for thin films patterning and a suitable barrier foil was selected for the fabrication of OLEDs. In the Chapter 4, a flexible laser patterned OLED device has been demonstrated using an excimer 248 nm laser in collaboration with the Holst Centre, The Netherlands. Knowing the shorter life time of fabricated OLED devices, the detail investigation was indeed necessary for the laser process and optimization. In Chapter 5, the Time of Flight Secondary Ion Mass Spectrometry (TOFSIMS) analysis technique is proposed for the investigation of ablated areas after laser patterning. The experiments were conducted for PEDOT:PSS thin films on the flexible barrier. The detailed monolayer investigation of the laser patterned PEDOT:PSS surfaces was carried out at University of Antwerp, using a TOFSIMS equipment. Chapter 6 is dedicated to the "Ultra-short laser pulse patterning" of thin organic films, which is relevant to OLED as well for OPV applications. After discussion about the OLED patterning, the Chapter 7 explains about the "Resonant Infrared Ablation" of bulk polymer Poly Methyle Methacrylate(PMMA), and the proof-of-concept for thin film patterning using RIA is demonstrated. The last chapter on the experimental part Chapter 8, describes the thin film patterning using RIA for OPV layers, the materials investigated are absorbers (donors) or hole transport materials. Finally, Chapter 9 concludes the overall results and provides the future scope of this work.

1.6 Research Context and Related Projects

The thin film patterning work for flexible OLED applications has been carried out in collaboration with Holst Center, The Netherlands. The collaboration with Holst Center in Technical Program 6 (TP6) was during the period of 2011 to 2013. The monolayer investigation of the PEDOT:PSS samples using the TOFSIMS equipment was carried out at the University of Antwerp, Belgium. For the OPV related work, the organic thin film patterning was carried out under the European Commission's FP7 (EC-FP7) project "IMPROV" (Innovative Mid-infrared high Power source for Resonant ablation of Organic based photoVoltaic devices). This project was started in the year 2010 and ended on 2014. The mid-IR nanosecond high power source was provided at IMEC, UGent through the collaboration of the project in the year 2012. Experimental work using nanosecond systems was carried out at IMEC/ CMST, UGent, whereas the pi-

cosecond laser experiments were conducted at Multitel, Mons. The samples were provided by Heliatek, Germany which recently developed materials for OPV applications. Some experiments were also performed at Thales Research and Technology, France at 4.50 µm and 4.77 µm wavelengths. The analysis of the samples during the IMPROV project was jointly carried out at IMEC, UGent and Heliatek, Germany.

To summarize, the following partners have contributed either in collaboration or through the projects during this PhD work:

- Holst Center, Eindhoven The Netherlands
- Multitel, Mons Belgium
- Thales Research and Technology, Paris France
- University of Antwerp, Antwerp Belgium
- Heliatek, Dresden Germany

1.7 Research Dissemination

1.7.1 Journal papers

- Sanjeev Naithani, David Schaubroeck, Yannick Vercammen, Rajesh Mandamparambil, Iryna Yakimets, Luc Van Vaeck and Geert Van Steenberge. "Excimer laser patterning of PEDOT : PSS thin-films on flexible barrier", *Applied Surface Science*, Vol. 280, 504-511 (2013), [Online].

- Sanjeev Naithani, Rajesh Mandamparambil, Henri Fledderus, David Schaubroeck and Geert Van Steenberge. "Fabrication of a laser patterned flexible organic light-emitting diode on an optimized multilayered barrier". *Applied Optics*, Vol. 53, 2638-2645 (2014), [Online].

- Sanjeev Naithani, Arnaud Grisard, David Schaubroeck, Eric Lallier and Geert Van Steenberge. "Mid-infrared resonant ablation of PMMA". *Journal of Laser Micro Nanoengineering*, Vol. 9, 147-152 (2014), [Online].

1.7.2 International conference proceedings

- Sanjeev Naithani, Rajesh Mandamparambil, Ferdie Van Assche, David Schaubroeck , Henri Fleddreus, An Prenen, Geert Van Steenberge and Jan Vanfleteren. "Influence of barrier absorption properties on laser patterning thin organic films". *Proceedings of SPIE, The International Society for Optical Engineering, SPIE*, Vol. 8435, 843505-1-843505-9 (2012), [Oral], Brussels, Belgium.

- Rajesh Mandamparambil, Geert Van Steenberge, Henri Fledderus, Sanjeev Naithani, An Prenen, Sandeep Perinchery and Iryna Yakimets. "Additive and Subtractive laser processes for printed electronics". *International Laser and Coating Symposium, ILaCoS*, (2012) [Oral], Dresden, Germany.

- Sanjeev Naithani, Arnaud Grisard, David Schaubroeck, Eric Lallier and Geert Van Steenberge. "Mid-infrared resonant ablation of PMMA". *Proceedings of 6th International Congress on Laser Advanced Materials Processing, LAMP*, Vol. 5 (2013), [Oral], Niigata, Japan.

- Geert Van Steenberge, Henri Fledderus, Thomas Hoegen, Sanjeev Naithani, David Schaubroeck, Rajesh Mandamparambil and Iryna Yakimets. "Ultrafast DPSS laser interaction with thin-film barrier stacks". *Large Area, Organic and Printed Electronics Convention, LOPE-C*, (2013) [Oral], Munich, Germany.

- Sanjeev Naithani, Charles Duterte, Marieta Levichkova, Arnaud Grisard, David Schaubroeck, Eric Lallier, Yves Hernandez, Karsten Walzer and Geert Van Steenberge. "Mid-infrared resonant ablation for selective patterning of thin organic films". *Proceedings of SPIE, The International Society for Optical Engineering, SPIE*, Vol. 9135, 91350K-1-91350K-12 (2014), [Oral], Brussels, Belgium.

- Sanjeev Naithani, David Schaubroeck, Rajesh Mandamparambil, Henri Fleddreus and Geert Van Steenberge "Ultrafast laser patterning of inorganic / organic thin-films for OLED / OPV applications". *Annual Symposium of the IEEE Photonics Benelux Chapter*, (2014), [Oral], Enschede, The Netherlands.

References

[1] Tang, C. W. and VanSlyke, S. A., "Organic electroluminescent diodes", *Applied Physics Letters*, vol. 51, no. 12, pp. 913–915, 1987. [Online].

[2] J. H. Burroughes, D. D. C. Bradley, A. R. Brown, R. N. Marks, and K. Mackay, "Light-Emitting Diodes Based on Conjugated Polymers", *Nature*, vol. 347, no. 6293, pp. 539–541, 1990. [Online].

[3] F. Ebisawa, T. Kurokawa, and S. Nara, "Electrical properties of polyacetylene / polysiloxane interface", *Journal of Applied Physics*, vol. 54, no. 6, pp. 3255–3259, 1983. [Online].

[4] K. Kudo, M. Yamashina, and T. Moriizumi, "Field-Effect Measurement of Organic Dye Films", *Japanese Journal of Aaapiled Physics Part 1-Regular Papers Short Notes & Review Papers*, vol. 23, no. 1, p. 130, 1984. [Online].

[5] A. Tsumura, H. Koezuka, and T. Ando, "Macromolecular electronic device: Field effect transistor with a polythiophene thin film", *Applied Physics Letters*, vol. 49, no. 18, pp. 1210–1212, 1986. [Online].

[6] Dimitrakopoulos, C.D. and Malenfant, P.R.L., "Organic Thin Film Transistors for Large Area Electronics", *Advanced materials*, vol. 14, no. 2, pp. 99–117, 2002. [Online].

[7] C. M. Bernanose A and V. P, "A new method of emission of light by certain organic compounds", *Journal de Chimie Physique et de Physico-Chimie Biologique*, vol. 50, no. 65, 1953.

[8] A. Bernanose, "Electroluminescence of organic compounds", *J. Appl. Phys.*, vol. 6, no. S54, 1955. [Online].

[9] H. Kallmann and M. Pope, "Positive Hole Injection into Organic Crystals", *The Journal of Chemical Physics*, vol. 32, no. 1, pp. 300–301, 1960. [Online].

[10] H. P. Kallmann and M. Pope, "Theory of Hole Injection and Conductivity in Organic Materials", *The Journal of Chemical Physics*, vol. 36, no. 9, pp. 2482–2485, 1962. [Online].

[11] R. McNeill, R. Siudak, J. H. Wardlaw, and D. E. Weiss, "Electronic Conduction in Polymers. I. The Chemical Structure of Polypyrrole", *Australian Journal of Chemistry*, vol. 16, no. 6, pp. 1056–1075, 1963. [Online].

[12] H. Shirakawa, E. J. Louis, A. G. MacDiarmid, C. K. Chiang, and A. J. Heeger, "Synthesis of Electrically Conducting Organic Polymers: Halogen Derivatives of Polyacetylene, CH_x", *J. Chem. Soc., Chem. Commun.*, pp. 578–580, 1977. [Online].

[13] H. Koezuka, A. Tsumura, and T. Ando, "Field-effect transistor with polythiophene thin film", *Synthetic Metals*, vol. 18, no. 1, pp. 699–704, 1987, Proceedings of the International Conference of Science and Technology of Synthetic Metals. [Online].

[14] "The Nobel Prize in Chemistry 2000, Nobel Media", *nobelprize.org*, 2014. [Online].

[15] Y. Taur and T. H. Ning, in *Fundamentals of Modern VLSI Devices, Second Edition*, Cambridge University Press, Cambridge, 1998, p. 11. [Online].

[16] P. K. Weimer, "The TFT A New Thin-Film Transistor", *Proceedings of the IRE*, vol. 50, no. 6, pp. 1462–1469, 1962. [Online].

[17] H. Klauk, "Organic thin-film transistors", *Chem. Soc. Rev.*, vol. 39, pp. 2643–2666, 7 2010. [Online].

[18] H. Kallmann and M. Pope, "Bulk Conductivity in Organic Crystals", *Nature*, vol. 186, pp. 31–33, 1960. [Online].

[19] M. Pope, H. P. Kallmann, and P. Magnante, "Electroluminescence in Organic Crystals", *The Journal of Chemical Physics*, vol. 38, no. 8, pp. 2042–2043, 1963. [Online].

[20] W. A. Hartman and H. L. Armstrong, "Electroluminescence in Organic Polymers", *Journal of Applied Physics*, vol. 38, no. 5, pp. 2393–2395, 1967. [Online].

[21] "Universal Display Corporation", *http://www.udcoled.com/*, Viewed on December-2014. [Online].

[22] M. C. Gather, A. Kohnen, and K. Meerholz, "White Organic Light-Emitting Diodes", *Advanced Materials*, vol. 23, no. 2, pp. 233–248, 2011. [Online].

[23] "Sony XEL-1: The world's first OLED TV", *http://www.oled-info.com/*, Viewed on December-2014. [Online].

[24] C. Lambardi, "Sony unveils ultrathin rollable OLED", *www.cnet.com/*, 2010. [Online].

[25] J. Nelson, "Organic photovoltaic films", *Current Opinion in Solid State and Materials Science*, vol. 6, no. 1, pp. 87–95, 2002. [Online].

[26] H. Hoppe and N. S. Sariciftci, "Organic solar cells: An overview", *Journal of Materials Research*, vol. 19, pp. 1924–1945, 07 2004. [Online].

[27] R. Pandey and R. J. Holmes, "Organic Photovoltaic Cells Based on Continuously Graded Donor-Acceptor Heterojunctions", *Selected Topics in Quantum Electronics, IEEE Journal of*, vol. 16, no. 6, pp. 1537–1543, 2010. [Online].

[28] Shinar J. and Shinar R., in *An Overview of Organic Light-Emitting Diodes and their Applications*, Elsevier B.V., 2011, pp. 74–101.

2

Fundamentals of Polymer Ablation

In this chapter, the basic concepts of the laser polymer ablation and its application in the thin film patterning are provided. As the selective patterning is crucial in organic electronics device fabrication, therefore the requirements for the selective ablation and ablation parameters are discussed in more depth. The focus is on the parameters such as laser based (wavelength, fluence, pulse length), material related (optical, thermal, photo-physical), and the basic ablation mechanisms are explained.

2.1 Introduction

The word "laser" is an acronym for "light amplification by stimulated emission of radiation". The foremost prediction of stimulated emission was done by Albert Einstein in 1916 [1, 2]. In 1928, Rudolph W. Ladenburg confirmed the existence of stimulated emission and negative absorption [3]. However, for the stimulated emission process to occur the population inversion was necessary. The possibility of population inversion was noted by Valentin A. Fabrikant in 1940 [4]. After seven years, Lamb and Retherford demonstrated the stimulated emission for the first time in Hydrogen spectra [5]. Meanwhile, at Columbia University the first device based on stimulated emission called "maser" was invented by Charles H. Townes in 1951 [6, 7]. The

word “maser” refers to “microwave amplification by stimulated emission of radiation”. In the same year, “maser” was independently invented by two different groups, one at Lebedev Laboratories, Moscow and another at University of Maryland. The first detailed paper describing an “optical maser” by Schawlow and Townes in 1958 was credited for the invention of laser [8], and two years later in 1960 they have patented the laser. However, the first working laser based on a ruby crystal was invented by Theodore Maiman in 1960 at Huges Research Laboratories [9].

Since its invention, lasers have been in practice for industrial as well as scientific investigations. Due to the highly coherent beam, laser light can be extremely focused, which allows to achieve very high energy densities. These properties of laser light makes it suitable for the high resolution material processing. The controlled removal of material by laser using vaporization or chipping of surface is termed as “ablation”. The mechanism of laser ablation depends on many parameters, some are related to the laser itself and others are material related. The monochromaticity of a laser beam permits the selective ablation, and the wavelength of the laser can be tuned to a particular electronic transition or molecular vibrational transition. In this chapter , the laser material processing is focused on polymer materials only, as polymer thin films are widely used in organic electronics devices. The pioneering work of polymer laser ablation was first reported by R. Srinivasan at IBM laboratories in 1982 [10, 11], in which the laser used was excimer laser (ultraviolet wavelengths). In the same year, photo-etching of the polymethyle methacrylate (PMMA) using excimer laser was reported by Kawamura [12].

2.2 Ablation Principles

The polymer laser ablation is mainly described by the threshold fluence and ablation rate. These parameters depend on the laser wavelength and absorption coefficient of the material.

2.2.1 Fluence

The term “fluence” is defined as the laser pulse energy per unit area or energy density. In laser polymer ablation, the fluence is an important parameter as it determines the ablation threshold of material to be ablated. In general, fluence can be described as follows:

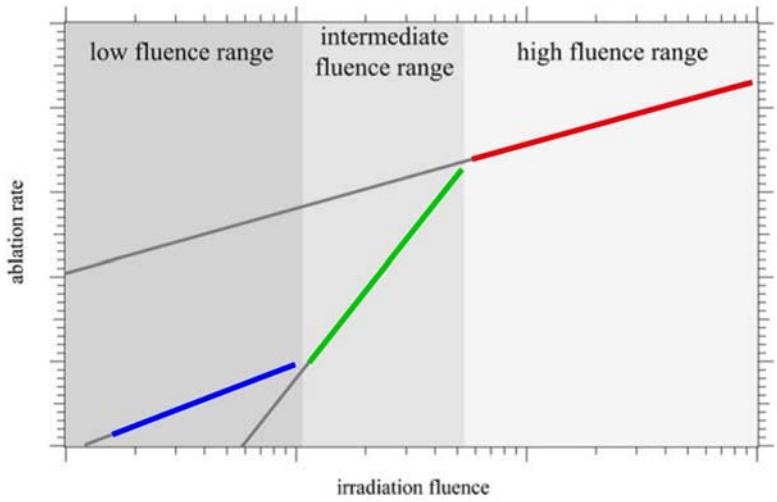

Figure 2.1: Schematic plot of the three fluence ranges which are typically observed for polymers. At low fluence range (blue line), there is incubation effect observed, medium fluence range (green line) efficient decomposition of polymer and at high fluence range (red line) the incident laser light is screened by solid, liquid, and gaseous ablation products and the laser produced plasma [13].

$$Fluence = \frac{Laser\ pulse\ energy\ (\text{Joules})}{Area\ of\ the\ focal\ spot\ (\text{cm}^2)}$$

The minimum fluence at which the material removal or onset of ablation is observed, is known as "ablation threshold or threshold fluence" of the material. A schematic diagram indicating the relationship of ablation rate with fluence for polymers is shown in Figure 2.1. In case of polymer laser ablation, there are three possible fluence ranges [13]:

1. **Low fluence range**: At low fluences the ablation threshold is determined and the incubation effect is mostly observed in this regime.

2. **Intermediate fluence range**: Increase of the slope of the ablation rate, which is caused by a more efficient decomposition

of the polymer. Energy that has been gained from an exothermic decomposition of the polymer can also increase the ablation rate.

3. **High fluence range**: In this case, the incident laser light is screened by solid, liquid, and gaseous ablation products and the laser produced plasma. This leads to similar ablation rates for many polymers [14] at high fluences.

2.2.2 Absorption coefficient

The absorption coefficient is a characteristic of any medium, a high absorption coefficient indicates that the beam is absorbed quickly in the medium whereas a low absorption coefficient means the material is transparent to the wavelength of irradiation or light. The absorption coefficient can be defined with Beer-Lambert's law [15].

$$I(z) = I(0)e^{-\alpha z}$$

where, $I(z)$ is the transmitted intensity of light after passing through a medium of thickness z, while $I(0)$ is the incident intensity of light. This can be illustrated as in Figure 2.5. The exponent α is the absorption coefficient, and it depends on the material, the wavelength of radiation and the intensity.

2.2.3 Ablation rate

The ablation rate is defined as the ablation depth per pulse for single pulse ablation, or the slope of the curve plotted between ablation depth versus number of pulses in case of a multi-pulse experiment. The ablation threshold fluence is the minimum energy density required for the onset of the ablation process. The ablation process can be explained with the following equation [16, 17]:

$$d = \frac{1}{\alpha_{eff}} \ln\left(\frac{F_0}{F_{th}}\right)$$

where, d is the ablation rate, α_{eff} is the effective absorption coefficient of the material. The parameter F_0 is the applied maximum laser fluence and F_{th} is the laser threshold fluence.

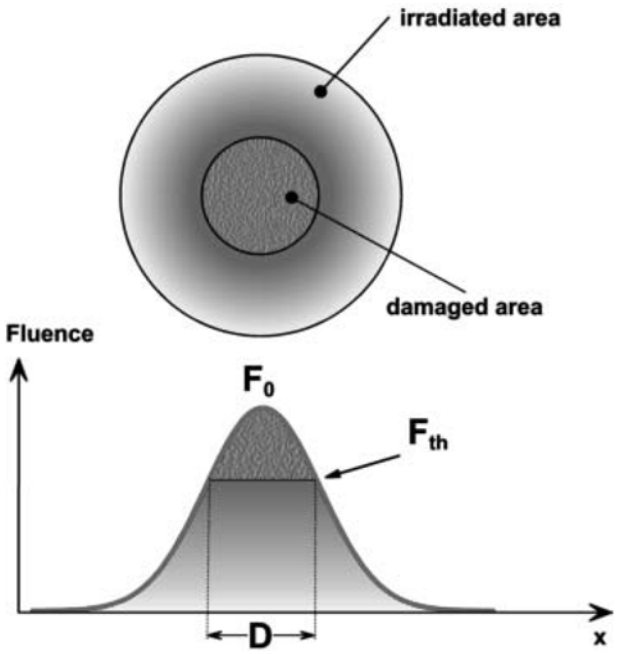

Figure 2.2: Schematic diagram of laser-induced ablation on the samples (top) and corresponding Gaussian fluence profile along x-axis (bottom), D indicates the diameter of the ablated area [19].

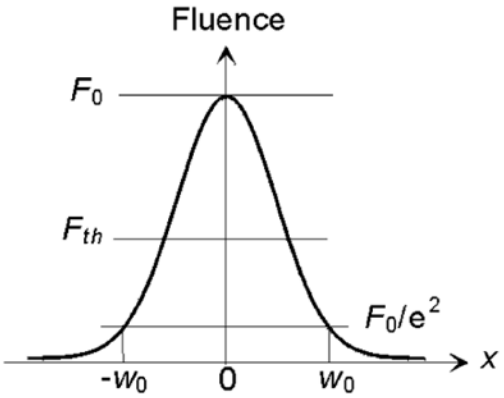

Figure 2.3: Schematic of a spatially Gaussian beam profile. F_0 and F_{th} denote the maximum laser fluence and the ablation threshold fluence, respectively. The distance $2W_0$ represents the $1/e^2$-Gaussian beam diameter [19].

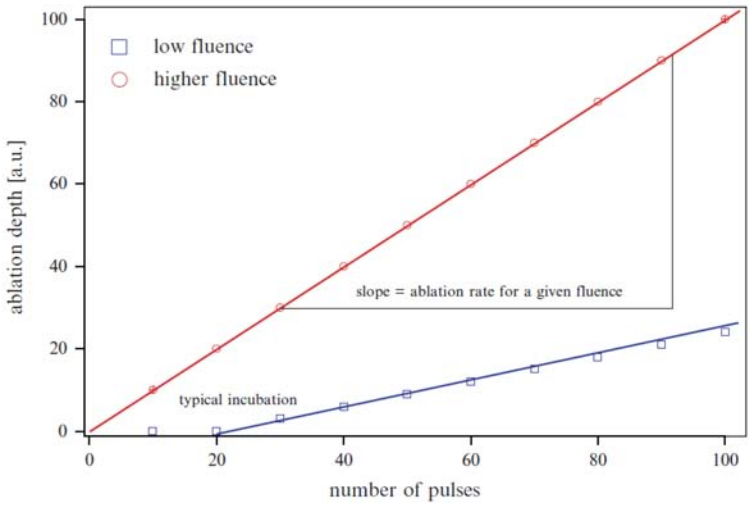

Figure 2.4: Plot of ablation depth vs. number of pulses, which is used to determine the ablation rate at a given fluence. The typical feature of incubation, i.e. ablation starts only after certain number of pulses, is shown for the low fluence curve [13].

Assuming the Gaussian beam profile as shown in Figure 2.2, the relation between diameter (D) of laser ablated crater and the maximum laser fluence (F_0) can be written as [18]:

$$D^2 = 2W_0^2 \times \ln\left(\frac{F_0}{F_{th}}\right)$$

where, W_0 is the Gaussian beam radius. The Gaussian beam diameter is defined as the separation between two points in the spatial Gaussian profile (Figure 2.3) at which the fluence is reduced to $1/e^2$ of its maximum value.

A plot of ablation depth versus number of pulses is shown in Figure 2.4, which clearly shows that the ablation rate is dependent on fluence. However, in some cases of polymer laser ablation, there is no removal of material with single pulse or first few pulses, and more number of pulses are required to have a depth of ablation which can be measured. This particular case is shown in the ablation plot (Figure 2.4) with a blue line, where minimum 20 pulses are needed for the onset of ablation, this mechanism is known as "incubation". The

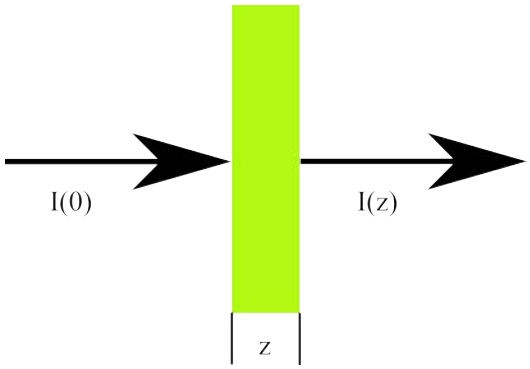

Figure 2.5: Schematic diagram to represent Beer-Lambert law for absorption of light in a medium.

pulse energy dumped into the material prior to ablation, is used in the modification of physical and chemical material properties, which results often in the increase of absorption at the irradiation wavelength. The incubation phenomenon is usually observed for the polymers with lower absorption coefficients such as poly (methyl metacrylate) (PMMA). A relationship between the single-pulse (damage) threshold $F_{th}(1)$ and the multi-pulse threshold $F_{th}(N)$ has been established and described as [19]:

$$F_{th}(N) = F_{th}(1) \times N^{\xi-1}$$

where ξ is a material-dependent incubation parameter. The values of incubation parameter are lesser than unity ($\xi \leq 1$), and $\xi = 1$ means that no incubation effect is observable.

2.2.4 Selective ablation

Selective ablation is a technique of removing one material or thin film from a substrate or another thin film without any damage on the underneath layer. As OLED/OPV devices consist of a multi-layered stack of thin films, selective ablation can be applicable to pattern these thin organic films. The selectivity is a critical issue. Selectivity of the ablation process mainly depends on the threshold fluence of materials and the laser wavelength. A simple illustration to understand the concept of selective ablation is shown in Figure 2.6, for a polymer on another polymer. In such cases, the absorption of the laser wavelength should be maximum for the layer to be ablated,

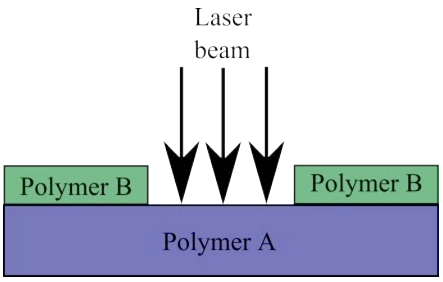

Figure 2.6: Schematic to represent selective ablation of "Polymer B" on "Polymer A" with a laser.

however it should be minimum for the underneath layer. For selective removal of a thin polymer film (Polymer B) from another polymer (Polymer A), the fluence of laser F_{Laser} should follow the condition:

$$F_{th}(PolymerB) < F_{Laser} < F_{th}(PolymerA)$$

where, F_{th} indicates the ablation threshold fluence of the material. This equation is valid in case of photochemical and photothermal ablation, however there can be deviation in case of photo-mechanical stress ablation. A detail discussion about the ablation mechanisms will be presented in the following sections. Selectivity is difficult to achieve as thin films of 100 nm or even lower thickness (as in case of OLED or OPV stack) are very sensitive, hence the laser wavelength should be very selective to remove one thin film without damaging the other. The polymer ablation using excimer lasers has been reported frequently for photonics [20, 21] and microsystem applications [22]. Furthermore, the patterning of conducting oxides such as Indium Tin Oxide (mostly used in organic electronics applications) on glass substrate [23–25] and also on the flexible substrates [26, 27] has been studied. Moving a step further to the conducting polymers as they are most suitable for organic electronics, the PEDOT:PSS has been successfully ablated using excimer lasers [28, 29]. However, the selective patterning of a polymer on another polymeric substrate has always been a challenging task, there are only limited studies of selective patterning of polymers on polymeric substrates or flexible substrates using lasers [30, 31].

2.3 Laser Parameters

The laser ablation of any material depends on several parameters, some are laser related and other depends on material. In this section, the focus is on the parameters which depends on the laser source such as wavelength, output power, pulse energy and pulse length.

2.3.1 Wavelength selection

The lasers are developed in a variety of wavelength range from ultraviolet (UV) to infrared (IR). These radiations have different energies, and the energy of a photon is given by:

$$E = h\nu$$

where, h is the Plank's constant and ν is the frequency of the electromagnetic radiation. Plugging in some numerical values, at the wavelength of visible light (450 nm) the energy of the photon is 2.77 eV. However, the energy required to break the chemical bonds is 3 eV to 10 eV, therefore visible radiations have not enough energy to break the chemical bonds. The alternative ways for material processing are possible as [32]:

- To increase the temperature of material by absorption of laser energy, which leads to a thermal or pyrolitic (thermo-mechanical decomposition) process.
- Higher energy photons (UV) which have an energy 3 eV to 7 eV can be used for breaking chemical bonds, especially for polymers or plastic materials. This is a photochemical process.
- The third option is using lasers, those deliver an extreme density of photons in time and space so that electrons are hit by several photons simultaneously i.e. allowing multi-photon absorption. Absorption of multiphotons has the same result as a single high energetic photon.

The lasers mostly used in the industrial applications are CO_2, Nd:YAG and excimers. For the polymer ablation, the use of excimer lasers was first reported by R. Srinivasan in 1982 [11]. Excimer lasers are very suitable for the ablation of polymers [33] and therefore they are used for the polymer thin film patterning in the industry. The

Table 2.1: Nanosecond laser systems available at CMST.

Type	Excimer	Nd:YAG	CO_2
Wavelength	248 nm	355 nm	10.6 µm
Average power (W)	0.3 - 5	> 5	60
Pulse energy (mJ)	1 - 20	0.5	400
Pulse duration (ns)	3 - 7	30	70

Table 2.2: Ultrafast laser systems available at CMST.

Duetto	Time Bandwidth (picosecond)
Wavelengths	1064 nm, 532 nm, 355 nm
Pulse duration	< 12 ps
Pulse repetition rate	50 kHz - 8 MHz
Pulse energy	up to 200 μJ
Output power	10 W - 15 W
Beam quality (M^2)	1.30
Satsuma	**Amplitude Systems (femtosecond)**
Wavelength	1030 nm
Pulse duration	400 fs - 10 ps
Pulse repetition rate	0 upto 5 MHz
Max.Pulse energy	10 μJ @ 100 kHz
Output power	5 W @ 1 - 5 MHz
Beam quality (M^2)	1.25

laser systems available for material processing at Center for Microsystems Technology (CMST) are shown in Table 2.1 (nanosecond laser systems) and Table 2.2 (ultrafast systems).

2.3.2 High pulse power

In the previous section, the selection of the laser wavelength has been discussed and it depends on the material optical absorption properties. Now, the next step is to achieve high pulse power and energy. The method of achieving high pulse power through a laser is known as "Q switching". It has been so designated because the optical Q of the resonator cavity is altered when this technique is used [34]. Q is known as the quality factor of a laser resonator cavity, and is defined as the ratio of the energy stored in the cavity to the

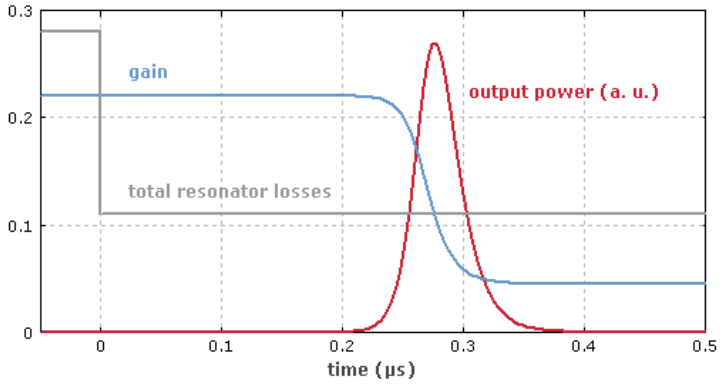

Figure 2.7: Generation of a Q-switched pulse, a technique for obtaining energetic pulses from laser by modulating the losses in the resonator cavity, picture adapted from [35].

energy loss per cycle. The higher the quality factor of the cavity, the lower the losses. In this method, first the energy is stored in the amplifying medium by optical pumping, while the cavity Q is lowered to prevent the onset of laser emission. As the energy is stored and the gain in the active lasing medium is high, the cavity losses are also high, the population inversion reaches a level far above the threshold for normal lasing action, but lasing action is still prohibited. When the cavity is switched from low Q value to a high Q value, the stored energy is suddenly released in the form of a very short pulse of light. Because the high gain created by the stored energy in the active material, the excitation is discharged in an extremely short time. The peak power of the resulting pulse exceeds that obtainable from an ordinary long pulse by several orders of magnitude. The Q-switch can be an actively controlled element such as electro-optic or acousto-optic modulator (active Q-switching) or it can be achieved by using saturable absorbers in the cavity (passive Q-switching). The basic principle of Q-switching is shown in Figure 2.7, where the cavity loss and generated high power pulse is illustrated.

2.3.3 Short pulse length

The quality of the ablated polymer material also depends on the pulse length of the laser. The shorter pulse length has advantages over the longer pulses in polymer ablation [31, 35, 36]. The ultrashort

pulse duration (picosecond, femtosecond) fundamentally changes the laser-matter interaction. The main differences between conventional nanosecond and ultrashort (ps/fs) laser ablation are summarized as [37]:

- Very high laser peak intensities ($(> 10^{14}\ W/cm^2)$) can be achieved with the focused beam, which are powerful enough to ionize and machine any material.
- The motion of the emerging ablated matter and its associated complexities for material removal can be ignored. There is no laser plasma interactions involved above the illuminated surface and hence no laser attenuation losses on target.
- The ablation mechanism for pulses below a few picoseconds ($1\,\text{ps} = 10 \times 10^{-12}\,\text{s}$) in duration decouples for most materials the ablation process from stochastic thermal processes. This has important implications on overall quality and reproducibility.
- The non-linear photon absorption process enables ablation of virtually any material, even materials that have band-gaps above the incident photon energy. It means by controlling the laser fluence in such a manner that only a smaller portion of the focused beam exceeds the ablation threshold by non-linear photon absorption.

Knowing that shorter pulses are producing less thermal effects and better quality of the ablated region, it is obvious to think about "how can we generate such short pulses?". The typical pulse width obtained from a Q-switched laser is on the order of 10-20 nanoseconds for most systems. With the cavity dumping technique, the pulse width can be reduced to a minimum of 1-2 nanoseconds. The limitation is the length of the cavity, which determines the pulse length. Ultrashort pulses with pulse widths in the picosecond or femtosecond regime are obtained from a solid state laser by "mode locking". In this technique, the longitudinal modes of the laser are locked in phase and the pulse width is inversely related to the bandwidth of the laser emission. In general, the output from the laser oscillators is subject to strong fluctuations; which originates from the interference of longitudinal resonator modes with random phase relations. In the mode locking, by establishing a fixed phase relationship among the longitudinal modes, a powerful well defined single pulse circulating

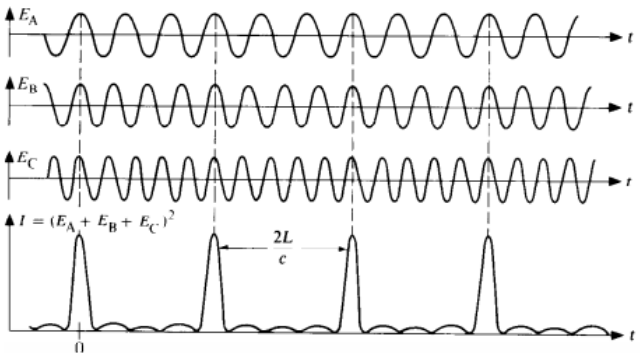

Figure 2.8: Mode locked or phase locked pulses in a resonator cavity, a technique to obtain ultrashort duration (ps/fs) pulses. E - field, I - Intensity, L - the length of cavity and c is the velocity of light [39].

in the resonator can be generated [34]. A schematic diagram of mode locked pulses in a resonator cavity is shown in Figure 2.8. Mode locking results in a train of pulses whose repetition period is twice the cavity transit time (t_r), and can be expressed as:

$$PRF = \frac{1}{t_r} = \frac{c}{2L}$$

where, PRF is the pulse repetition frequency, t_r is the separation of individual pulses, L is the length of resonator cavity and c is the velocity of light. The pulse width (t_p) of the mode-locked pulses is roughly equal to the cavity round trip time (t_r) divided by the number of phase locked modes (N):

$$t_p \approx \frac{t_r}{N} \approx \frac{1}{\Delta\nu}$$

where, $\Delta\nu$ is the gain bandwidth of the laser.

The mode locking requires a mechanism that results in a lower loss for a more intensive radiation peak compared to the average intensity in the resonator. This can be provided by two different ways:

- **Passive mode locking**: The radiation in combination with the saturable absorbers generates a periodic modulation that

leads to a fixed relationship of the longitudinal modes. Examples of such types of saturable absorbers are organic dyes or semiconductors.

- **Active mode locking**: An acousto-optic modulator provides a phase or frequency modulation exactly at the frequency separation of adjacent modes that leads to a higher gain for a train of mode locked pulses compared to continuous wave (cw) operation.

The short pulses (ps, fs) generated by the mode locking technique have the energy level in the order of few nanojoules only. In order to amplify these pulses, chirped pulse amplification (CPA) method is used to reach the energy levels from a few nanojoules to a few joules. The measurement of the duration of ultrafast pulses, where electronic apparatus would be too slow to respond, is done by using an autocorrelator trace.

2.3.4 Beam optics and delivery

The beam optics has significant importance in the quality of the laser ablated grooves. Beam parameters which have influence on the laser ablation process are beam profile, polarization, lens numerical aperture (NA), number of pulses (translational speed of stage), pulse repetition rate, drilling method, delivery method, environmental conditions and surface focal plane. The beam profile in general is Gaussian distribution, and in some applications a flat top beam profile is preferred. The polarization state of the light with repetitive pulses shows a strong influence on the micro- and nano-morphology of the machining results. Linear polarization of repeated pulses cause "ripples" parallel to the electric field vector, however the circular polarization results in cone-like nano-structure arrays exhibiting the periodicity of ripples for linear polarization [19]. When rotating the polarization and keeping the target fixed, the ripple orientation follows the polarization, independent of the material structure [38]. The effect of polarization state on laser induced periodic surface texture is shown in Figure 2.9.

The numerical aperture of the objective has a great influence on the cross section of the laser patterned trenches. The rectangular cross sections are achieved with lower numerical aperture values ($<$ 0.25). For example, the fabrication of polymeric mold inserts the steep sidewalls and well defined contours of edges are required, in

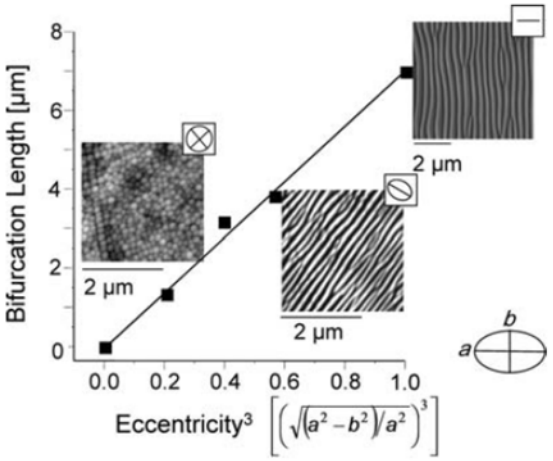

Figure 2.9: Dependence of self organized structures on the state of polarization after ablation [40].

such cases numerical aperture of ≈ 0.10 objectives are used [22]. The higher pulse repetition rates result in lower pulse energy. For any patterning application, the translation speed of the sample stage can be determined as:

$$Speed = \left(\frac{Spot\ size}{N}\right) \times PRF$$

where, N is number of laser pulses per unit area and PRF indicates the pulse repetition frequency. The spot size is measured on the sample, it can be the diameter of a beam or the spot dimensions depending on the mask size. When the patterning is required such as a line or an area, the overlapping of pulses is carried out and the corresponding speed is varied in the proportionate ratio. The laser drilling for microfabrication can be performed in various ways; such as single pulse, multiple pulse (percussion) or trepanning as shown in Figure 2.10. Beam delivery for patterning or structuring can be performed through a mask or directly, the mask dimension depends on the application.

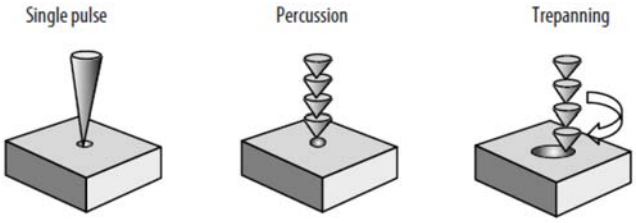

Figure 2.10: Laser drilling methods for via drilling or microfabrication [41].

Table 2.3: Material properties relevant to laser ablation.

Optical	Thermal	Physical
Refractive index	Thermal expansion coefficient	Density
Absorption coefficient	Melting point	Hardness
Reflectivity	Boiling point	Poison Ratio
	Vapor pressure	Surface roughness

2.4 Material Parameters

For successful selective patterning of any material, the material parameters are as important as the laser parameters. Some of the material properties which are relevant to the laser ablation are listed in the Table 2.3. While considering any material for ablation, the first task is to obtain its absorption spectrum. Depending on the absorption characteristics, next step is to find an appropriate laser or wavelength which can be absorbed by the material. Polymer materials have significant absorption at the UV wavelengths, therefore these material are excellently ablated with the excimer lasers. The shorter the laser wavelength, the higher the photon energy and thus it is easier to break the chemical bond. A summary of the typical laser wavelength regimes and corresponding energy is given in Table 2.4. As most of the polymer materials are carbon chains connected through chemical bonds, the bond energies are taken into consideration. A list of typical chemical bond energies of polymer materials is given in Table 2.5.

Table 2.4: Examples of typical laser wavelength regimes and corresponding photons energy [41].

Source	Wavelength (µm)	Regime	Frequency (Hz)	Energy (eV)
Excimer	0.248	UV	1.2×10^{15}	4.90
Argon	0.488	Visible	6.1×10^{14}	2.53
Nd:YAG	1.064	IR	2.8×10^{14}	1.16
CO_2	10.60	IR	2.8×10^{13}	0.12

Table 2.5: Polymer chemical bonds and corresponding energies [41].

Type of bond	C−C	C=C	C≡C	C−H	C−N	C−S
Energy (eV)	3.62	6.40	8.44	4.30	3.04	4.96

2.5 Ablation Mechanisms

The laser parameters and material properties are required prior to the ablation experiments to be conducted. After laser ablation, another crucial aspect is to know the ablation mechanisms by which the material removal was possible. There is no general rule of thumb to be definite about the ablation mechanism, it can be a combination of photochemical, photothermal and photomechanical processes. When the ablation process is mainly governed by thermalization of material it is known as photothermal, whereas when it is dominated by the chemical transitions it is known as photochemical. If both thermal and nonthermal mechanisms are significant then the process is referred to as photophysical [39]. If the laser processing is thermally activated, the state of the system is described by the laser-induced temperature distribution. On the other hand, photochemical laser processing is determined by the selectivity of the excitation either it is electronic or molecular vibrational. Some of the main aspects of the ablation mechanisms can be summarized as [13]:

1. **Direct bond breaking**: When the laser pulse strikes the polymer, first of all there is a possibility of direct bond breaking due to the absorption of photons by the polymer. This absorption depends on the energy of the photon, UV radiations (e.g. excimer lasers) have higher energy compared to IR radiations (e.g. CO_2, Nd:YAG lasers). The direct bond breaking is a very rapid

process in the time scales of picoseconds or femtoseconds. It implies that if the process is carried out with nanosecond lasers, then the primary decomposed ablation products can also be decomposed with laser photons. The direct bond breaking of polymers is assumed to be "cold ablation" as there is no thermal process involved.

2. **Temperature rise**: However, not all the photon energy is used for breaking the bonds, means some of the energy is transferred to the polymer matrix which eventually increases the temperature. These reactions create different structures with different absorption properties and quantum yields for their further decomposition. Energy can be released from exothermic decomposition reactions, which again gives rise to temperature increase.

3. **Pressure rise**: The primary and secondary decomposition reactions lead to small products formation which increases the pressure in the volume. Due to higher temperature, the thermal decomposition starts very quickly which results in the increase of pressure. Moreover, the fast increase in temperature can also increase the quantum yield and subsequent reactions such as unzipping the polymer chains. These kind of small reactions also leads to increase in pressure of the overall volume.

4. **Incubation phenomenon**: Delayed ablation is another consideration, when the polymer is modified first with the absorption of photons through incubation mechanisms, and ablation of modified material becomes easier than the original polymer.

On the basis of above considerations, it is difficult to model the ablation mechanism, it is a complex process. An ablation mechanism is interrelated to thermal, chemical and photophysical processes. There are three different models proposed to explain the ablation mechanisms in details:

- **Photochemical model**: The photonic energy is sufficient for electronic excitations which leads to direct bond breaking. The photochemical model has been reported in literature [40–44].

- **Photothermal model**: The electronic excitation is thermalized in picosecond time scales, which results in thermal bond breaking [14, 16, 45–47].

Table 2.6: Ablation regimes based on the energy transfer rate into material [41]

Energy transfer rate	Removal mechanisms	Main interaction
Slow	Thermal heating Photothermal effects Thermal stress	Evaporation Spallation
Medium	Photochemical Photophysical	Evaporation
Fast	Coloumb explosion Mechanical shock	Evaporation Mechanical Thermal Coloumb

- **Photophysical model**: In this case, both thermal and non-thermal processes contribute significantly to the ablation of material. Direct and thermal bond breaking are considered two independent channels to model [48, 49] or, different bond breaking energies for ground state and electronically excited states chromophores are applied [50, 51] in this model. This model is most adequate for short laser pulses in the picosecond and femtosecond range.

Considering the organic electronics, we are interested in the polymer structuring and patterning applications. In order to pattern a polymer without any debris on the surface, the photochemical ablation is recommended. In case of photochemical ablation the polymer can absorb the wavelength of radiation and eventually evaporates, which results in no thermal damage on surrounding material. The ablation regimes at different rates of energy transfer into the material are listed in Table 2.6.

2.6 Conclusions

In this chapter, a general theoretical background of the laser polymer ablation was provided. The basics of ablation principles, laser parameters and material parameters are explained. Although, not all the details have been covered fully but the curious reader can follow

the references for more in depth knowledge about those fundamentals from the cited articles/ books. Moreover, the ablation mechanisms are briefly discussed, and three basic mechanisms: photo-thermal, photo-chemical and photo-physical are mentioned. Furthermore, the basic laser polymer ablation models are shortly discussed, however the complete modeling can be followed with the given references.

References

[1] A. Einstein, "Strahlungs-Emission und Absorption nach der Quantentheorie", German, vol. 18, pp. 318–323, 1916. [Online].

[2] A. Einstein and P. Ehrenfest, "Zur Quantentheorie des Strahlungsgleichgewichts", German, *Zeitschrift fur Physik*, vol. 19, no. 1, pp. 301–306, 1923. [Online].

[3] W. M. Steen and J. Mazumder, "Background to Laser Design and General Applications", English, in *Laser Material Processing*, Springer London, 2010, pp. 11–78. [Online].

[4] M. Bertolotti, "Background to Laser Design and General Applications", English, in *Masers and lasers: An historical approach*, Bristol, Adam Hilger, Ltd., 1983, p. 278. [Online].

[5] W. E. Lamb and R. C. Retherford, "Fine Structure of the Hydrogen Atom. Part I", *Phys. Rev.*, vol. 79, pp. 549–572, 4 1950. [Online].

[6] J. P. Gordon, H. J. Zeiger, and C. H. Townes, "Molecular Microwave Oscillator and New Hyperfine Structure in the Microwave Spectrum of NH_3", *Phys. Rev.*, vol. 95, pp. 282–284, 1 1954. [Online].

[7] J. P. Gordon, C. H. Townes, and H. J. Zeiger, "The Maser - New Type of Microwave Amplifier, Frequency Standard, and Spectrometer", *Phys. Rev.*, vol. 99, pp. 1264–1274, 4 1955. [Online].

[8] A. L. Schawlow and C. H. Townes, "Infrared and Optical Masers", *Phys. Rev.*, vol. 112, pp. 1940–1949, 6 1958. [Online].

[9] T. H. Maiman, "Stimulated Optical Radiation in Ruby", *Nature*, vol. 187, pp. 493–494, 4 1960. [Online].

[10] R. Srinivasan and V. Mayne Banton, "Self developing photoetching of poly(ethylene terephthalate) films by far ultraviolet excimer laser radiation", *Applied Physics Letters*, vol. 41, no. 6, pp. 576–578, 1982. [Online].

[11] R. Srinivasan and W. Leigh, "Ablative photodecomposition: action of farultraviolet (193 nm) laser radiation on poly(ethylene terephthalate) films", *Journal American Chemical Society*, vol. 104, no. 24, pp. 6784–6785, 1982. [Online].

[12] Y. Kawamura, K. Toyoda, and S. Namba, "Effective deep ultraviolet photoetching of polymethyl methacrylate by an excimer laser", *Applied Physics Letters*, vol. 40, no. 5, pp. 374–375, 1982. [Online].

[13] T. Lippert, "UV Laser Ablation of Polymers: From Structuring to Thin Film Deposition", English, in *Laser-Surface Interactions for New Materials Production*, ser. Springer Series in Materials Science, A. Miotello and P. M. Ossi, Eds., vol. 130, Springer Berlin Heidelberg, 2010, pp. 141–175. [Online].

[14] S. Lazare and V. Granier, "Ultraviolet Laser Photoablation of Polymers: A Review and Recent Results", *Laser Chemistry*, vol. 10, no. 1, pp. 25–40, 1989. [Online].

[15] D. W. Bauerle, in *Laser Processing and Chemistry*, ser. Springer Advanced Texts in Physics, Springer, 2000. [Online].

[16] J. E. Andrew, P. E. Dyer, D. Forster, and P. H. Key, "Direct etching of polymeric materials using a XeCl laser", *Applied Physics Letters*, vol. 43, no. 8, pp. 717–719, 1983. [Online].

[17] R. Srinivasan and B. Braren, "Ablative photodecomposition of polymer films by pulsed far-ultraviolet (193 nm) laser radiation: Dependence of etch depth on experimental conditions", *Journal of Polymer Science: Polymer Chemistry Edition*, vol. 22, no. 10, pp. 2601–2609, 1984. [Online].

[18] J. M. Liu, "Simple technique for measurements of pulsed Gaussian beam spot sizes", *Optics Letters*, vol. 7, no. 5, pp. 196–198, 1982. [Online].

[19] J. Kruger and W. Kautek, "Ultrashort Pulse Laser Interaction with Dielectrics and Polymers", in *Polymers and Light*, ser. Advances in Polymer Science, T. K. Lippert, Ed., vol. 168, Springer Berlin Heidelberg, 2004, pp. 247–290. [Online].

[20] K. Naessens, H. Ottevaere, P. V. Daele, and R. Baets, "Flexible fabrication of microlenses in polymer layers with excimer laser ablation", *Applied Surface Science*, vol. 208, pp. 159–164, 2003, Physics and Chemistry of Advanced Laser Materials Processing. [Online].

[21] P. Dyer, R. Farley, R. Giedl, and D. Karnakis, "Excimer laser ablation of polymers and glasses for grating fabrication", *Applied Surface Science*, vol. 96, pp. 537–549, 1996, Proceedings of Symposium F: Third International Symposium on Laser Ablation of the 1995 E-MRS Spring Conference. [Online].

[22] W. Pfleging, M. Przybylski, and H. J. Bruckner, *Excimer laser material processing: state-of-the-art and new approaches in microsystem technology*, 2006. [Online].

[23] J. G. Lunney, R. R. O Neill, and K. Schulmeister, "Excimer laser etching of transparent conducting oxides", *Applied Physics Letters*, vol. 59, no. 6, pp. 647–649, 1991. [Online].

[24] T. Szorenyi, L. Laude, I. Bertoti, Z. Kantor, and Z. Geretovszky, "Excimer laser processing of indium tin oxide films: An optical investigation", *Journal of Applied Physics*, vol. 78, no. 10, pp. 6211–6219, 1995. [Online].

[25] G. Raciukaitis, M. Brikas, M. Gedvilas, and G. Darcianovas, *Patterning of ITO with picosecond lasers*, 2006. [Online].

[26] Tsai, Hong-Yin and Yang, Hsiharng and Pan, Chengtang and Chou, Min-Chieh, "Laser patterning indium tin oxide (ITO) coated on PET substrate", *Proc. SPIE*, vol. 4230, pp. 156–163, 2000. [Online].

[27] S. Xiao, S. A. Fernandes, and A. Ostendorf, "Selective Patterning of ITO on flexible PET Substrate by 1064 nm picosecond Laser", *Physics Procedia*, vol. 12, Part B, pp. 125–132, 2011, Lasers in Manufacturing 2011 - Proceedings of the Sixth International WLT Conference on Lasers in Manufacturing. [Online].

[28] M. Schaefer, J. Holtkamp, and A. Gillner, "Ablation of PEDOT/PSS with excimer lasers for micro structuring of organic electronic devices", *Synthetic Metals*, vol. 161, no. 11, pp. 1051–1057, 2011. [Online].

[29] N. Semaltianos, C. Koidis, C. Pitsalidis, P. Karagiannidis, S. Logothetidis, *et al.*, "Picosecond laser patterning of PEDOT:PSS thin films", *Synthetic Metals*, vol. 161, no. 5, pp. 431–439, 2011. [Online].

[30] S. Naithani, D. Schaubroeck, Y. Vercammen, R. Mandamparambil, I. Yakimets, *et al.*, "Excimer laser patterning of PEDOT:PSS thin-films on flexible barrier foils: A surface analysis study", *Applied Surface Science*, vol. 280, pp. 504–511, 2013. [Online].

[31] R. Mandamparambil, H. Fledderus, G. Van Steenberge, and A. Dietzel, "Patterning of Flexible Organic Light Emitting Diode (FOLED) stack using an ultrafast laser", *Optics Express*, vol. 18, no. 8, pp. 7575–7583, 2010. [Online].

[32] J. Meijer, K. Du, A. Gillner, D. Hoffmann, V. Kovalenko, *et al.*, "Laser Machining by short and ultrashort pulses, state of the art and new opportunities in the age of the photons", *CIRP Annals - Manufacturing Technology*, vol. 51, no. 2, pp. 531–550, 2002. [Online].

[33] R. Srinivasan and B. Braren, "Ultraviolet laser ablation of organic polymers", *Chemical Reviews*, vol. 89, no. 6, pp. 1303–1316, 1989. [Online].

[34] W. Koechner, English, in *Solid State Laser Engineering*, ser. Springer Series in Optical Science, Springer, 2006. [Online].

[35] A. Serafetinides, C. Skordoulis, M. Makropoulou, and A. Kar, "Picosecond and subpicosecond visible laser ablation of optically transparent polymers", *Applied Surface Science*, vol. 135, no. 1, pp. 276–284, 1998. [Online].

[36] D. Karnakis, A. Kearsley, and M. Knowles, "Ultrafast Laser Patterning of OLEDs on Flexible Substrate for Solid-state Lighting", *Journal of Laser Micro/Nanoengineering*, vol. 4, no. 3, pp. 218–223, 2009. [Online].

[37] X. Liu, D. Du, and G. Mourou, "Laser ablation and micromachining with ultrashort laser pulses", *IEEE Journal of Quantum Electronics*, vol. 33, no. 10, pp. 1706–1716, 1997. [Online].

[38] J. Reif, "Basic Physics of Femtosecond Laser Ablation", English, in *Laser-Surface Interactions for New Materials Production*, ser. Springer Series in Materials Science, A. Miotello and P. M. Ossi, Eds., vol. 130, Springer Berlin Heidelberg, 2010, pp. 19–41. [Online].

[39] D. W. Bauerle, English, in *Laser Processing and Chemistry*, ser. Springer Advanced Texts in Physics, Springer, 2011. [Online].

[40] S. R. Cain, "A photothermal model for polymer ablation: chemical modification", *The Journal of Physical Chemistry*, vol. 97, no. 29, pp. 7572–7577, 1993. [Online].

[41] S. R. Cain, F. C. Burns, and C. E. Otis, "On single photon ultraviolet ablation of polymeric materials", *Journal of Applied Physics*, vol. 71, no. 9, pp. 4107–4117, 1992. [Online].

[42] G. C. DCouto and S. V. Babu, "Heat transfer and material removal in pulsed excimer laser induced ablation: Pulsewidth dependence", *Journal of Applied Physics*, vol. 76, no. 5, pp. 3052–3058, 1994. [Online].

[43] N. Bityurin, N. Arnold, B. Luk'yanchuk, and D. Bauerle, "Bulk model of laser ablation of polymers", *Applied Surface Science*, vol. 127, pp. 164–170, 1998. [Online].

[44] N. Arnold, B. Luk'yanchuk, and N. Bityurin, "A fast quantitative modelling of ns laser ablation based on non-stationary averaging technique", *Applied Surface Science*, vol. 127, pp. 184–192, 1998. [Online].

[45] T. F. Deutsch and M. W. Geis, "Self developing UV photoresist using excimer laser exposure", *Journal of Applied Physics*, vol. 54, no. 12, pp. 7201–7204, 1983. [Online].

[46] E. Sutcliffe and R. Srinivasan, "Dynamics of UV laser ablation of organic polymer surfaces", *Journal of Applied Physics*, vol. 60, no. 9, pp. 3315–3322, 1986. [Online].

[47] G. D. Mahan, H. S. Cole, Y. S. Liu, and H. R. Philipp, "Theory of polymer ablation", *Applied Physics Letters*, vol. 53, no. 24, pp. 2377–2379, 1988. [Online].

[48] V. Srinivasan, M. A. Smrtic, and S. V. Babu, "Excimer laser etching of polymers", *Journal of Applied Physics*, vol. 59, no. 11, pp. 3861–3867, 1986. [Online].

[49] H. Schmidt, J. Ihlemann, B. Wolff-Rottke, K. Luther, and J. Troe, "Ultraviolet laser ablation of polymers: spot size, pulse duration, and plume attenuation effects explained", *Journal of Applied Physics*, vol. 83, no. 10, pp. 5458–5468, 1998. [Online].

[50] B. Luk'yanchuk, N. Bityurin, N. Arnold, and D. Bauerle, "The role of excited species in ultraviolet-laser materials ablation III. Non-stationary ablation of organic polymers", *Applied Physics A*, vol. 62, no. 5, pp. 397–401, 1996. [Online].

[51] B. Luk'yanchuk, N. Bityurin, S. Anisimov, and D. Bauerle, "The role of excited species in UV-laser materials ablation", *Applied Physics A*, vol. 57, no. 4, pp. 367–374, 1993. [Online].

3

Barrier Influence on Thin Film Patterning

In this chapter, we present the study of selective ablation of thin organic films (PEDOT:PSS - Poly 3, 4 ethylenedioxythiophene: polystyrene sulfonate and LEP-Light Emitting Polymer) using a 248 nm excimer laser on various kinds of multilayered barrier foils for the development of Organic Light Emitting Diodes (OLEDs). Different Silicon Nitride barrier foils with dedicated absorption spectra are taken into account for this purpose. An optimization of laser parameters like fluence and number of shots has been carried out for the various types of barrier foils. After complete investigations, one multilayer barrier foil with optimized ablation results has been selected for the fabrication of an OLED.

3.1 Introduction

Organic electronics devices such as OLEDs are well developed industrially, although the use of transparent conducting oxides (TCOs) or metal films for the electrodes still exists. Patterning of transparent conducting oxides is important because of their wide range of applications in liquid crystal displays, electroluminescent displays, solar cells and organic devices [1]. Among the transparent conducting ox-

ides the most industrially employed is Indium Tin Oxide (ITO). First (1047 nm), second (524 nm), third (349 nm) and fourth (262 nm) harmonics of the Nd:YLF (Neodymium-doped Yttrium Lithium Fluoride) laser were applied to study the effect of wavelengths on laser processing of ITO thin films deposited on glass substrates and good etching results were found using ultra-violet (UV) light [2]. ITO patterning on glass substrates with different Nd:YAG (Neodymium-doped Yttrium Aluminium Garnet) laser wavelengths (266 nm, 355 nm and 532 nm) has been studied and a clean removal of ITO was found for 266 nm wavelength [3], which lies in the UV region also. A comparison of ITO ablation characteristics using excimer laser (248 nm) and Nd:YAG laser (262 nm, 532 nm) has been carried out; and ITO is well patterned by the Excimer laser [4]. There has been some studies of ITO selective removal using ultrafast lasers on glass substrates. For instance, the ITO ablation on a glass substrate using ultrafast laser (Ti: Sapphire laser, 150 fs, 810 nm) for OLED application has been demonstrated by Park *et al.* [5], and the patterning results with different number of pulses are shown in the Figure 3.1. Some authors also demonstrated the enormous commercial potential of Laser Direct Write (LDW) versus wet-etch lithography to pattern ITO on glass, for the manufacturing of Plasma Display Panels (PDPs) [6]. In a nutshell, it has been observed from the literature that the patterning of ITO on glass substrates using UV laser pulses is very successful as compared to higher wavelengths.

During the 90s, glass was the main substrate for laser patterning of thin films. However, the processing of thin films on glass substrates is limited due to its brittleness, heavy-weight and difficulty in producing larger sizes. Later on the successful ablation of ITO on Poly Ethylene Terephthalate (PET) with an excimer laser was reported by Tsai, Hong-Yin and Yang, Hsiharng and Pan, Chengtang and Chou, Min-Chieh [7]. In case of roll-to-roll production of display devices like OLEDs or Flat Panel Displays (FPDs), the need for a flexible substrate is a primary requirement. Direct laser structuring of thin film conducting oxides (TCOs) on both rigid glass and flexible polymer (polyimide, PET) substrates has been demonstrated[8]. It has been found that the polymeric substrate patterning was very sensitive to processing parameters, including the positioning speed and wavelength. This investigation shows that the UV radiation was most appropriate for patterning TCOs on polymeric substrates in terms of quality.

Nowadays, the PEDOT:PSS has been a subject of great research

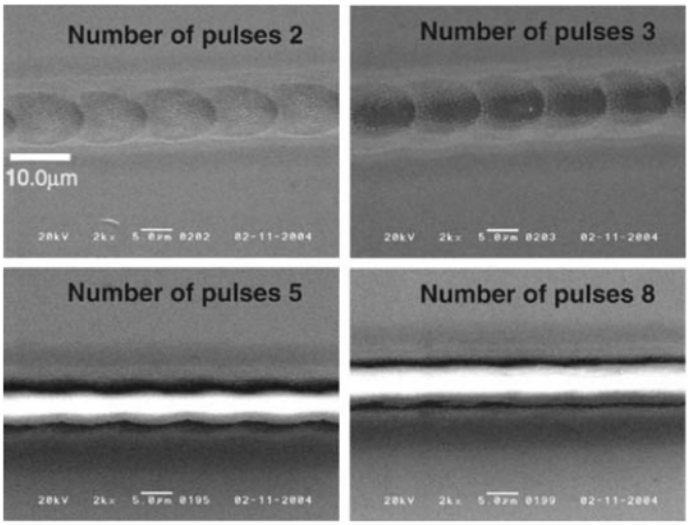

Figure 3.1: Ultrafast laser patterning of ITO thin film on a glass substrate for OLED application, picture adopted from Park et al. [5].

and discussion in the field of organic electronics; as it is a transparent, highly ductile and conductive polymer. If some specific organic compounds such as dimethyl sulfoxide or sorbitol are added to PEDOT:PSS, its conductivity can be increased manifolds [9, 10]. Due to these enhanced properties it can be used as a transparent electrode in the devices such as touchscreens, OLEDs and electronic paper (e-paper); making it a conductive polymer alternative to thin film transparent conductive oxide ITO. The laser patterning of PEDOT:PSS has been recently revealed by some research groups for organic device applications [11, 12], however the substrate used in these cases was a metallic layer. Moreover, the successful laser patterning of the PEDOT:PSS thin films on a glass substrate has been presented as well[13]. In addition, a comparison of ablation patterns of PEDOT:PSS by using different excimer lasers (193 nm, 248 nm) has been reported [14], where an inorganic colorless solid Calcium Fluoride (CaF_2) has been used as a substrate. The laser patterning of an OLED stack consisting of LEP and PEDOT:PSS on a fully flexible substrate PET or Polyethylene naphthalate (PEN) has been successfully demonstrated by Mandamparambil *et al.* [15], even in this case the use of ITO for anode has its crucial role. On the other

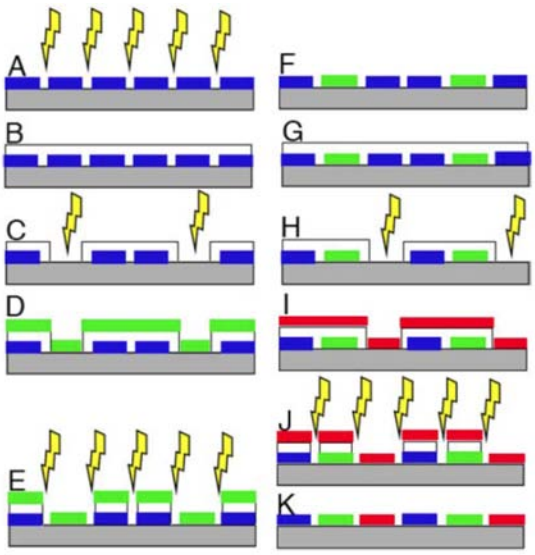

Figure 3.2: Laser assisted patterning process for organic electronics, the thickness of thin polymer films is 100 nm, picture adopted from [16].

hand, the laser patterning of light emitting polymer (LEP) in combination with water soluble sacrificial resists has been reported by Lidzey *et al.* [16], in this procedure of patterning the various steps are illustrated in Figure3.2.

In the laser ablation mechanism, the role of the substrate has a major effect on the patterned region and grooves. The most of the literature we have discussed here, was based on rigid glass or solid substrates, and only few studies based on flexible polymer substrates. In OLED applications, the patterning of LEP and PEDOT:PSS on a barrier is of crucial importance as it is highly responsible to protect the device against any water or oxygen permeation into the stack. Moreover, the structuring and pattering of thin films is significantly dependent on the substrate, the effect of substrate absorption on laser patterning of ITO on rigid glass has been published [17]. Still, there is a need to further investigate and understand the effect of the substrate on thin film pattering especially when the substrate is not rigid glass but a flexible barrier foil.

In this chapter, the concept of varying optical absorption properties of the barrier (substrate), for the selective ablation of LEP or PEDOT:PSS on different barriers and a flexible PEN substrate, will

be discussed[18]. An excimer laser (248 nm) is used for pattering thin organic films like PEDOT:PSS and LEP, because the absorption of UV light for such aromatic functionalized organic materials is strong. The selective removal of any polymer on a barrier needs maximum absorption of the laser wavelength by the top organic films while minimum absorption by the barrier (substrate). Five different types of Silicon Nitrides barrier foils are evaluated to understand the influence of the variation of the absorption properties of the barrier layer on the patterning of thin organic films. Each barrier layer consists of different organic and inorganic layers, so termed as multilayer barrier. After all the experimental investigations and evaluations, an optimized multilayered barrier foil has been eventually selected for the fabrication of an OLED device.

3.2 Ablation Set-up

An industrial short pulse excimer laser ATLEX-200/300i (supplied by ATL Lasertechnik GmbH) was used to carry out these experiments. It is an extremely compact, air-cooled UV-laser with integrated power supply and microprocessor controller unit. This laser set-up has the capabilities of producing nanosecond pulses of 1 mJ to 20 mJ energies, pulse repetition rate can be chosen 100 Hz; 200 Hz or 300 Hz depending on application and the pulse length varies in between 3 nm and 7 nm (Full Width Half Maximum). In this investigation, ablation experiments were performed with a pulsed, nanosecond KrF excimer laser at 248 nm wavelength and pulse repetition rate of 100 Hz.

The schematic diagram of the ablation set-up is shown in the Figure 3.3. The laser beam emitted from the excimer source is deflected by two mirrors and then passes through a variable attenuator, which controls the power. Afterwards, the beam passes across a variable mask wheel, where an appropriate mask, depending on the task to be carried out, is selected. In this study, a square mask of 2000 µm × 2000 µm is chosen. In these experiments, a focusing lens which is also adjustable in the vertical direction for accurate focusing, with a demagnification of 10 was used. This combination of mask and demagnification results in a spot size of 200 µm × 200 µm on the sample. The fluence is controlled with an attenuator plate and the pulse energy at each fluence is measured with a pyro-electric energy meter (Coherent J25LP-MUV, in combination with FieldmaxII TOP) placed at the end of the beam axis. The samples were mounted on a motorized automated translation stage, perpendicular to the beam

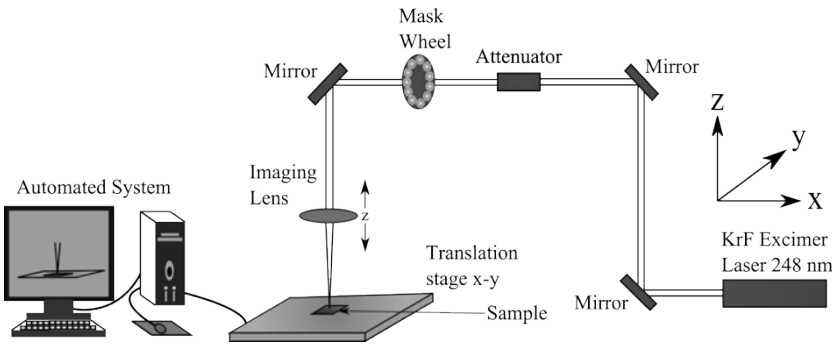

Figure 3.3: Nanosecond ablation set-up.

with the thin film facing the incident laser beam. The laser ablation of the hole transport layer (PEDOT:PSS) and active layer (LEP) is carried out under atmospheric conditions. The ablation set-up is equipped with a suction head, which removes the generated ablation byproducts from the process site leading to a controlled process.

3.3 Why a Multilayer Barrier?

In any OLED design, one of the biggest challenges is to have higher life time. The life time of an OLED mainly depends on the barrier and encapsulation layers. In case of a flexible OLED design the stack must be protected from both sides, anode side (bottom electrode) as well as cathode side (top electrode). The barrier layer is used at the bottom side below the anode, while the encapsulation layer covers the complete OLED stack from the top cathode side. These barrier and encapsulation layers are designed to protect the fabricated OLED stack from moisture (or water) and oxygen penetration. The permeation of moisture or oxygen into the stack starts the oxidation of the cathode which is responsible for the electron injection into the organic emissive polymer. Due to such oxidation, it is not possible to inject the electron at that specific area, which results in a black spot on the display during the device operation. The cathode in the OLED design usually consists of a thin layer of a Barium (Ba) covered with a relatively thick layer of Aluminium (Al). Barium is preferred for this purpose as it has a low work function which is suitable for the injection of the electrons. To protect the Barium from moisture or oxygen a layer of Aluminium is used on top of it. Even though, there are some small pinholes through which permeation of water or

oxygen into the device stack is possible, and it starts the degradation mechanism at the cathode layer. This degradation rate depends on the diffusion rate of the water or oxygen into the stack through pinholes. Water Vapor Transmission Rate (WVTR) and Oxygen Transmission Rate (OTR) are the two well defined parameters to address this degradation mechanism. At the moment, it is important to think about the design of such a barrier or encapsulation layer which can slow down this diffusion rate. Indeed, single layer Silicon Nitride thin film can be used for barrier purpose, nevertheless there is a high need of improvement in terms of its properties to slow down permeation of moisture or oxygen.

In cooperation with Holst Center, we propose a multilayer barrier design consisting of inorganic-organic-inorganic thin films. In this design, five different kinds of Silicon Nitride thin films have been utilized for the inorganic layer. A thin organic film is used for the planarization purpose in between inorganic layers, to reduce the diffusion rate. A detailed schematic of the multilayered barrier consisting of organic and inorganic layers is illustrated in Figure 3.4(a).

3.4 Thin Film Patterning

Knowing that a multilayer barrier is a better option for the protection of an OLED stack, the samples of thin organic films were prepared on the multilayered barrier and a flexible substrate. Thin organic films of PEDOT:PSS and LEP were investigated on different kinds of multilayered barrier foils with an excimer laser. Three different types of thin film stacks were prepared as shown in Figure 3.4(b), 3.4(c) and 3.4(d). The thin film stack 3.4(b) consists of 125 µm PEN as a flexible substrate on top of which a multilayered barrier consisting of 150 nm inorganic Silicon Nitride, was deposited by Plasma Enhanced Chemical Vapor Deposition (PECVD). Subsequently, a thin PEDOT:PSS layer (100 nm) was spin coated on the barrier stack. Next, Figure 3.4(c) shows the same layered configuration of a PEN substrate and barrier foil except the top layer is an active conjugated light emitting polymer (LEP), with a thickness of about 80 nm. These two stacks were prepared to investigate the ablation behavior of the PEDOT:PSS and LEP thin organic films on different barriers separately. The third thin film stack as shown in Figure 3.4(d), was prepared to be identical to the layered structure of a flexible OLED stack. In this case, a LEP layer (80 nm) was spin coated on top of PEDOT:PSS (100 nm), while keeping the barrier and flexible substrate PEN iden-

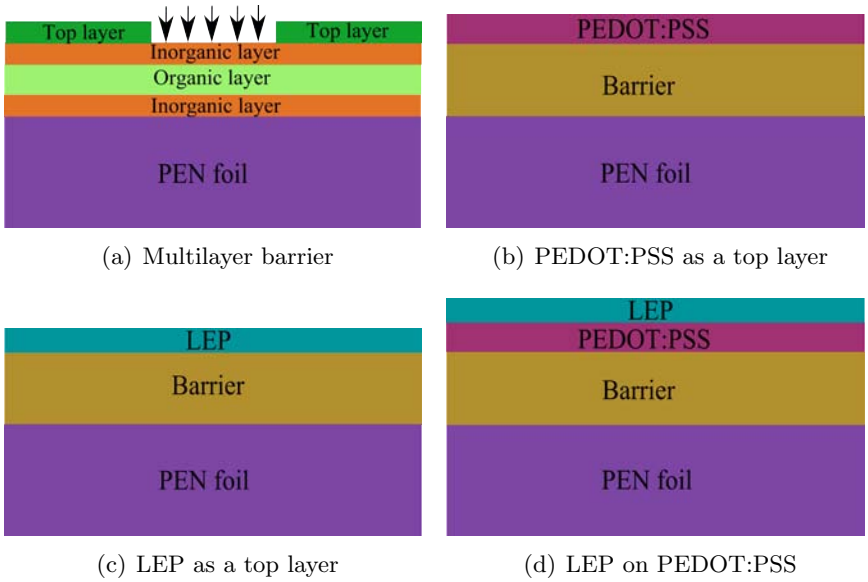

(a) Multilayer barrier

(b) PEDOT:PSS as a top layer

(c) LEP as a top layer

(d) LEP on PEDOT:PSS

Figure 3.4: Samples prepared with thin organic films on a multilayered barrier and flexible PEN substrate: (a) illustrates the general concept and (b) to (d) describe specific sample structure.

tical to the previous two cases.

3.4.1 Thin films absorption spectra

The absorption spectra of PEDOT:PSS and LEP were characterized before ablation experiments. These optical absorption spectra were measured by depositing thin polymer layers, with the same thicknesses as required in the stack (80 nm LEP and 100 nm PEDOT:PSS), on a quartz substrate of 2 inch × 2 inch. A UV-Vis spectrometer (JASCO), which is able to measure below 300 nm was utilized to measure these thin films absorption spectra. Consequently, the measured optical absorption spectra of the thin organic films PEDOT:PSS and LEP are shown in Figure 3.5. From the spectral information, it is observed that LEP absorbs quite heavily from 200 nm to 450 nm. However, PEDOT:PSS is almost transparent for the wavelengths higher than 300 nm. This means that the selection of a laser source for the ablation of these thin films in the nanosecond pulse regime should be in this absorption band. The natural choice would be UV lasers, either 193 nm or 248 nm excimer, because thin polymer films have

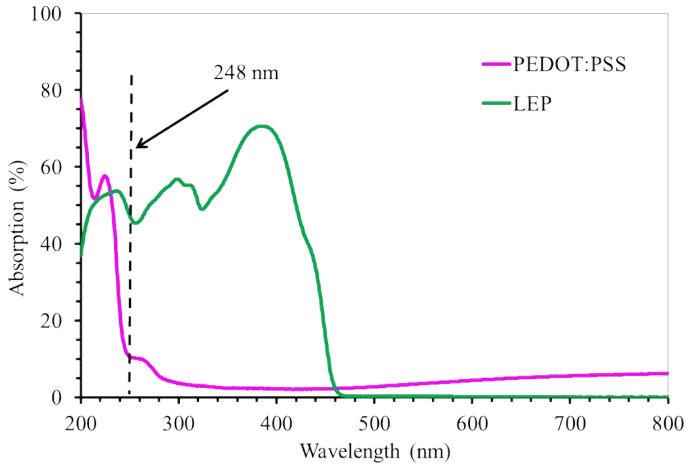

Figure 3.5: The UV absorption spectra of PEDOT:PSS and LEP thin organic films.

comparatively higher absorption at these wavelengths. Since, the 248 nm excimer laser is well industrialized and is also available at our laboratory, this laser has been chosen to carry out these experiments.

3.4.2 Barriers absorption spectra

In order to investigate the influence of barrier absorption on the selective ablation process, five different types of Silicon Nitride inorganic barriers were evaluated. The absorption spectra of these inorganic barrier foils were characterized with a UV-Vis spectrometer, and are illustrated in Figure 3.6. The different Silicon Nitrides were prepared by varying the ratio of Silane and Ammonia in the Plasma Enhanced Chemical Vapor Deposition (PECVD) method. For the convenience, these barrier foils are referred to as SiN(1), SiN(2), SiN(3), SiN(4) and SiN(5). Looking at the Figure 3.6, it is observed that at the wavelength of ablation (248 nm), the optical absorption of these barrier foils differs. The SiN(1) has the least absorption and SiN(4) indicates the highest absorption at 248 nm wavelength. It would be very much of interest to know how this variation in absorption effects the ablation process. The critical issue in the selective patterning is the removal of top layer without damaging the underneath layer.

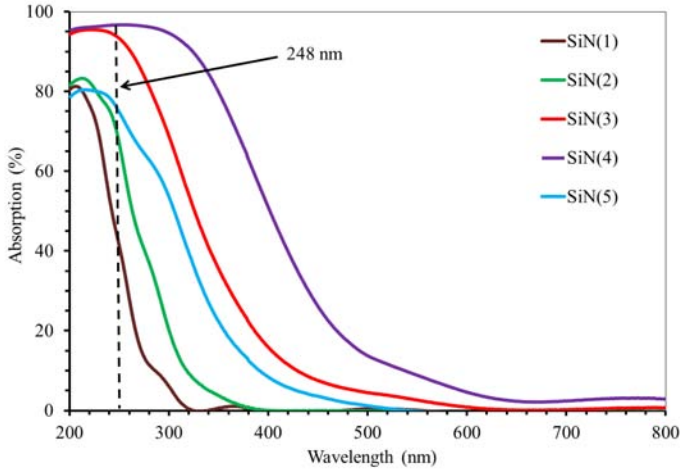

Figure 3.6: The absorption spectra of different kinds of Silicon Nitrides used in multilayered barrier foils.

3.4.3 Thin films selective ablation

A series of experiments were conducted to understand the ablation mechanisms, and to determine the ablation thresholds of the thin films on different kinds of barrier foils. In the first stage of this research, experiments were carried out on samples covered with the 100 nm thin film of PEDOT:PSS as shown in Figure 3.4(b). The laser fluences ranging from 75 mJ/cm^2 to 250 mJ/cm^2 with 1 pulse, 2 pulses and 5 pulses per location were applied. The experiments were performed separately for SiN(1), SiN(2), SiN(3), SiN(4) and SiN(5) barrier foils. After the experiments, ablated crater depths were measured using a mechanical profiler (Tencor Alphastep 200). The plots of fluence against ablation depth were generated for 1 pulse, 2 pulses and 5 pulses per location. In order to compare ablation depths on different kinds of Silicon Nitrides, the SiN(1) and SiN(4) were taken into consideration as they have the least optical absorption (SiN(1)) and the most optical absorption (SiN(4)) at 248 nm wavelength, among all barrier types. The ablation results of PEDOT:PSS on SiN(1) and SiN(4) barrier foils are plotted as shown in Figure 3.7(a) and Figure 3.7(b), respectively.

As shown in Figure 3.7(a), for the least absorbing SiN(1) barrier foil there is a very little increase in the depth from fluence of 75 mJ/cm^2 with 1 pulse to 150 mJ/cm^2 with 5 pulses. The depth

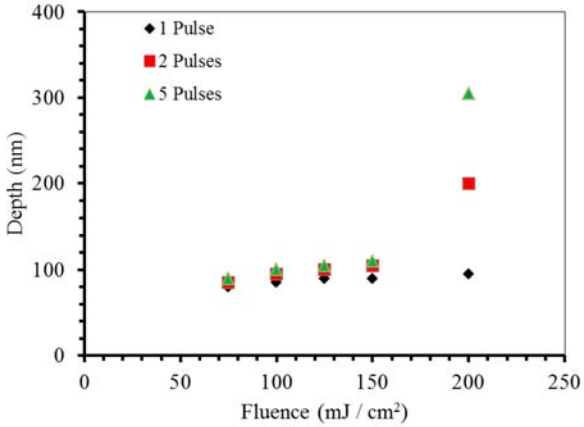

(a) PEDOT:PSS on SiN(1)

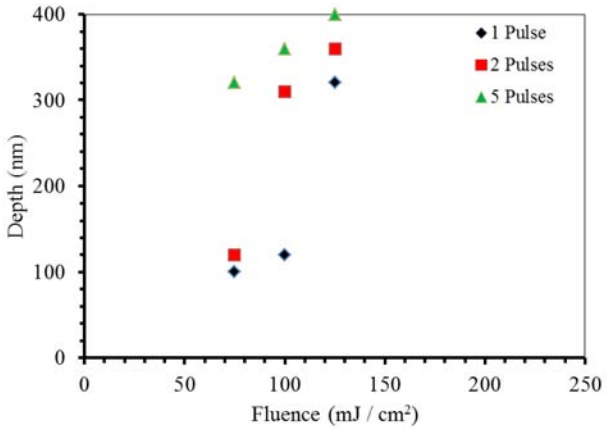

(b) PEDOT:PSS on SiN(4)

Figure 3.7: Ablation plots for least absorbing (a) and most absorbing (b), Silicon Nitrides barrier foils.

at 125 mJ/cm^2 with 2 pulses is about 100 nm, which is identical to the thickness of the PEDOT:PSS thin film. It indicates that a single layer of PEDOT:PSS of 100 nm has been selectively removed from the SiN(1) barrier. If we increase the fluence further to 200 mJ/cm^2 and with 1 pulse, the same thickness of 100 nm removal indicates the PEDOT:PSS layer selective ablation. However, with 2 shots at this fluence (200 mJ/cm^2) the depth of crater is about 200 nm, which is higher than the PEDOT:PSS thickness, clearly implicates a damage on SiN(1) barrier foil. The ablation plot shows that at a fluence of 250 mJ/cm^2 even with 1 pulse the ablation depth is about 200 nm, leading to a damage on the underneath barrier layer. Therefore, the operation between 75 mJ/cm^2 to 200 mJ/cm^2 with 1 pulse is a processing range (working window) for the selective removal of PEDOT:PSS on SiN (1) barrier foil.

On the other hand, in case of most absorbing SiN(4) barrier foil as shown in Figure 3.7(b), the depth of 100 nm indicates the removal of PEDOT:PSS thin film at 75 mJ/cm^2 with 1 pulse. At a fluence of 100 mJ/cm^2 even with 1 pulse the ablation depth obtained is more than 100 nm, which is an indication of damage on the SiN(4) barrier. The depth at a fluence of 75 mJ/cm^2 with 2 pulses is also more than 100 nm (PEDOT:PSS thickness) and at 100 mJ/cm^2 with 2 pulses is about 300 nm; both settings indicate the damage on SiN (4) barrier layer. Hence, there is hardly any processing range for the laser patterning of PEDOT:PSS on a SiN (4) barrier.

The optical microscopic images of PEDOT:PSS selective ablation on SiN(1) and SiN(4) barrier foils for identical laser parameters (125 mJ/cm^2, 1 pulse) are shown in Figure 3.8. Those microscopic images indicate the removal of material, and the layer removal is clean. However, the exact thickness of the removed layer is not clear without the analysis of depth measurements. The depth measurement plots as shown in Figure 3.7(a) and Figure 3.7(b), indicate that at a fluence of 125 mJ/cm^2 with 1 pulse per location the thickness of the removed layer in case of SiN(1) is 100 nm, which is exactly the same as of the PEDOT:PSS thin film; whereas for SiN(4) it is about 300 nm. The optical images also show that the thin film layer removal is complete and clean from the barrier SiN(1). In contrast, for the identical parameters, there is an abrupt breaking and removal of SiN(4) resulting in higher depth. As the thickness of the inorganic Silicon Nitride is about 150 nm and the thickness of PEDOT:PSS thin film is about 100 nm, removal of both layers consequently gives a thickness higher than 250 nm.

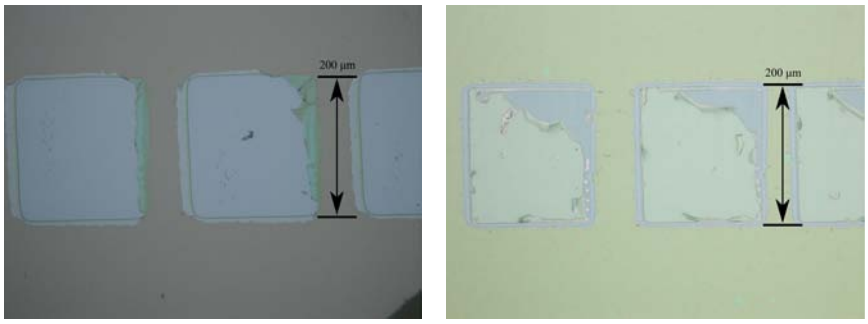

(a) PEDOT:PSS on SiN(1) at 125 mJ/cm^2 and 1 pulse

(b) PEDOT:PSS on SiN(4) at 125 mJ/cm^2 and 1 pulse

Figure 3.8: A comparison of PEDOT:PSS ablation on SiN(1) and SiN(4) barrier foils for identical ablation parameters.

Apart from the static pulse ablation, for structuring and patterning applications dynamic laser processing is necessary. In this case, line patterning of PEDOT:PSS on SiN(1) and SiN(4) barriers is compared for identical processing parameters as illustrated in Figure 3.9. At a fluence of 125 mJ/cm^2 with 2 pulses per location the PEDOT:PSS ablation on SiN(1) is clean and there is no visible damage on the line track. On the other hand, for SiN(4) barrier foil there is a damage visible on barrier and some vertical lines at regular intervals are seen. The depth for SiN(1) at 125 mJ/cm^2 with 2 pulses is about 100 nm whereas for SiN(4) the depth is about 350 nm. In a nutshell, it is clear that PEDOT:PSS line patterning is very successful on SiN(1) barrier foil, but with identical laser processing parameters there is a complete removal of SiN(4) barrier, which is not a desired virtue.

In a similar fashion, selective ablation results of the Light Emitting Polymer (LEP) on SiN(1) and SiN(4) barrier foils are illustrated in Figure 3.10. The ablation plot for LEP on SiN(1) barrier indicates the selective removal of LEP (thickness 80 nm) is possible until the fluence of 150 mJ/cm^2. When the fluence increases further, the removed layer thickness is higher than the LEP thickness. For instance, at a fluence of 200 mJ/cm^2 with 5 pulses per location the ablation depth is about 200 nm, this implicates a damage on the barrier foil. Nevertheless, selective ablation of LEP is possible from 75 mJ/cm^2 to 200 mJ/cm^2 with 2 pulses. Consequently, this fluence range is the process window for selective ablation of LEP on SiN(1) barrier foil. Next, from the ablation plot of LEP on SiN(4) barrier the depth of

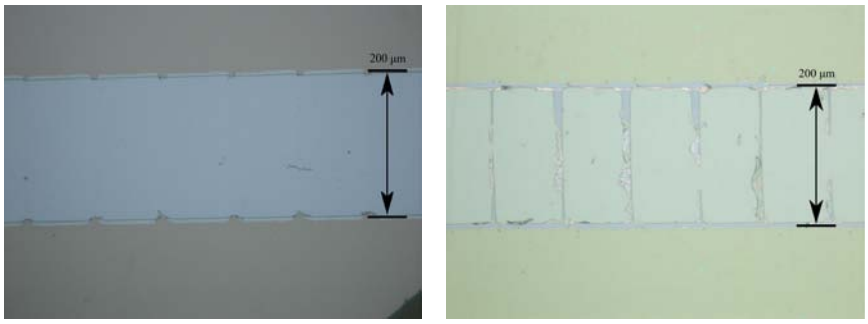

(a) PEDOT:PSS on SiN(1) (b) PEDOT:PSS on SiN(4)

Figure 3.9: A comparison of PEDOT:PSS ablation on SiN(1) and SiN(4) barriers, (a) Clean removal on SiN (1) (b) Damage on barrier SiN(4); for identical ablation parameters: Fluence 125 mJ/cm^2, 2 Pulses.

ablation at 100 mJ/cm^2 with 2 pulses is about 80 nm. If we increase the number of pulses from 2 to 5 at this fluence, the depth of ablation increases very rapidly to about 360 nm, which is in turn much higher than the targeted thickness (80 nm). Moreover, if we observe the ablation depth at a fluence of 125 mJ/cm^2 with 2 pulses, it is slightly higher than 80 nm an implication of the damage on the SiN(4) barrier. Therefore, the selective removal of LEP on SiN(4) barrier is possible but there is not sufficient processing range for ablation.

Furthermore, the optical microscopic images illustrated in Figure 3.11 show the LEP ablation on SiN(1) and SiN(4) barriers at a fluence of 125 mJ/cm^2 with 1 pulse per location. The ablation depth for this particular setting is about 80 nm, which is the thickness of LEP. From the pictures, the ablation seems to be clean and without any detectable damage on the barrier foils. In fact, there is no significant difference in the behavior of two barriers at 125 mJ/cm^2 with 1 pulse, as can be easily inferred from the ablation plots as well.

Looking at the patterning results, a clear illustration of the line patterning is depicted in Figure 3.12 for LEP selective ablation at 75 mJ/cm^2 with 5 pulses. The SiN(1) barrier has a debris free ablation track, whereas there is noticeable damage on the SiN(4) barrier. The ablation plots (Figure 3.10) show the depth at 75 mJ/cm^2 with 5 pulses is about 80 nm for SiN(1) and 350 nm for SiN(4). This indicates that SiN(1) barrier is suitable for LEP patterning and it has a wider working process window.

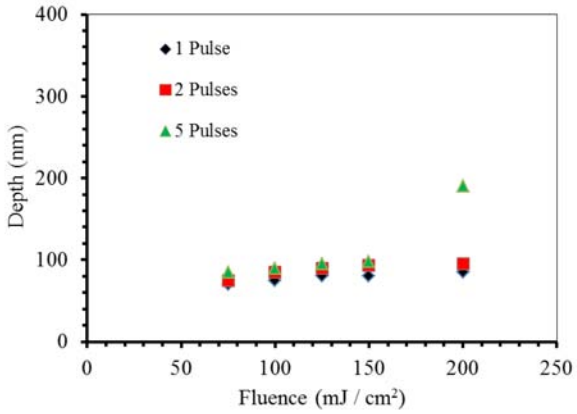

(a) LEP on SiN(1)

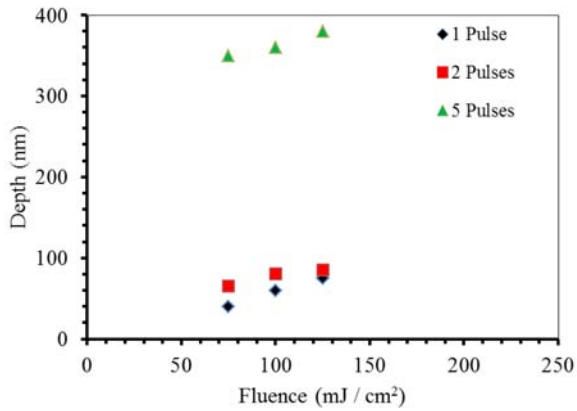

(b) LEP on SiN(4)

Figure 3.10: Ablation plots for LEP on least absorbing and most absorbing Silicon Nitrides barrier foils.

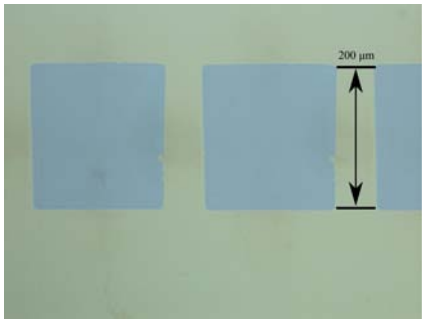

(a) LEP on SiN(1) at 125 mJ/cm^2 and 1 pulse

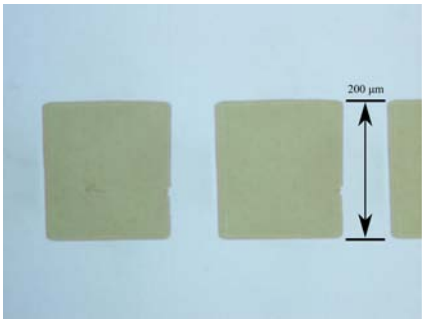

(b) LEP on SiN(4) at 125 mJ/cm^2 and 1 pulse

Figure 3.11: A comparison of LEP ablation on SiN(1) and SiN(4) barrier foils for identical ablation parameters.

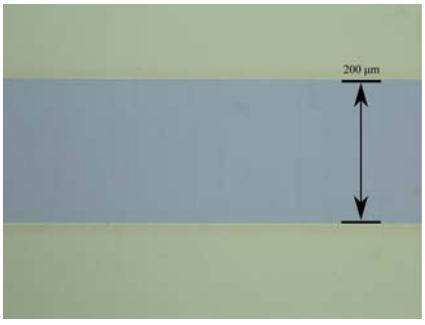

(a) LEP on SiN(1)

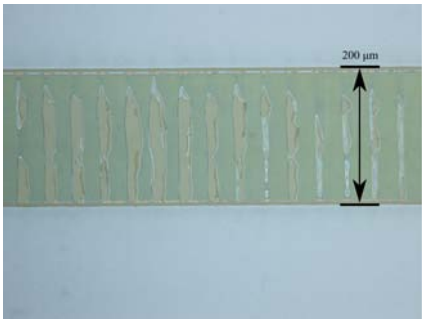

(b) LEP on SiN(4)

Figure 3.12: A line patterning comparison of LEP ablation on SiN(1) and SiN(4) barrier foils for at 75 mJ/cm^2 and 5 pulses.

Finally, the ablation results of LEP and PEDOT:PSS together (LEP - PEDOT:PSS) on the different Silicon Nitrides are analyzed. The ablation plots for SiN(1) and SiN(4) barrier are shown in Figure 3.13. From the plot of SiN(1) it is inferred that at a fluence of 75 mJ/cm^2 with 2 pulses, the ablation depth is about 80 nm. It indicates the removal of LEP on PEDOT:PSS, as the thickness of LEP is 80 nm. Furthermore, at a fluence of 100 mJ/cm^2 with 5 pulses, the ablation depth is about 180 nm, which is indeed the total thickness of LEP and PEDOT:PSS. This implies that at this particular setting (fluence and number of pulses), the LEP and PEDOT:PSS can be selectively removed from the SiN(1) barrier. Now, referring to the ablation plot for SiN(4), it shows a depth of about 180 nm at the fluence of 75 mJ/cm^2 with 2 pulses. This is an indication of the selective removal of both LEP and PEDOT:PSS together, from the SiN(4) barrier. However, at the fluence of 100 mJ/cm^2 with 5 pulses the ablation depth is about 360 nm, which is higher than the thickness of thin films and barrier. Hence, in this case the barrier (thickness 150 nm) and both thin films (180 nm) have been removed, which is not desired. Therefore, these plots indicate that SiN(1) barrier foil is suitable as compared to SiN(4) for patterning and structuring of LEP and PEDOT:PSS thin organic films.

3.5 Barrier Influence on Patterning

It has been clearly noticed that the substrate plays a crucial role in laser patterning of thin organic films. Different kinds of barriers foils (SiN(1), SiN(2), SiN(3), SiN(4) and SiN(5)) were tested and investigated. PEDOT:PSS, LEP and LEP on PEDOT:PSS have shown their different ablation characteristics on different barrier foils. The SiN(1) barrier foil has the widest working process window and excellent ablation results as compared to other barrier foils. Due to a very narrow processing range, SiN(4) barrier is not suitable for patterning applications. All the results have been compiled for the determination of the damage thresholds of these barrier foils. Assuming three different top layers on the barriers, the damage thresholds of the barriers are tabulated in the Table 3.1.

From this table, it is deduced that the damage thresholds for SiN(1) barrier with PEDOT:PSS thin film as top layer is 200 mJ/cm^2, whereas this value is only 75 mJ/cm^2 for SiN(4) barrier. When LEP acts as a top layer, the value of damage threshold is 200 mJ/cm^2 for SiN(1) and is reduced to 100 mJ/cm^2 for SiN(4) barrier foil. These

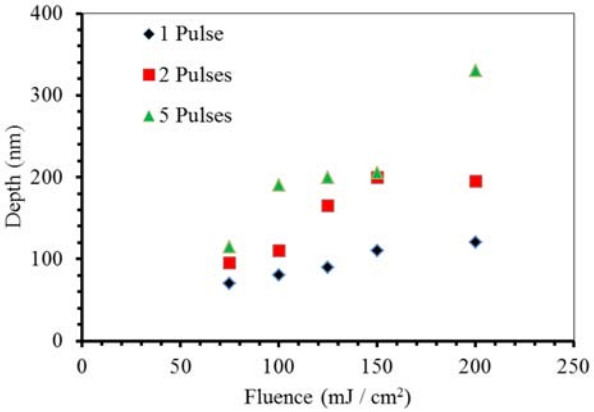

(a) LEP on PEDOT:PSS, on SiN(1)

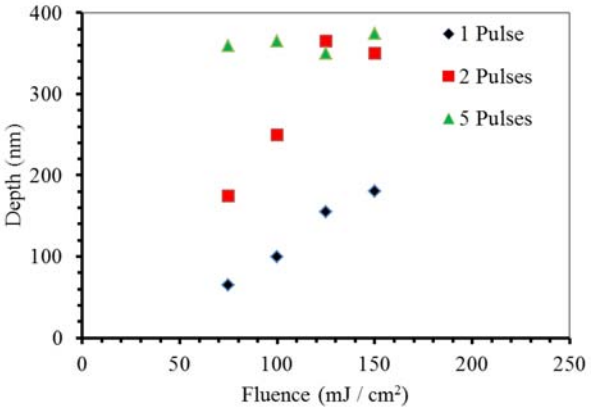

(b) LEP on PEDOT:PSS, on SiN(4)

Figure 3.13: Ablation plots for LEP and PEDOT:PSS on (a) SiN(1) barrier (b) SiN(4) barrier.

Table 3.1: Damage thresholds (values in mJ/cm^2) with 2 pulses.

Top Layer	SiN (1)	SiN (2)	SiN (3)	SiN (4)	SiN (5)
PEDOT:PSS	200	125	100	75	100
LEP	200	150	100	100	100
LEP-PEDOT:PSS	250	125	125	100	125

results are in agreement with the barriers absorption spectra shown in Figure 3.6, where at the wavelength of operation (248 nm) the SiN(1) barrier has minimum absorption and SiN(4) has the maximum optical absorption.

3.6 Conclusions

We have studied the influence of barrier absorption on laser patterning of thin organic films. The organic thin films were successfully patterned using nanosecond UV excimer laser on multilayered barrier foils. The concept of using different types of Silicon Nitride barrier foils with dedicated absorption properties is applied and implemented. It has been found that the barrier foil having minimum absorption at the wavelength of operation (248 nm) has the largest working process window for selective ablation of PEDOT:PSS and LEP thin films, without any observable damage on the stopping layer. In contrast, the barrier foil having the maximum absorption at the same wavelength of operation has the narrowest process window for selective ablation. These results are in agreement with the absorption spectra of the barrier foils. It is concluded that the optical absorption of the barrier plays a significant role in the selective ablation mechanism of thin organic films. However, it is known that the thermoelastic behavior and adhesion between layers are also important in such ablation processes.

References

[1] J. G. Lunney, R. R. O Neill, and K. Schulmeister, "Excimer laser etching of transparent conducting oxides", *Applied Physics Letters*, vol. 59, no. 6, pp. 647–649, 1991. [Online].

[2] R. Tanaka, T. Takaoka, H. Mizukami, T. Arai, and Y. Iwai, "Laser etching of indium tin oxide thin films by ultra-short pulsed laser", *Proc. SPIE*, vol. 5063, pp. 370–373, 2003. [Online].

[3] G. Raciukaitis, M. Brikas, M. Gedvilas, and T. Rakickas, "Patterning of indium tin oxide on glass with picosecond lasers", *Applied Surface Science*, vol. 253, no. 15, pp. 6570–6574, 2007. [Online].

[4] K. Lee and C. Lee, "The comparison of ITO ablation characteristics using KrF excimer and Nd: YAG laser", in *2nd International Symposium on Laser Precision Microfabrication, Singapore, May 16-18, 2001*, ser. Proceedings of SPIE, vol. 4426, 2002, 260–263. [Online].

[5] M. Park, B. H. Chon, H. S. Kim, S. C. Jeoung, D. Kim, *et al.*, "Ultrafast laser ablation of indium tin oxide thin films for organic light-emitting diode application", *Optics and Lasers in Engineering*, vol. 44, no. 2, pp. 138–146, 2006. [Online].

[6] M. Henry, P. M. Harrison, and J. Wendland, "Laser Direct Write of Active Thin-Films on Glass for Industrial Flat Panel Display Manufacture", *Journal of Laser Micro Nanoengineering*, vol. 2, no. 1, 49–56, 2007. [Online].

[7] Tsai, Hong-Yin and Yang, Hsiharng and Pan, Chengtang and Chou, Min-Chieh, "Laser patterning indium tin oxide (ITO) coated on PET substrate", *Proc. SPIE*, vol. 4230, pp. 156–163, 2000. [Online].

[8] G. Raciukaitis, M. Brikas, G. Darcianovas, D. Ruthe, and K. Zimmer, "Laser structuring of conducting films on transparent substrates - art. no. 67320C", in *International Conference on Lasers, Applications, and Technologies 2007: Laser-assisted Micro and Nanotechnolgies*, Panchenko, V and Louchev, O and Malyshev, S, Ed., ser. Proc. of SPIE, vol. 6732, 2007, p. C7320. [Online].

[9] J. Kim, J. Jung, D. Lee, and J. Joo, "Enhancement of electrical conductivity of poly(3,4-ethylenedioxythiophene)/poly(4-styrenesulfonate) by a change of solvents", *Synthetic Metals*, vol. 126, no. 2, pp. 311–316, 2002. [Online].

[10] Y. Chen, K. Kang, K. Han, K. Yoo, and J. Kim, "Enhanced optical and electrical properties of PEDOT:PSS films by the addition of MWCNT-sorbitol", *Synthetic Metals*, vol. 159, no. 17, pp. 1701–1704, 2009. [Online].

[11] A. F. Lasagni, P. Shao, J. L. Hendricks, C. M. Shaw, D. C. Martin, *et al.*, "Direct fabrication of periodic patterns with hierarchical sub-wavelength structures on poly(3,4-ethylene dioxythiophene)-poly(styrene sulfonate) thin films using femtosecond laser interference patterning", *Applied Surface Science*, vol. 256, no. 6, 1708–1713, 2010. [Online].

[12] A. F. Lasagni, J. L. Hendricks, C. M. Shaw, D. Yuan, D. C. Martin, *et al.*, "Direct laser interference patterning of poly(3,4-ethylene dioxythiophene)-poly(styrene sulfonate) (PEDOT-PSS) thin films", *Applied Surface Science*, vol. 255, no. 22, pp. 9186–9192, 2009. [Online].

[13] N. Semaltianos, C. Koidis, C. Pitsalidis, P. Karagiannidis, S. Logothetidis, *et al.*, "Picosecond laser patterning of PEDOT:PSS thin films", *Synthetic Metals*, vol. 161, no. 5, pp. 431–439, 2011. [Online].

[14] M. Schaefer, J. Holtkamp, and A. Gillner, "Ablation of PEDOT/PSS with excimer lasers for micro structuring of organic electronic devices", *Synthetic Metals*, vol. 161, no. 11, pp. 1051–1057, 2011. [Online].

[15] R. Mandamparambil, H. Fledderus, G. Van Steenberge, and A. Dietzel, "Patterning of Flexible Organic Light Emitting Diode (FOLED) stack using an ultrafast laser", *Optics Express*, vol. 18, no. 8, pp. 7575–7583, 2010. [Online].

[16] D. G. Lidzey, M. Voigt, C. Giebeler, A. Buckley, J. Wright, *et al.*, "Laser-assisted patterning of conjugated polymer light emitting diodes", *Organic Electronics*, vol. 6, no. 5, pp. 221–228, 2005. [Online].

[17] O. Yavas, C. Ochiai, and M. Takai, "Substrate-assisted laser patterning of indium tin oxide thin films", English, *Applied Physics A*, vol. 69, no. 1, S875–S878, 1999. [Online].

[18] S. Naithani, R. Mandamparambil, F. van Assche, D. Schaubroeck, H. Fledderus, *et al.*, "Influence of barrier absorption properties on laser patterning thin organic films", in *Photonics Europe*, Brussels, Belgium: SPIE, 2012, pp. 843 505–843 509. [Online].

4

Flexible OLED Fabrication

In this chapter, the fabrication of a flexible organic LED (OLED) using laser patterning and structuring has been discussed. The OLED stack consists of a polyethylene naphthalate (PEN) flexible substrate, a multilayered Silicon Nitride foil as barrier, poly(3,4-ethylene dioxythiophene):poly(styrene sulfonate) (PEDOT:PSS) thin organic film acts both for hole injection and anode electrode, Chromium-Aluminum-Chromium (Cr-Al-Cr) bus bar, light emitting polymer (LEP) and at the top a cathode of Barium capped with Aluminum (Ba-Al). Following the process optimization, a laser processed flexible OLED has been fabricated, thin film encapsulated and its operation is demonstrated in atmospheric conditions.

4.1 Introduction

Organic electronics is an emerging field where rapid advances are made in finding novel applications due to its inherent advantages such as flexibility, stretchability and adaptability towards roll-to-roll production. The invention of the first OLED in 1987 [1], created much research attention for developing efficient materials and fabrication techniques for OLED devices [2–4]. In lighting applications, flexible OLEDs have significant advantages over conventional incandescent or fluorescent lighting devices due to its light weight, improved dura-

bility, higher impact resistance, inherent flexibility and energy efficiency (up to 150 lm/W). Moreover, these devices are environmental friendly (no heavy metals involved) and cost-effective (roll-to-roll fabrication). Nowadays, the research in this area is mainly focused on the development of generic technologies for cost effective roll-to-roll production of flexible OLEDs [5].

One of the major challenges in fabricating reliable flexible OLEDs is to maintain higher device life times by protecting the device from moisture and oxygen permeation [6, 7]. In addition, the fabrication of OLED on a flexible substrate is rather complicated as it must be encapsulated from top and bottom sides, contrary to glass based OLEDs. In such a case, the role of a flexible moisture barrier which has similar optical properties as that of glass is vital for flexible OLEDs. In order to fabricate the flexible OLEDs in a roll-to-roll manner, different post patterning techniques of active device layers are considered of which laser ablation is favored. Laser ablation has several inherent advantages such as non-contact, dry processing, high speed, less environmental pollution (no hazardous wet-chemicals) and high accuracy, which makes it suitable for roll-to-roll production on flexible substrates. The use of lasers for the fabrication of these devices implicates that selective ablation process of optically thin organic device layers has to be developed. The influence of the optical absorption properties of the barrier layer, in the selective removal of the thin organic films like PEDOT:PSS or LEP, is crucial in the process of patterning OLED layers.

PEDOT:PSS and LEP have classically been deposited using spin-coating technologies or inkjet printing. Spin-coating results in significant quantities of material waste. Inkjet printing has been largely investigated for small area substrates. However, in case of large area substrates, large amounts of material have to be deposited. Hence, the layer flatness and deposition speed are questionable [8, 9]. Homogeneity and high overlay accuracy of the PEDOT:PSS and LEP are essential for the functionality of an OLED which can be attained by using large area deposition techniques for high volume production. Slot-die coating can be considered as fast, simple and cost-effective deposition technique for both PEDOT:PSS and LEP layers in a roll-to-roll fashion. However, the slot-die coating requires a post-patterning technique amongst which laser ablation is a very suitable candidate. Large area deposition of stacked layers followed by laser processing can preserve better layer homogeneities compared to patterned deposition techniques mentioned before. Proper power density

adjustment and wavelength / pulse-width selection of the laser beam has to be effectively utilized for selective removal of different thin layers which is crucial during OLED processing [10–16].

In this chapter, we demonstrate a fully functional laser patterned OLED on a flexible PEN substrate with a multilayered barrier stack [17]. In the previous chapter, various multilayered barrier foils with different optical absorption properties were discussed and laser processing parameters were optimized to obtain a selective ablation process. The challenge is to selectively remove a thin film organic layer, deposited on top of an inorganic layer, without any damage or (organic) leftovers present. An industrially qualified 248 nm KrF (Krypton Fluoride) excimer laser is used to structure and pattern flexible OLED stack layers. Subsequently, functional OLED devices are fabricated and encapsulated using thin film technology. A flexible substrate, which is 125 µm thick PEN, is laminated on a 6 inch × 6 inch glass carrier (1.1 mm thick) with a thermally activated release layer. On top of the laminated PEN substrate, a multilayer barrier stack is deposited with various deposition techniques. The device layers are then spin coated on the barrier stack on which selective laser ablation has been carried out. The samples were fabricated on the least absorbing Silicon Nitride (SiN(1)) multilayer barrier (referred as "barrier" afterward in this chapter) as it has shown the widest working process window (Chapter 3). The ablation experiments were conducted for the patterning and structuring of the thin films stack of the OLED device.

Consequently, a fully functional flexible OLED was fabricated and its operation has been demonstrated under environmental conditions. Still, this is a verification of the selective laser process investigation for the roll-to-roll production of flexible OLEDs and further life time testing will be the focus of future work.

4.2 Organic Light Emitting Diodes

4.2.1 General principle

An OLED is a light emitting diode with the organic material as main component for the emission of radiation. In a simple structural form, it consists of several thin films: anode, hole transport layer, emissive layer and a cathode, as shown in Figure 4.1. A thin organic material film is sandwiched between two electrodes. The anode is usually a transparent conducting material which is connected to the

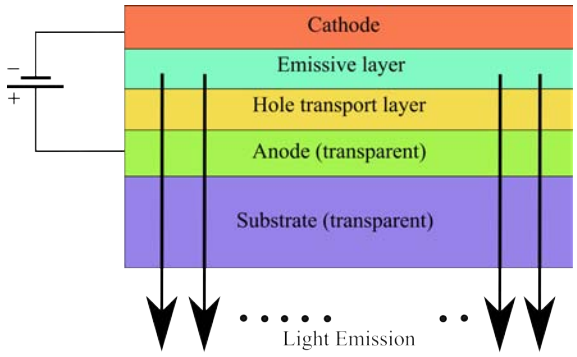

Figure 4.1: A simple schematic diagram of the OLED layered structure.

positive terminal. For instance, Indium Tin Oxide (ITO) has been widely used as anode in OLED design for many years. Recently, PEDOT:PSS replaced ITO as it is a transparent and conducting polymer (organic) alternative. Moreover, PEDOT:PSS also plays the role of hole transport layer. The organic materials used in organic light emitting devices are divided into two categories: based on conducting polymers and small molecules. The polymers which are suitable for this purpose are dominantly derivatives of poly(p-phenylene vinylene) and polyfluorene. The article "Organic electroluminescent diodes" by C.W. Tang and S.A. VanSlyke from Eastman Kodak, New York in the year 1987 was the first efficient demonstration of a small molecule based OLED [1]. In their double layered organic film structure, the luminescent film of 8-hyroxyquinoline aluminum (Alq_3) was used. The small molecules exploited for emission purpose in OLED design are usually organometallic chelates, fluorescent and phosphorescent dyes, and conjugated dendrimers. The cathode comprises of a low work function material suitable for the injection of electrons. Barium and Calcium are indeed qualifying for this purpose but they are reactive and hence starts degrading in due course of time. In practice, to protect the cathode from degradation, a layer of Aluminum is usually used as a cover. The substrate can be either rigid glass or flexible PET or PEN foil. For the flexible OLED fabrication, only polymeric substrates such as PET or PEN are suitable.

An OLED operates in forward bias, a positive voltage is applied at anode and relatively negative voltage at the cathode electrode. On application of voltage the electrons moves from cathode to anode. The organic material is semiconducting in nature, the conductivity

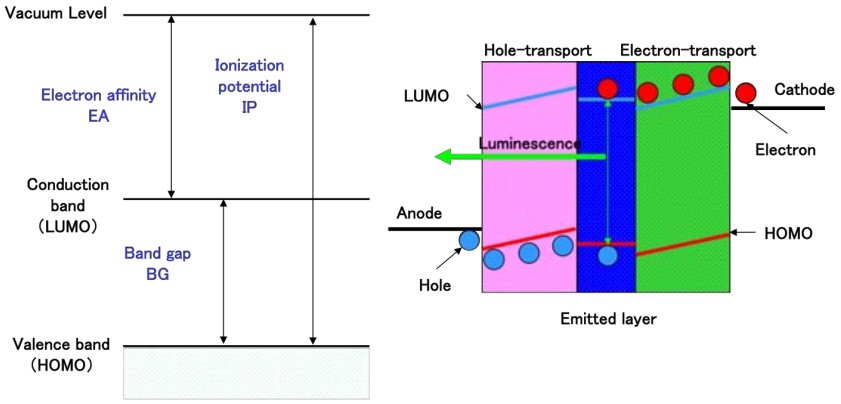

Figure 4.2: Model of energy band diagram for organic semiconductor material and operation of OLED [19].

lies in between insulators and conductors. The lowest unoccupied molecular orbital (LUMO) and highest occupied molecular orbital (HOMO) of organic materials are analogous to the conduction band and valence band of inorganic semiconductors. Electrons injects into LUMO at cathode and releases from HOMO at anode. The recombination process of electrons and holes, creates a bound "exciton" state. When the exciton decomposes, the electron relaxes to lower energy level and a radiation of frequency released. This frequency of radiation depends on the energy band gap between LUMO and HOMO, a simple illustration is shown in Figure 4.2.

4.2.2 Life time and efficiency

The life time and efficiency are the two big issues in the current OLED design. A satisfactory performance for indoor and portable display applications requires a brightness of about $100\,\mathrm{cd/m^2}$ at an operating voltage of between 5 and 15 V, an efficiency of about $15\,\mathrm{lm/W}$ and a continuous operational lifetime of at least 10000 hours [18]. In general, the life of the polymer based OLEDs is substantially shorter than that of small-molecule based devices [19]. Indeed, a lot of research work has been carried out in last two decades to improve the life time and efficiency of OLEDs. These devices fail because of the exposure to oxygen, moisture, high electric fields and high intensity illuminations. The degradation of these devices is due to the improper encapsulation / sealing after fabrication. Because of the penetration

of oxygen or moisture into the electrode starts decomposing it. P.E. Burrows et.al reported that the failure develops through the formation and growth of non-emissive dark spots that are initiated by the electrode defects [20]. In another study, a major cause of degradation in OLEDs has been found to be the electrochemical reaction between the two electrodes [21]. Such reaction leads to corrosion and to micro-structural changes in both electrode materials. Different types of barrier films can be used for encapsulation and sealing purpose, which eventually stop the oxygen/ moisture permeation. Using roll-coating techniques, a composite thin film barrier (Batrix TM) has been applied to commercially available polymers, which restricts moisture and oxygen to undetectable levels [22]. An alternative approach to increase the life time of the OLED is by doping into either hole transport layer or electron injection layer. The life extension of organic LEDs by the use of aromatic hydrocarbon dopants in the hole transport layer has been reported [23]. The OLEDs require a lot of improvement in the efficiency, in order to compete with other display technologies. The improvement in efficiency of electroluminescent devices by the introduction of a fluorescent dye has been reported [24]. Phosphorescent dyes offer a means of achieving improved light emission efficiencies as emission may result from both singlet and triplet states. The improved performance of OLED has been demonstrated with metal (Cesium) doped electron transport layer [25]. They have used a silver cathode which provides a reduction in driving voltage by 2.59 volts, a 47.3 percent increase in current efficiency and a 3.14 times enhancement in operation life.

4.3 Silicon Nitride Barrier Threshold

In order to selectively remove the thin film from a substrate, it is necessary to know the damage threshold of the substrate and ablation threshold of the thin film. In this study, a silicon nitride multilayered barrier has been used for the fabrication of the OLED. The multilayered barrier as described in the previous chapter consists of an inorganic, organic and inorganic thin films stack. The thickness of the top layer of inorganic Silicon Nitride in the barrier is 150 nm and overall barrier thickness is about 20 µm as shown in the Figure 4.3. The processing is carried out with an excimer 248 nm laser at 100 Hz pulse repetition rate. In the previous chapter (Chapter 3) it has been mentioned that due to the higher UV absorption of the polymers, excimer lasers are suitable for this patterning. A series

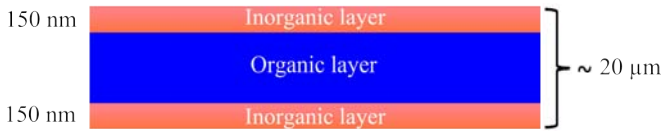

Figure 4.3: A multilayered barrier used for the fabrication of flexible OLED.

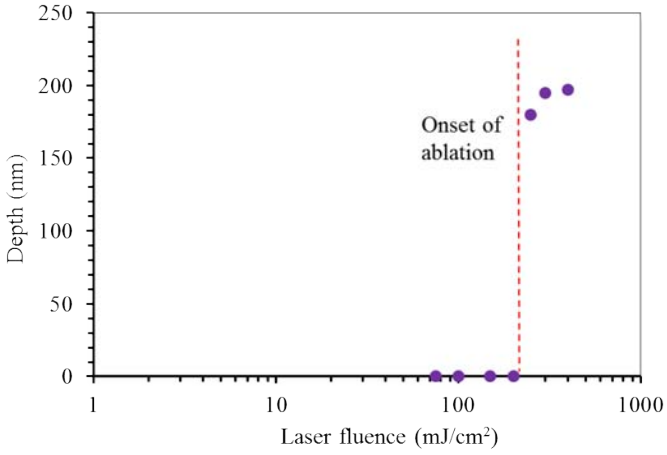

Figure 4.4: Silicon Nitride barrier threshold at 248 nm wavelength.

of experiments was conducted for the determination of the damage threshold of Silicon Nitride barrier. The laser fluence ranging from 75 mJ/cm^2 to 250 mJ/cm^2 were used. The processing was controlled by applying 1 pulse, 2 pulses and 5 pulses per location. Consequently, the ablation depth plot of the Silicon Nitride barrier is shown in the Figure 4.4. This plot shows that there is no removal of the material until a fluence of 200 mJ/cm^2. At fluences higher than 200 mJ/cm^2 the thickness abruptly increases to 150 nm and higher. It indicates that at fluences higher than 200 mJ/cm^2 the Silicon Nitride top layer (150 nm) has been completely removed.

4.4 Thin Films Ablation Thresholds

The ablation thresholds of PEDOT:PSS (Agfa Orgacon^{TM}) and LEP (Merck Livilux^{TM}) thin films on the barrier has crucial importance in the patterning of OLED thin films stack. We have determined the ablation threshold values for these films on the barrier. The PEDOT:PSS and LEP are spin coated on the multilayered barrier. The thicknesses of PEDOT:PSS and LEP are 100 nm and 80 nm respectively. The experiments were conducted in the similar manner as in the previous section, varying the fluence from 75 mJ/cm^2 to 250 mJ/cm^2 and controlling the ablation depth with 1, 2, 5 pulses. As a result, the ablation depth vs fluence plots for PEDOT:PSS and LEP are illustrated in Figure 4.5.

From this figure, it is observed that the threshold of layer removal in both cases is 75 mJ/cm^2 from single pulse experiments. This information is important to define a process for patterning both layers in subsequent steps on the barrier layer. Since the threshold of ablation of the barrier is found to be more than twice that of the fluence required for ablating any of these organic layers, there is a high probability of patterning these thin films without any damage to the underlying barrier layer. Therefore, a wide and sufficient process working window is available for selective ablation. Multi-pulse laser ablation studies at various fluences were carried out to determine the optimized process windows.

The optical microscopic images of onset of ablation at 75 mJ/cm^2 with 1 pulse per location are shown in Figure 4.6. It appears that the ablation of thin film is about to start and a slightly higher energy is sufficient to remove the thin film. When the fluence increases to 100 mJ/cm^2 with 1 pulse per location, the optical microscopic images are shown in Figure 4.7. If we compare these images, in case of PEDOT:PSS (images (a)) the variation in the two optical microscopic images is clearly visible for the fluence of 75 mJ/cm^2 and 100 mJ/cm^2, but there is no visible recognizable change in the two images for LEP (images (b)). Only the depth measurements of the ablated craters can provide information about depth and film removal. This kind of optimization of the laser processing parameters has been discussed in Chapter 3, where the exact depths are plotted against fluence.

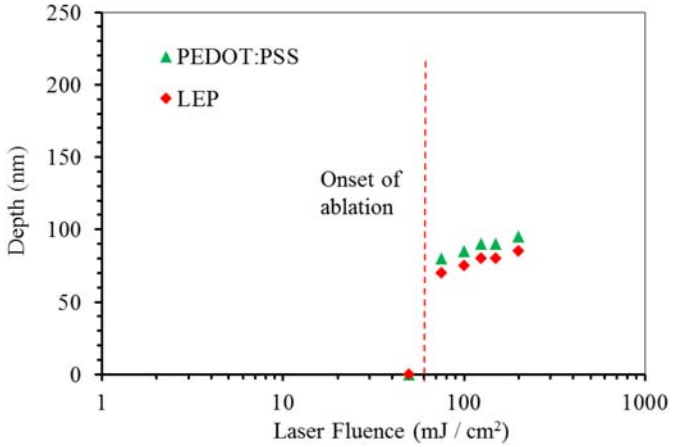

Figure 4.5: Onset of ablation for the PEDOT:PSS and LEP thin films on an optimized multilayered barrier.

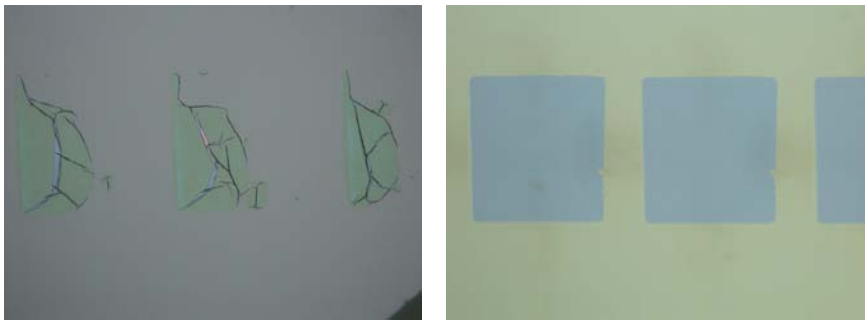

(a) Fluence 75 mJ/cm^2, 1 Pulse (b) Fluence 75 mJ/cm^2, 1 Pulse

Figure 4.6: The optical microscopic images at the onset of ablation for thin organic films (a) PEDOT:PSS and (b) LEP.

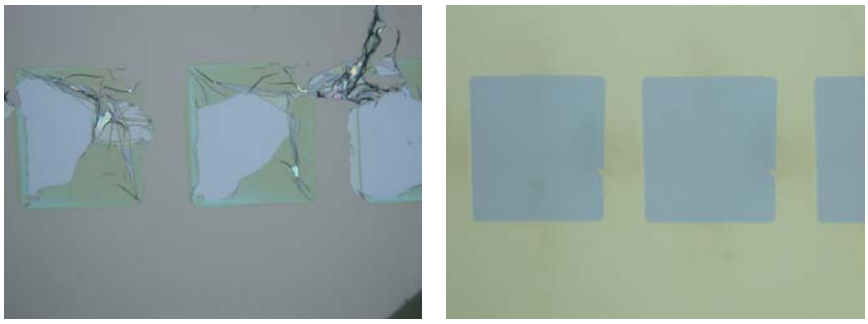

(a) Fluence 100 mJ/cm^2, 1 Pulse (b) Fluence 100 mJ/cm^2, 1 Pulse

Figure 4.7: The selective removal of thin organic films from barrier with single pulse (a) PEDOT:PSS and (b) LEP.

4.5 Flexible OLED Fabrication

A complete thin films layered stack has been prepared on the multilayered barrier and PEN substrate for the fabrication of a flexible OLED. Two laser patterning steps involving organic thin films PEDOT:PSS (≈100 nm) and LEP (≈80 nm) have been carried out. There are two challenges to be considered for the realization of a laser patterned device. First, to selectively ablate the organics without damaging the top inorganic barrier layer. Secondly, to protect the bus bar which is a multilayer stack of Chromium and Aluminum (Cr-Al-Cr) beneath, during this ablation process. The selective removal of thin films definitely requires the overlapping of pulses to scan the area as required. The line patterning of PEDOT:PSS, has been optimized in terms of fluence and number of shots. Selective line patterning of organic thin film of PEDOT:PSS at a fluence of 125 mJ/cm^2 and 2 pulses per location is illustrated in Figure 4.8 (a). The corresponding depth profile with a non-contact optical profiler is shown in Figure 4.8 (b). It is observed that the ablated line track is clean and debris free, however in this image there are some external dust particles present during analysis, which can be blown away. Furthermore, the measured depth of ablated region is about 111 nm, which is slightly higher than the thickness of the PEDOT:PSS thin film. This difference can be attributed to roughness of the ablated track and also to the roughness of the PEDOT:PSS film. However, there is no detectable damage on the inorganic barrier layer which is about 150 nm. During the analysis of different Silicon Nitride barrier

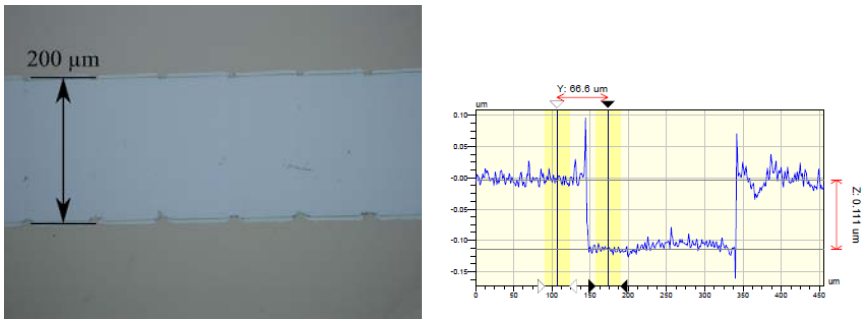

(a) PEDOT:PSS line patterning (b) Depth profile

Figure 4.8: PEDOT:PSS thin film line patterning on barrier (a) Optical microscopic image and (b) Wyko depth profile.

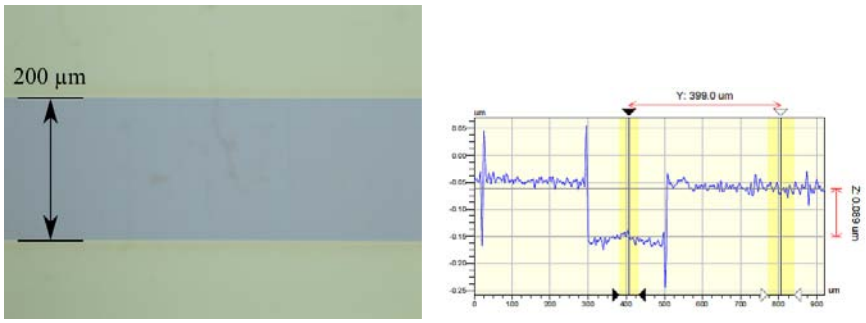

(a) LEP line patterning (b) Depth profile

Figure 4.9: LEP thin film line patterning on barrier (a) Optical microscopic image and (b) Wyko depth profile.

samples it has been observed that the detection of the damage on Silicon Nitride is usually represented with a color change and cracks on the layer.

In order to selectively ablate the light emissive polymer organics, the laser process has been optimized on the barrier layer. A fluence of 100 mJ/cm^2 with 2 to 5 pulses, provides a suitable working window for this patterning. For instance, line patterning of LEP on the inorganic barrier layer at a fluence of 100 mJ/cm^2 with 5 pulses per location is shown in Figure 4.9. This figure indicates that the depth profile is clean and no debris present on the ablated groove. Apart from that, there is no visible and detectable damage on the inorganic Silicon Nitride barrier layer. On the right image the measured depth

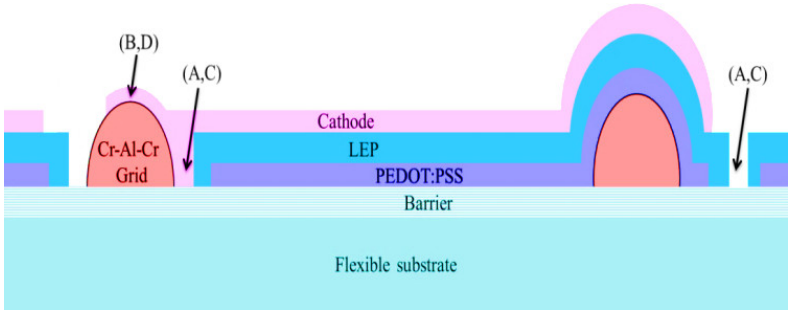

Figure 4.10: Schematic of a flexible OLED layered structure and various selective ablation steps for patterning: (A) To ablate PEDOT:PSS on a barrier (B) To ablate PEDOT:PSS on bus bar (C) To ablate LEP on the barrier (D) To ablate LEP on the bus bar.

profile is depicted, which indicates to a depth of 89 nm. As in case of the PEDOT:PSS, the measured depth is slightly higher than the actual thickness of the LEP thin film i.e. 80 nm.

A simple schematic illustration of the device layers with necessary laser process steps is given in Figure 4.10. The PEDOT:PSS and LEP laser patterning steps are validated on a 15 cm × 15 cm flexible OLED device platform incorporating 9 individual OLED devices. A detailed overview of thicknesses and processing methodology of various layers is summarized in the Table 4.1. The hole injection layer (PEDOT:PSS) is deposited on top of the barrier stack by spin coating from an aqueous solution followed by a heating step for solvent removal. Laser patterning of this layer leads to electrical contact separation between anode and cathode, as well as top barrier encapsulation structures. Subsequently, LEP is deposited by spin coating followed by laser patterning which removes the layer at specific regions for device encapsulation. The device layers are then covered by a low work-function Barium (Ba) cathode layer capped with Aluminum (Al). Finally, a barrier layer is deposited on the whole OLED stack to form the top encapsulation, which will hermetically seal the fabricated device.

Sequential ablation steps of PEDOT:PSS and LEP are required for processing the OLED device. It is important to remove both the organic layers (LEP and PEDOT:PSS) from the barrier layer. After laser processing of the device layers, thin film encapsulation is made on the top-side by depositing identical barrier layer over the

Table 4.1: Layer composition, thicknesses and deposition methods of the OLED stack

Layer	Role in OLED stack	Thickness	Deposition
Ba-Al	Cathode	100 nm	Evaporation
LEP	Active emissive layer	80 nm	Spin coating
Cr-Al-Cr	Bus-bar	150 nm	Sputtering
PEDOT:PSS	Hole injection/Anode	100 nm	Spin coating
Silicon Nitride	Top layer of barrier	150 nm	Plasma deposition
PEN	Flexible substrate	125 µm	–

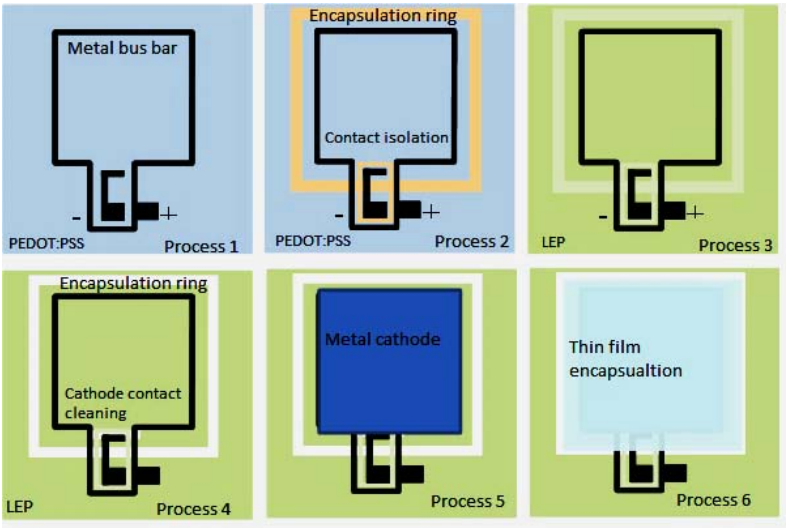

Figure 4.11: Process flow for the laser patterned flexible OLED device.

whole device surface. This process should ensure that the top and the bottom barrier stack form a hermetical seal. If the laser process leaves an incompletely removed layer, then there is a possibility of improper sealing between barrier and encapsulation layers, this acts as a moisture ingress path which eventually leads to the damage of the device.

The Figure 4.12 demonstrates a laser patterned flexible OLED, which lights up on application of an electrical power supply. It can be seen from this figure that, after the device is turned ON, the OLED works in ambient conditions.

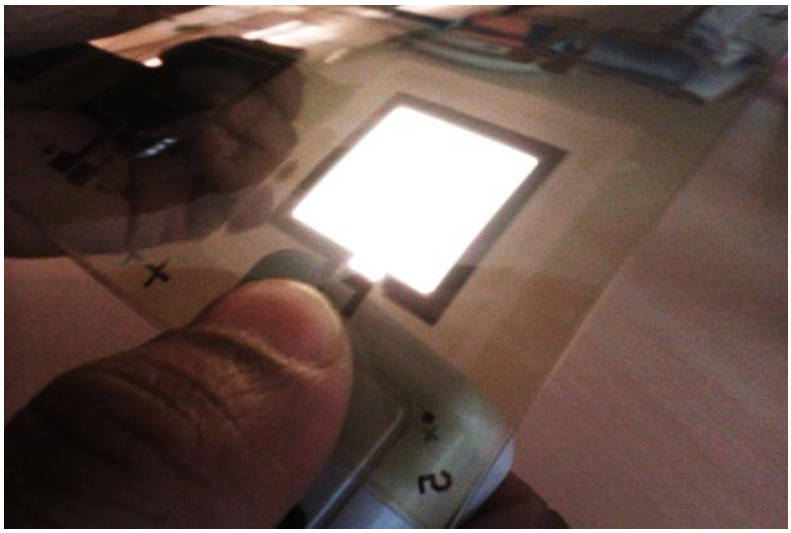

Figure 4.12: A functional flexible OLED device incorporating PEDOT:PSS and LEP selective ablation using excimer laser, demonstration under environmental conditions.

4.6 Conclusions

The process investigation on selective ablation of thin organic films on a multilayered barrier foil has been performed. After selection of an optimized barrier foil, feasibility of the laser process for patterning and structuring of various OLED layers has been investigated. Minimal debris field and layer delamination are observed in the ablated zone. Multi-pulse laser processes were optimized for the removal of both PEDOT:PSS and LEP organic layers on a flexible substrate containing a multilayer barrier stack. A functional flexible laser processed OLED device has been fabricated and its operation has been demonstrated under environmental conditions.

References

[1] Tang, C. W. and VanSlyke, S. A., "Organic electroluminescent diodes", *Applied Physics Letters*, vol. 51, no. 12, pp. 913–915, 1987. [Online].

[2] A. N. Krasnov, "High-contrast organic light-emitting diodes on flexible substrates", *Applied Physics Letters*, vol. 80, no. 20, pp. 3853–3855, 2002. [Online].

[3] M. Eritt, C. May, K. Leo, M. Toerker, and C. Radehaus, "OLED manufacturing for large area lighting applications", English, *Thin Solid Films*, vol. 518, no. 11, 3042–3045, 2010. [Online].

[4] D. A. Pardo, G. E. Jabbour, and N. Peyghambarian, "Application of Screen Printing in the Fabrication of Organic Light-Emitting Devices", *Advanced Materials*, vol. 12, no. 17, pp. 1249–1252, 2000. [Online].

[5] "www.holstcentre.com", *Holst Center, The Netherlands*, viewed on 2014. [Online].

[6] P. van de Weijer and T. van Mol, "White paper on the characterisation of thin-film barrier layers for protection of organic Light-Emitting Diodes", *ICT-216641 Fast2light*, pp. 1–17, 2009.

[7] J.-S. Park, H. Chae, H. K. Chung, and S. I. Lee, "Thin film encapsulation for flexible AM-OLED: a review", *Semiconductor Science and Technology*, vol. 26, no. 3, 2011. [Online].

[8] G. E. Jabbour, R. Radspinner, and N. Peyghambarian, "Screen printing for the fabrication of organic light-emitting devices", *Selected Topics in Quantum Electronics, IEEE Journal of*, vol. 7, no. 5, pp. 769–773, 2001. [Online].

[9] S.-C. Chang, J. Liu, J. Bharathan, Y. Yang, J. Onohara, *et al.*, "Multicolor Organic Light-Emitting Diodes Processed by Hybrid Inkjet Printing", *Advanced Materials*, vol. 11, no. 9, pp. 734–737, 1999. [Online].

[10] D. G. Lidzey, M. Voigt, C. Giebeler, A. Buckley, J. Wright, *et al.*, "Laser-assisted patterning of conjugated polymer light emitting diodes", *Organic Electronics*, vol. 6, no. 5, pp. 221–228, 2005. [Online].

[11] Y.-H. Tak, C.-N. Kim, M.-S. Kim, K.-B. Kim, M.-H. Lee, *et al.*, "Novel patterning method using Nd:YAG and Nd:YVO4 lasers for organic light emitting diodes ", *Synthetic Metals*, vol. 138, no. 3, pp. 497–500, 2003. [Online].

[12] C. Liu, G. Zhu, and D. Liu, "Patterning cathode for organic light-emitting diode by pulsed laser ablation", *Displays*, vol. 29, no. 5, pp. 536–540, 2008. [Online].

[13] N. Bityurin and A. Malyshev, "Bulk photothermal model for laser ablation of polymers by nanosecond and subpicosecond pulses", *Journal of Applied Physics*, vol. 92, no. 1, pp. 605–613, 2002. [Online].

[14] R. Stoian, A. Rosenfeld, D. Ashkenasi, I. V. Hertel, N. M. Bulgakova, *et al.*, "Surface Charging and Impulsive Ion Ejection during Ultrashort Pulsed Laser Ablation", *Physical Review Letters*, vol. 88, p. 097 603, 9 2002. [Online].

[15] R. Mandamparambil, H. Fledderus, G. Van Steenberge, and A. Dietzel, "Patterning of Flexible Organic Light Emitting Diode (FOLED) stack using an ultrafast laser", *Optics Express*, vol. 18, no. 8, pp. 7575–7583, 2010. [Online].

[16] S. Naithani, R. Mandamparambil, F. van Assche, D. Schaubroeck, H. Fledderus, *et al.*, "Influence of barrier absorption properties on laser patterning thin organic films", in *Photonics Europe*, Brussels, Belgium: SPIE, 2012, pp. 843 505–843 509. [Online].

[17] S. Naithani, R. Mandamparambil, H. Fledderus, D. Schaubroeck, and G. V. Steenberge, "Fabrication of a laser patterned flexible organic light emitting diode on an optimized multilayered barrier", *Applied Optics*, vol. 53, no. 12, pp. 2638–2645, 2014. [Online].

[18] P. E. Burrows, S. R. Forrest, and M. E. Thompson, "Prospects and applications for organic light-emitting devices", *Current Opinion in Solid State and Materials Science*, vol. 2, no. 2, pp. 236–243, 1997. [Online].

[19] S. A. Van Slyke, C. H. Chen, and C. W. Tang, "Organic electroluminescent devices with improved stability", *Applied Physics Letters*, vol. 69, no. 15, pp. 2160–2162, 1996. [Online].

[20] P. E. Burrows, V. Bulovic, S. R. Forrest, L. S. Sapochak, D. M. McCarty, *et al.*, "Reliability and degradation of organic light emitting devices", *Applied Physics Letters*, vol. 65, no. 23, pp. 2922–2924, 1994. [Online].

[21] H. Aziz and G. Xu, "A degradation mechanism of organic light-emitting devices", *Synthetic Metals*, vol. 80, no. 1, pp. 7–10, 1996. [Online].

[22] P. Burrows, G. Graff, M. Gross, P. Martin, M. Shi, *et al.*, "Ultra barrier flexible substrates for flat panel displays", *Displays*, vol. 22, no. 2, pp. 65–69, 2001. [Online].

[23] Z. Popovic, S. Xie, N. Hu, A. Hor, D. Fork, *et al.*, "Life extension of organic LED's by doping of a hole transport layer", *Thin Solid Films*, vol. 363, no. 12, pp. 6–8, 2000. [Online].

[24] M. A. Baldo, D. F. O'Brien, Y. You, A. Shoustikov, S. Sibley, *et al.*, "Highly efficient phosphorescent emission from organic electroluminescent devices", *Nature*, vol. 395, pp. 151–154, 1998. [Online].

[25] J.-H. Lee, M.-H. Wu, C.-C. Chao, H.-L. Chen, and M.-K. Leung, "High efficiency and long lifetime OLED based on a metal-doped electron transport layer", *Chemical Physics Letters*, vol. 416, no. 46, pp. 234–237, 2005. [Online].

5

Monolayer Investigation: TOFSIMS

In this chapter, a detailed analysis of the multilayer barrier surface after laser patterning of the PEDOT:PSS thin films is presented. While the use of a 3D surface profiler or a scanning electron microscope (SEM) allows to conclude whether the laser process is layer selective or not, analyzing the chemical surface composition is required to conclude whether the PEDOT:PSS organic film is completely removed or not. In fact, even a monolayer might be responsible for shortening the life time of organic electronics device, since in that case proper sealing and encapsulation can not be provided. Therefore, the use of Time-Of-Flight Static Secondary Ion Mass Spectrometry (TOF-S-SIMS) is proposed as an analytical method to analyze the outermost molecular surface layer of the barrier after laser patterning of thin films.

5.1 Introduction

The fabrication of a laser patterned flexible OLED is discussed in the previous chapter, eventually it turns out that shorter life-time and reliability issues are of the major concern [1–4]. There has been a lot of research efforts to improve the life time of OLEDs by different methods such as doping the hole/electron transport layers or using cavity structures [5–8]. The damage on the barrier or encapsulation

layer leads to shortening the life time of the OLED, as it introduces moisture or oxygen into the OLED stack which results in black non-emissive spots on it [9–11]. There is also a possibility of the remaining thin film of organics after laser processing. Due to such a remaining thin film, the sealing of bottom barrier layer and top encapsulation layer is not adequate, which opens a space for penetration of moisture or oxygen [12, 13]. Hence, it is highly important to know if there is any damage on the barrier layer during the selective laser processing and / or any left over traces of the organic material are still present. The optical microscopic, mechanical or optical depth profiling and SEM techniques have their limitations to identify and quantify the remaining thin film organics of the order of atomic, molecular size or monolayer(s) left after processing. Therefore, a high quality detection technique is necessary for the investigation of the laser ablated regions, which can provide the surface compositional information.

In this chapter, a highly qualitative surface analysis technique known as Time Of Flight Static Secondary Ion Spectrometry (TOF-S-SIMS) is introduced. This technique is capable to provide the information about surface composition after processing, which implicates if there is any thin organic film material present or not. The PEDOT:PSS thin films are investigated using TOF-SIMS technique after selective ablation process.

TOF-S-SIMS, (Time of Flight Static Secondary Ion Mass Spectrometry) is a surface analysis technique to provide the chemical elemental information. Static SIMS relies on the bombardment of the sample with a low intensity positive ion beam or neutral atoms. The ion beam from the ion gun (source) is called primary ion beam and the ions emitted from the surface of the sample are known as secondary ions. The ejected ion from the surface can be positive or negative ions. The mass spectrometer detects the positive and negative secondary ions at the another end. The detector system with an associated software calculates the time of flight of ion from the sample surface to the detector and determines the mass of the secondary ion. The time of arrival of the ion at the detector is directly related to the mass. Based on the sensitivity of the detector either positive or negative, the spectra can be either negative or positive respectively. A general schematic of the TOF-SIMS spectrometer is shown in Figure 5.1, it consists of the primary gun source, focusing optics for secondary ions to the detector and a mass analyzer. The TOF-SIMS method is much more surface sensitive compared to SEM/EDX to determine the elemental composition of the surface to

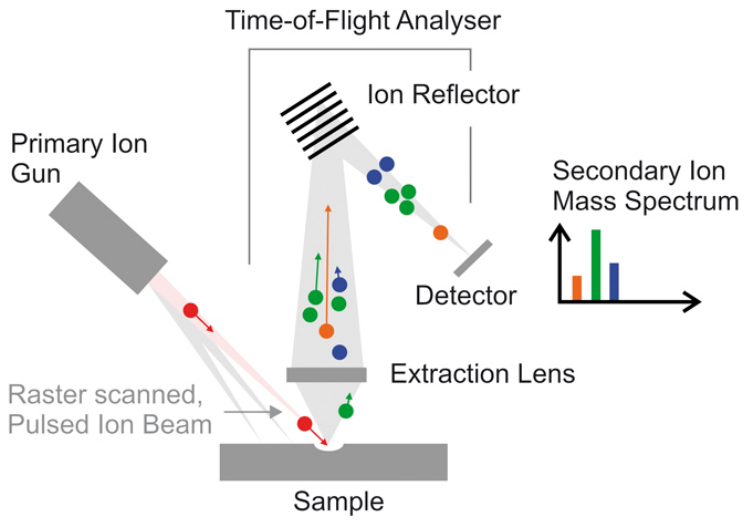

Figure 5.1: Schematic diagram of TOF-SIMS, indicating the primary gun bombardment on sample and detection of secondary ions [14].

a depth of 1 nm to 2 nm. It uses the primary ion beam for the surface investigation, whereas in case of SEM/EDX the electron beam is used for this purpose.

5.2 Materials and Methods

5.2.1 Sample preparation

The PEN foils (125 µm) have been used as flexible substrates, on top of which a multilayer barrier stack is deposited. The inorganic silicon nitride layer (deposited by plasma enhanced chemical vapour deposition) serves as a moisture or oxygen barrier; while the organic layer (applied by spin-coating) is intended to planarize the surface. The total thickness of the multilayer barrier stack is approximately 20 µm. The PEDOT:PSS thin-film is deposited by spin-coating from an aqueous solution, with a target layer thickness of 100 nm. The sample layered build-up is illustrated in Figure 5.2.

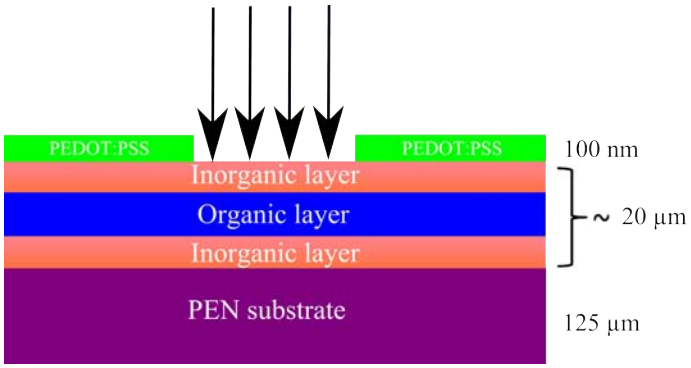

Figure 5.2: The PEDOT:PSS thin film on a multilayered barrier, sample prepared for TOF-SIMS analysis.

5.2.2 Ablation parameters

The ablation experiments were performed with a pulsed KrF excimer laser (ATL Lasertechnik SP300i, tFWHM = 3 ns to 7 ns) at 248 nm with a pulse repetition rate of 100 Hz (refer to Figure 3.3). A square mask with an aperture of 2 mm was used to utilize a homogeneous part of the beam, which was focused by a lens onto the sample with a demagnification of 10, yielding a spot size of 200 µm. The fluence was adjusted with an attenuator plate, and the pulse energy at each fluence was measured by a pyroelectric energy meter (Coherent J25LP-MUV, in combination with FieldmaxII TOP) placed at the end of the beam axis. A fluence of 125 mJ/cm^2 with different number of shots varying from 5 to 10 has been used for patterning the 1 mm × 1 mm area of the PEDOT:PSS.

5.2.3 Non-contact optical profiler

After laser processing, the samples were analysed with a non-contact optical profiler (Wyko NT3300). During these measurements, the foil was applied to a sticking surface (PDMS-Polydimethylsiloxane), minimizing the foil curvature. Since a stack of transparent layers might result in multiple reflections, a reflective layer was applied on top of the stack, by a gold sputter step.

5.2.4 Scanning electron microscopy

Scanning electron microscope (SEM) analysis has been performed on a JEOL JSM-5600. The apparatus was used in the secondary electron mode. Prior to analysis, all samples were coated with a thin gold layer (20 nm) via plasma magnetron sputter coating.

5.2.5 Plasma cleaning

To investigate whether residues of PEDOT:PSS which are not removed in the laser process can still be removed by other means, some samples were treated with two different types of cleaning processes. One set of samples has been treated with a Diener plasma system (Diener Electronic) using an O_2 gas chamber-pressure of 0.8 mbar and a power of 190 W at room temperature. This plasma surface activation and etching treatment has been carried out for time intervals of 1 minute, 2 minutes and 5 minutes. The second set of samples was processed in a Reactive Ion Etching (RIE) system (Plasma Therm, Batchtop), using a base pressure of 30 mTorr, oxygen flow of 40 sccm and 40 W RF power at room temperature. The RIE treatment has been carried out at three different time intervals of 1 minute, 2 minutes and 3 minutes.

5.2.6 TOF-SIMS equipment

The chemical surface composition has been investigated using TOF-SIMS. Positive and negative secondary ion mass spectra have been recorded using a TOF-SIMS V (ION-TOF, Munster, Germany) equipped with a Bi_3^+ liquid metal ion gun. The analysis has been performed in the so-called "high current bunched mode" featuring good mass resolution and a beam spot size of 2 µm. Depending on the sample, the field-of-view has been adjusted between 50 µm × 50 µm and 500 µm × 500 µm. Mass spectra have been recorded during 100 second to 150 second with a pulsed primary ion beam current of 0.4 pA to 0.5 pA. To compensate for positive charge build-up, an electron flooding has been applied in all analyses. Calibration of the positive ion mass spectra has been performed using the signals at m/z 1 (H^+), 15 (CH_3^+), 29 ($C_2H_5^+$) and 43 ($C_3H_7^+$). The ions at m/z 1 (H^-), 12 (C^-), 13 (CH^-), 16 (O^-) and 17 (OH^-) have been used for the negative ion mass spectra.

5.3 PEDOT:PSS Area Patterning

In the first stage of this investigation, the number of laser pulses has been optimized for area patterning of PEDOT:PSS. An excimer laser with a fluence of 125 mJ/cm^2 and different number of shots per location has been used for the area patterning experiments. Initially, the experiments have involved 5 to 10 shots per location keeping the fluence fixed. It has been observed that even with 5 shots per location, there is a removal of PEDOT:PSS but the ablated area is full of debris or re-deposited material as shown in Figure 5.3(a). As the number of shots is increased from 5 to 10, the ablated area becomes free of debris as shown in Figure 5.3(b) and Figure 5.3(c). For the given laser fluence, the ablation is driven by a combination of photomechanical and photochemical processes, still leading to quite some flakes which are being removed with increasing amount of laser shots. Therefore, a fluence of 125 mJ/cm^2 with 10 shots per location seems necessary and sufficient for the selective area patterning of the PEDOT:PSS thin film.

The depth of the ablated area has been measured using a non-contact optical profiler and is shown in Figure 5.4. The depth profile indicates a crater depth of about 100 nm to 110 nm, which is indeed closer to the specified PEDOT:PSS layer thickness (100 nm), suggesting a complete PEDOT:PSS layer removal, without digging into the barrier layer. In order to compare the surface of the laser ablated areas with bare silicon nitride, the samples were analyzed using a Scanning Electron Microscope (SEM). Figure 5.5 illustrates the high magnification SEM images of laser patterned areas and bare silicon nitride surfaces. In case of 5 and 7 pulses per location, the particles present on the ablated area can be ascribed to debris or non-ablated polymer residues. A particle free area is obtained when 10 pulses are applied. Moreover, the surface topography is similar to that of the bare silicon nitride surface.

5.4 TOF-SIMS Investigations and Analysis

In the second stage of this work, a detailed analysis of the ablated samples were carried out using TOF-SIMS analysis. Four different kinds of the samples have been prepared for the purpose of comparison, namely (1) un-ablated pure PEDOT:PSS (2) ablated PEDOT:PSS on barrier (3) ablated pattern with O_2 plasma treatment and (4) ablated pattern with mild RIE exposure. Before dis-

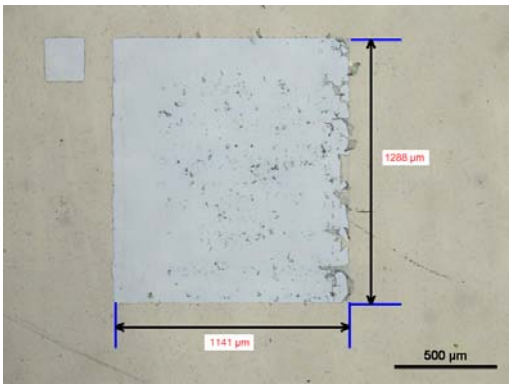

(a) 125 mJ/cm^2 and 5 pulses

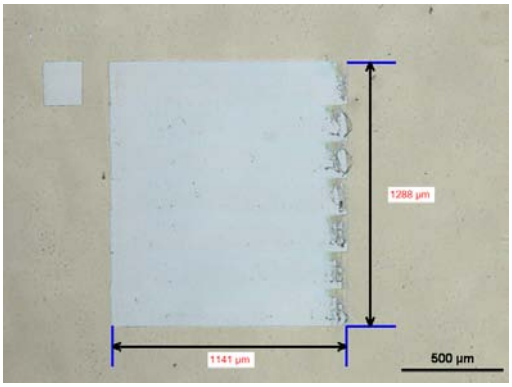

(b) 125 mJ/cm^2 and 7 pulses

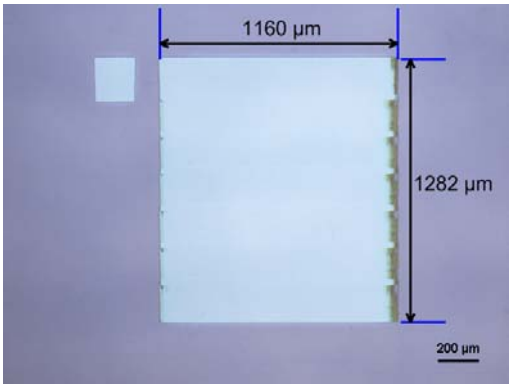

(c) 125 mJ/cm^2 and 10 pulses

Figure 5.3: Area patterning of PEDOT:PSS on barrier foil with different pulses. On the left top corner in all images there is a square mark, which is a reference mark during experiments.

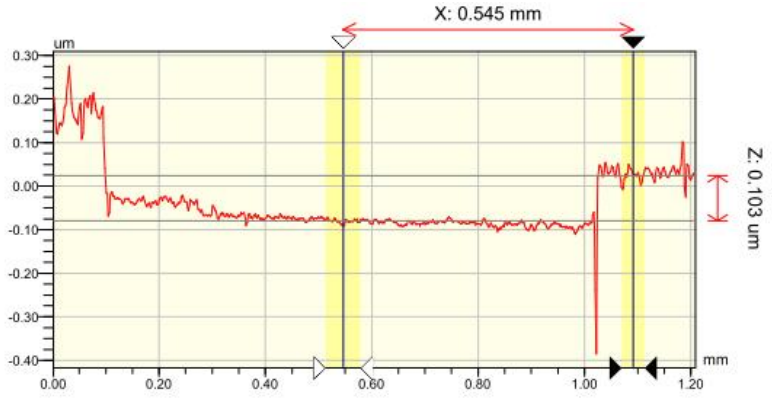

Figure 5.4: Depth profile of the laser ablated area using a non-contact optical profiler.

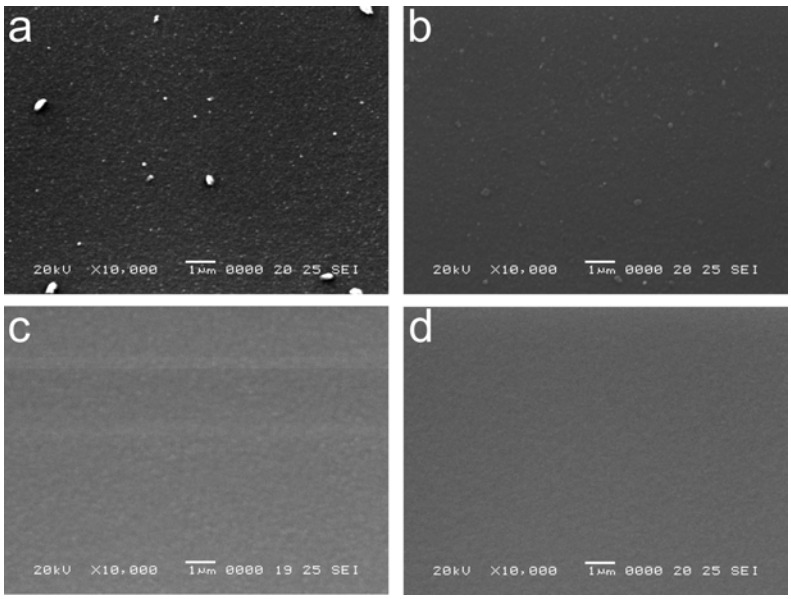

Figure 5.5: SEM micrographs of (a) the laser ablated area with 5 shots per location, shows the presence of debris particles (b) ablated crater with 7 shots per location, with few tiny sub-micron particles (c) selective removal of PEDOT:PSS with 10 shots per location, yielding a clean debris free ablated area. (d) bare Silicon Nitride surface, included for the purpose of comparison.

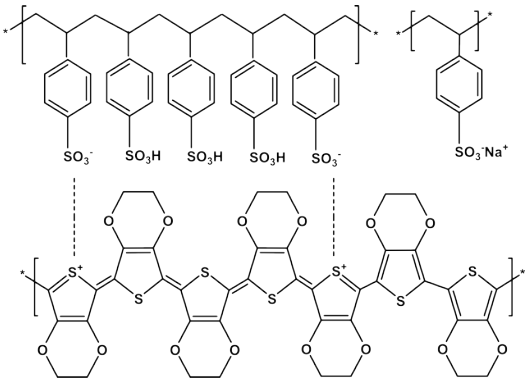

Figure 5.6: Chemical structure of PEDOT:PSS.

cussing the TOFSIMS results, it is necessary to understand the chemical structure of the the PEDOT:PSS. The general chemical structure of PEDOT:PSS is presented in Figure 5.6. PEDOT:PSS is obtained in its conductive cationic form by oxidative polymerization of 3,4-ethylenedioxythiophene in aqueous solution using sodium peroxodisulfate as the oxidant [14]. Therefore, it is possible that PSS^--Na^+ is also present in the final product. The PSS^- in the complex acts as the source for the charge balancing counter ion and keeps the PEDOT segments dispersed in the aqueous medium. Recently, Lang [15] discovered that thin films of PEDOT:PSS are composed of grains with a diameter in the range of 30 nm to 50 nm. These grains have a PEDOT-rich core and a PSS-rich shell with a thickness of 5 nm to 10 nm.

Figure 5.7 shows the positive secondary ion mass spectrum of the pure PEDOT:PSS layer. The main signals obtained in the spectrum characterize the PSS component of the system. Specifically, the signal at m/z 23 and 39 are due to Na^+ and K^+, respectively. The ions at m/z 126, 149, 165 and 181 have to be assigned to the molecular ion $Na_2SO_3{}^+$ and the adduct ions $Na_2SO_3Na^+$, $Na_2SO_4Na^+$ and /or $Na_2SO_3K^+$, and $Na_2SO_4K^+$ and /or $K_2SO_3Na^+$, respectively. The latter ions are typically detected in S-SIMS from inorganic sulphates and sulphites as well as from organic sulfonate salts and can be considered as structure specific. The repeat unit of PSS^-- Na^+ is detected as a whole in the form of a cationized molecule at m/z 229 (cf. Figure 5.8). These ions yield prominent signals that are superimposed on a complex pattern of peaks that is typical for the PS-like backbone structure of the layer. It is obvious that the PS polymer

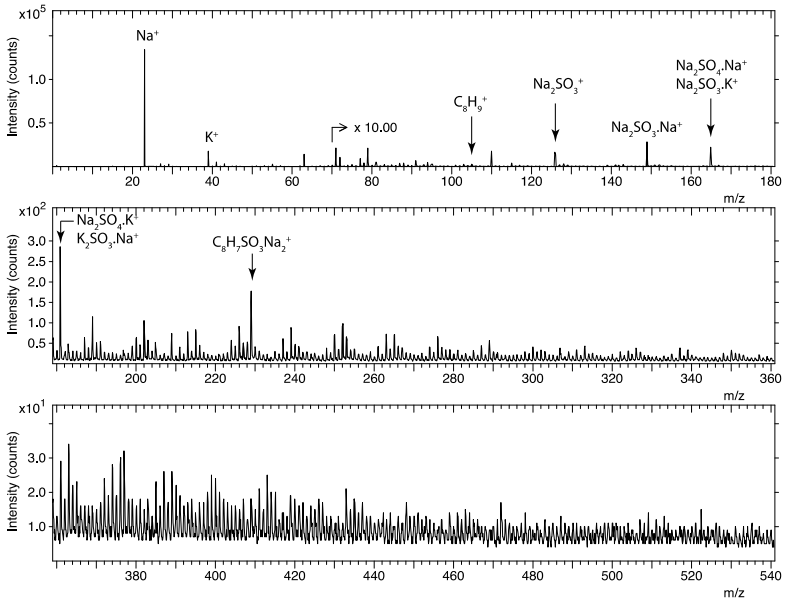

Figure 5.7: Positive ion mass spectrum recorded by TOF-S-SIMS from a pure PEDOT:PSS layer.

can be considered as a logical precursor for a fully aromatic system. Hence, the low intensity peak pattern is typical in that it contains significant signals at every two m/z. These signals are associated to the numerous fragments that can be generated from the PS repeat units undergoing different degree of aromatisation to stabilise the internal energy imparted by the primary ion bombardment. The prominent signal at m/z 105 is readily associated with the protonated styrene repeat unit of PS. Note that the assignment of all these structures is supported by accurate m/z measurements in that the relative difference between the experimental end theoretical mass of the ions stays within 100 ppm, although this level of mass accuracy is to be considered acceptable for a method operating at the nano-scale.

Strikingly, no evidence is found on the PEDOT part of the layer and this lack of information is not compensated by the negative ion mass spectrum of the layer in Figure 5.9. The main signals in the low m/z range can be readily assigned to inorganic ions such as m/z 32 (S^-), 33 (HS^-), 64 (SO_2^-), 80 (SO_3^-), 81 (HSO_3^-) and 97 (HSO_4^-). These ions are again typically generated from components with a sulphate or sulfonate group. Organic structural ions are detected at m/z

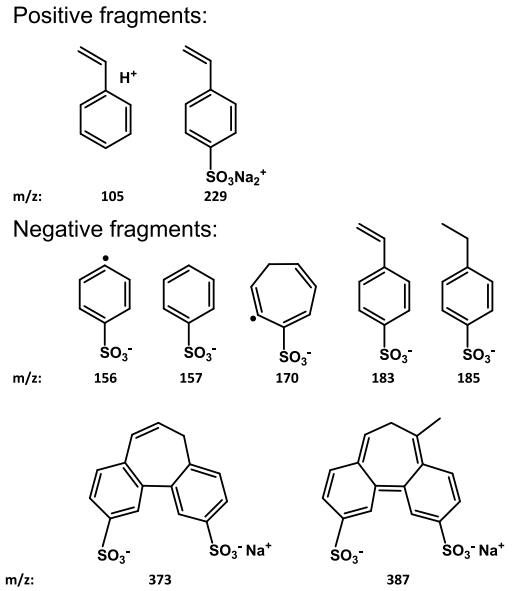

Figure 5.8: Tentative structural assignment of the positive and negative ions of major diagnostic interest detected from a pure PEDOT:PSS layer by S-SIMS.

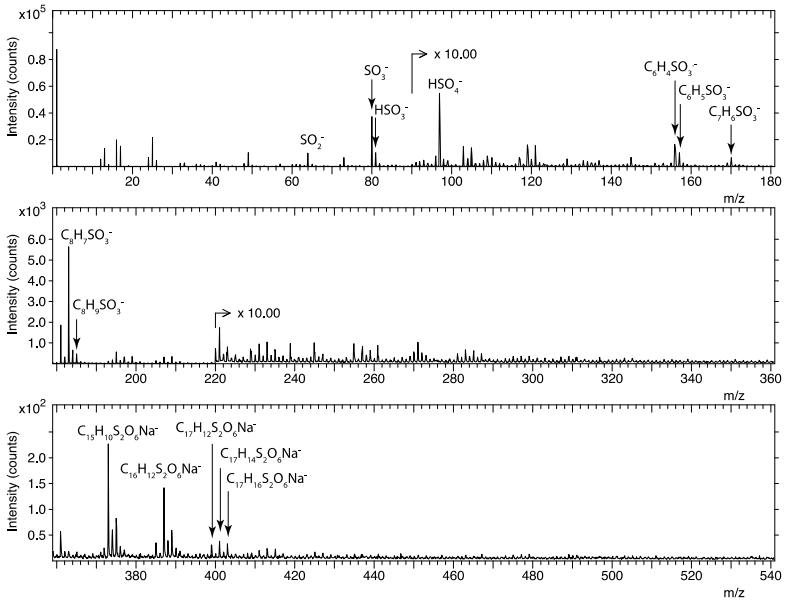

Figure 5.9: Negative ion mass spectrum recorded by TOF-S-SIMS from a pure PEDOT:PSS layer.

156 ($C_6H_4SO_3^-$), 157 ($C_6H_5SO_3^-$), 170 ($C_7H_6SO_3^-$), 183 ($C_8H_7SO_3^-$), 185 ($C_8H_9SO_3^-$), 373 ($C_{15}H_{10}S_2O_6Na^-$), 387 ($C_{16}H_{12}S_2O_6Na^-$), 399 ($C_{17}H_{12}S_2O_6Na^-$), 401 ($C_{17}H_{14}S_2O_6Na^-$) and 403 ($C_{17}H_{16}S_2O_6Na^-$). Figure 5.8 shows that these signals essentially confirm the presence of a sulfonated styrene structure as the repeat unit of the PSS system. The formation of the fragments at m/z 170 is believed to involve complex skeletal rearrangements that are typical for aromatic systems in S-SIMS. Also here, numerous low intensity signals are found referring to the formation of highly aromatised fragments from PS-like structures. The absence of fragments of PEDOT is consistent with the idea that the outermost surface layer(s) of PEDOT:PSS thin films are primarily composed of PSS [15–17].

Looking at the positive ion mass spectrum of the laser ablated PEDOT:PSS area in Figure 5.10, it is readily seen that the peak pattern consists of a dominating Na^+ peak (m/z 23) superimposed on the complex pattern that is typical for PS-like structures. Otherwise stated, the intense signals due to the sulfonated repeat unit of PSS component that have been detected in the pristine (cf. Figure 5.7) layer are no longer detected after laser ablation. It looks like the laser

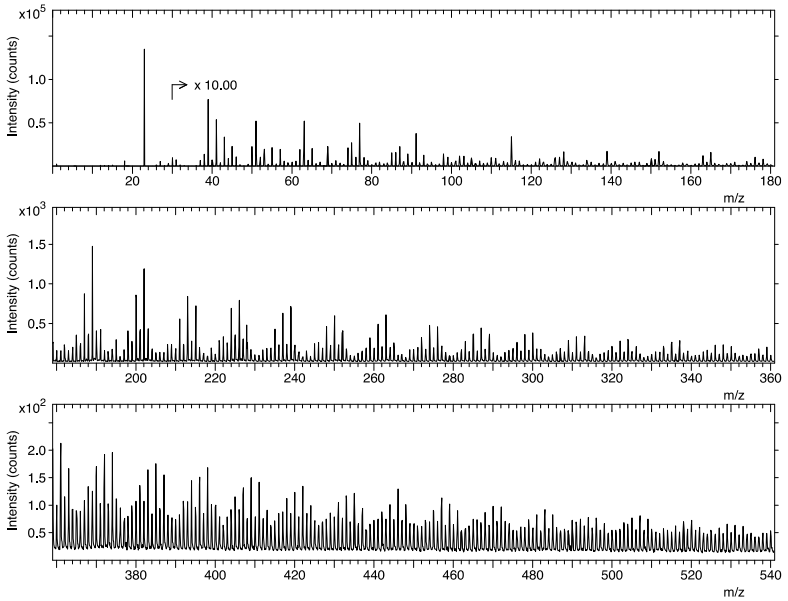

Figure 5.10: Positive ion mass spectrum recorded by TOF-S-SIMS from the crater after laser ablation (10 pulses).

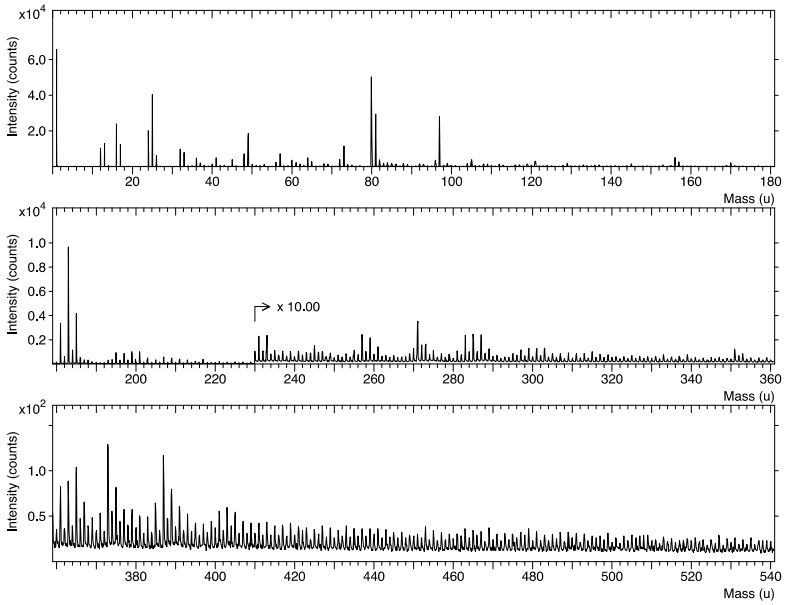

Figure 5.11: Negative ion mass spectrum recorded by TOF-S-SIMS from the crater after laser ablation (10 pulses).

ablation induces thermal degradation of the components in the subsurface, thereby leaving the PS backbone structures at the bottom of the crater. This behavior is confirmed from the negative secondary ion mass spectrum in Figure 5.11. Comparison with the spectrum in Figure 5.9 reveals that again the prevalent dominance of the peaks related to sulfonated PS is largely reduced in the ablated area. These measurements do not yet allow the precise mechanism occurring as a result of laser ablation to be determined. Specifically, distinction between partial decomposition of the PEDOT:PSS layers and the occurrence volatilisation and re-deposition of modified PEDOT:PSS (fragments) cannot be made. However, the SEM micrographs after laser ablation (Figure 5.5(c)) do not reveal the presence of small particles, when applying a magnification of 10000x. Therefore, if redeposition occurs, these particles should be smaller than app. 50 nm, which makes them very difficult to be observed.

Diener oxygen plasma treatment of the laser ablated area was executed in order to remove the remaining layer(s) after laser ablation. The analysis of the treated surface with TOF-S-SIMS yielded similar spectra as the one recorded for the laser ablated PEDOT:PSS samples as shown in Figure 5.10 and Figure 5.11. Even an exposure during 5 minutes has not allowed the PEDOT:PSS fragments to be removed from the laser ablated crater. However, a mild RIE treatment (1 minute) of the laser ablated area results in a completely different positive ion mass spectrum as depicted in Figure 5.12. Specifically, the low m/z range contains abundant signals from Na^+ (m/z 23), Si^+ (m/z 28) and $SiOH^+$ (m/z 45). Interestingly, the prevalent high m/z signals refer to adducts of structural units present in the surface layer of the sample according to the systematic that is typical for inorganic speciation [18]. For instance, the ions at m/z 121, 181, 241 and 301 are due to $(SiO_2)n.H^+$, the ions at m/z 199, 259 and 319 refer to $(SiO_2)n.H_2O.H^+$ and the ions at m/z 201, 261 and 321 are due to $Si_3N_4.(SiO_2)m.H^+$. The numerous organic signals from the PS-like structures seen before (cf. Figure 5.10) vanish almost completely.

The negative ion mass spectrum in Figure 5.13 contains an intense signal at m/z 19 due to F^-. Apparently, the RIE treatment causes contamination of the surface due to the presence of residual trifluoromethane from previous processing steps. The remaining prominent signals are due to logical adducts of SiO_2 such as $(SiO_2)n.O^-$ detected at m/z 76, 136 and 196, $(SiO_2)n.OH^-$ detected at m/z 77, 137, 197 and 257 and $(SiO_2)n.Na_2O.OH^-$ detected at m/z 139, 199 , 259 and 259. The presence of a signal at m/z 79 due to $Na_2O.OH^-$ fits with

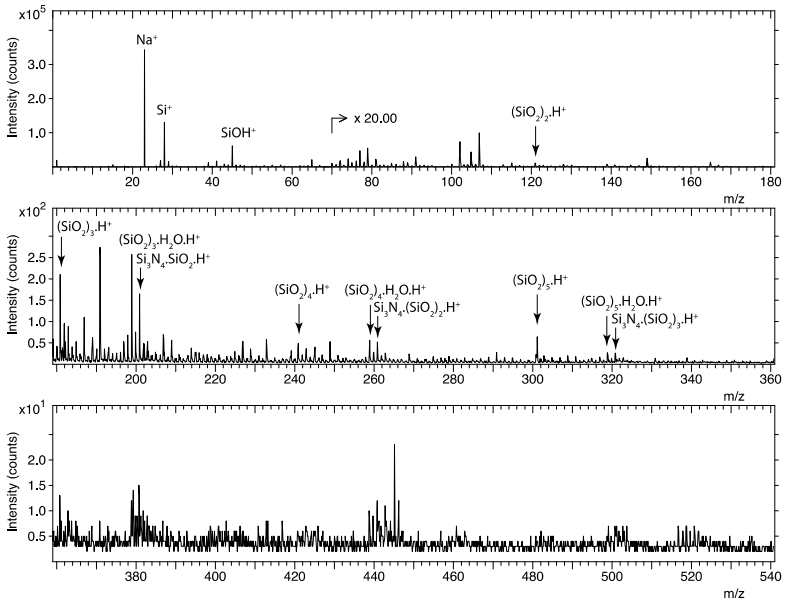

Figure 5.12: Positive ion mass spectrum recorded by TOF-S-SIMS from the crater after laser ablation (10 pulses) and subsequent RIE treatment (1 minute).

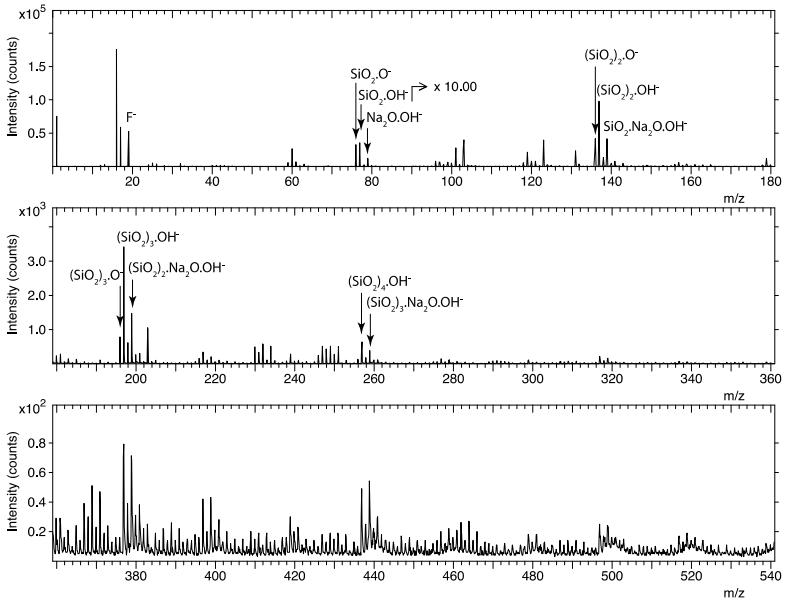

Figure 5.13: Negative ion mass spectrum recorded by TOF-S-SIMS from the crater after laser ablation (10 pulses) and subsequent RIE treatment (1 minute).

the observation of the higher m/z ions as well as the prominent Na^+ signal in the positive ion mass spectrum. The detection of SiO_2 based adducts in the negative as well as in the positive ion detection mode can be ascribed to an oxidized silicon nitride surface since silicon nitride surfaces are prone to oxidation in atmospheric environment [19, 20]. Finally, the organic signals originating from PSS like structures at m/z 156, 157, 170, 183 and 185 vanished almost completely in the negative spectrum (Figure 5.13).

Summarizing, the information contained in the mass spectra is consistent with the idea that the RIE treatments lead to the complete removal of residual PEDOT:PSS and /or the corresponding decomposition products generated by laser ablation. Therefore, we can conclude that the proposed laser ablation process followed by a mild RIE treatment is sufficient to completely remove (monolayer level) the PEDOT:PSS layer, without physically damaging the underlying silicon nitride layer.

5.5 Conclusions

The laser patterning of thin films of PEDOT:PSS on a multi-layered barrier and a flexible substrate has been carried out successfully. An area of about 1 mm × 1 mm was selectively patterned using an excimer laser. No debris and no damage on the underlying silicon nitride inorganic barrier layer have been observed using optical microscopy and SEM. Investigation of laser ablated area with TOF-S-SIMS has allowed the process to be described with unseen chemical specificity as opposed to the traditionally used characterization methods. Specifically, the excimer treatment of the PEDOT:PSS layer has been found to result in the prevalent presence of decomposition products of the PSS component. Basically, the sulfonate groups are removed leaving a PS-like structure. Additional treatment with RIE removes the remnants of the organic (decomposition) layer, exposing an oxidised silicon nitride surface. Although, it can not yet be concluded with certainty that the organic layer left after laser ablation treatment is the result of incomplete ablation or re-deposition, it is clear that the use of TOF-S-SIMS yields an interesting approach to obtain substantially refined insight in comparison to the optical and morphological characterisation of the craters.

References

[1] A. Berntsen, P. van de Weijer, Y. Croonen, C. Liedenbaum, and J. Vleggaar, "Stability of polymer light-emitting diodes", *Philips Journal of Research*, vol. 51, no. 4, pp. 511–525, 1998. [Online].

[2] S. A. Van Slyke, C. H. Chen, and C. W. Tang, "Organic electroluminescent devices with improved stability", *Applied Physics Letters*, vol. 69, no. 15, pp. 2160–2162, 1996. [Online].

[3] R. Gill, P. van de Weijer, C. Liedenbaum, H. Schoo, A. Berntsen, *et al.*, "Stability and characterization of large area polymer light-emitting diodes over extended periods", *Optical Materials*, vol. 12, no. 2, pp. 183–187, 1999. [Online].

[4] C. Charton, N. Schiller, M. Fahland, A. Hollander, A. Wedel, *et al.*, "Development of high barrier films on flexible polymer substrates", *Thin Solid Films*, vol. 502, no. 1, pp. 99–103, 2006. [Online].

[5] Z. Popovic, S. Xie, N. Hu, A. Hor, D. Fork, *et al.*, "Life extension of organic LED's by doping of a hole transport layer", *Thin Solid Films*, vol. 363, no. 12, pp. 6–8, 2000. [Online].

[6] J.-H. Lee, M.-H. Wu, C.-C. Chao, H.-L. Chen, and M.-K. Leung, "High efficiency and long lifetime OLED based on a metal-doped electron transport layer", *Chemical Physics Letters*, vol. 416, no. 46, pp. 234–237, 2005. [Online].

[7] C.-S. Li, S.-H. Su, H.-Y. Chi, Z.-B. Li, and M. Yokoyama, "Enhancing the lifetime of field-emission organic light-emitting diodes using a cavity structure", *Thin Solid Films*, vol. 517, no. 17, pp. 5330–5332, 2009. [Online].

[8] X. Zhang, Z. Wu, D. Wang, D. Wang, and X. Hou, "Improving the stability of organic light-emitting devices using a solution-processed hole-injecting layer", *Applied Surface Science*, vol. 255, no. 18, pp. 7970–7973, 2009. [Online].

[9] H. Aziz and G. Xu, "A degradation mechanism of organic light-emitting devices", *Synthetic Metals*, vol. 80, no. 1, pp. 7–10, 1996. [Online].

[10] Z. D. Popovic, H. Aziz, N.-X. Hu, A.-M. Hor, and G. Xu, "Long-term degradation mechanism of tris(8-hydroxyquinoline) aluminum-based organic light-emitting devices", *Synthetic Metals*, vol. 111, pp. 229–232, 2000. [Online].

[11] E. Lay, D.-S. Wuu, S.-Y. Lo, R.-H. Horng, H.-F. Wei, *et al.*, "Permeation barrier coatings by inductively coupled plasma {CVD} on polycarbonate substrates for flexible electronic applications", *Surface and Coatings Technology*, vol. 205, no. 17, pp. 4267–4273, 2011. [Online].

[12] J. Laubender, L. Chkoda, M. Sokolowski, and E. Umbach, "The influence of oxygen and air on the characteristics of organic light-emitting devices studied by in vacuo measurements", *Synthetic Metals*, vol. 111, pp. 373–376, 2000. [Online].

[13] J. S. Lewis and M. S. Weaver, "Thin-film permeation-barrier technology for flexible organic light-emitting devices", *Selected Topics in Quantum Electronics, IEEE Journal of*, vol. 10, no. 1, pp. 45–57, 2004. [Online].

[14] S. Kirchmeyer and K. Reuter, "Scientific importance, properties and growing applications of poly(3,4-ethylenedioxythiophene)", *Journal of Materials Chemistry*, vol. 15, pp. 2077–2088, 21 2005. [Online].

[15] U. Lang, E. Muller, N. Naujoks, and J. Dual, "Microscopical Investigations of PEDOT:PSS Thin Films", *Advanced Functional Materials*, vol. 19, no. 8, pp. 1215–1220, 2009. [Online].

[16] G. Greczynski, T. Kugler, and W. Salaneck, "Characterization of the PEDOT PSS system by means of X ray and ultraviolet photoelectron spectroscopy", *Thin Solid Films*, vol. 354, no. 1, pp. 129–135, 1999. [Online].

[17] G. Greczynski, T. Kugler, M. Keil, W. Osikowicz, M. Fahlman, *et al.*, "Photoelectron spectroscopy of thin films of PEDOT PSS conjugated polymer blend a mini-review and some new results", *Journal of Electron Spectroscopy and Related Phenomena*, vol. 121, no. 1, pp. 1–17, 2001, Electron Spectroscopy of polymer surfaces. [Online].

[18] H. Struyf, L. Van Vaeck, P. Kennis, R. Gijbels, and R. Van Grieken, "Chemical Characterization of Neo-ceramic Powders by Time-of-flight and Fourier Transform Laser Microprobe Mass Spectrometry", *Rapid Communications in Mass Spectrometry*, vol. 10, no. 6, pp. 699–706, 1996. [Online].

[19] S. Raider, R. Flitsch, J. Aboaf, and W. Pliskin, "Surface Oxidation of Silicon Nitride Films", *Journal of The Electrochemical Society*, vol. 123, no. 4, pp. 560–565, 1976. [Online].

[20] H. Du, R. Tressler1, K. Spear1, and C. Pantano, "Oxidation Studies of Crystalline CVD Silicon Nitride", *Journal of The Electrochemical Society*, vol. 136, no. 5, pp. 1527–1536, 1989. [Online].

6

Ultra-short Laser Pulses for Thin Film Patterning

The previous chapters were focused on nanosecond laser patterning of thin organic films. In those studies, thin films patterning was carried out with 248 nm UV nanosecond excimer laser; either for scribing lines, structuring / patterning OLED layers or patterning areas. Now, it is interesting to investigate thin film patterning with ultrashort pulses instead of nanosecond pulses. In this chapter, the focus is on picosecond laser patterning of thin organic films with 355 nm, 532 nm and 1064 nm wavelengths. The patterning of the PEDOT:PSS and Plexcore (poly(thiophene-3-[2[(2-methoxyethoxy)ethoxy]-2,5-diyl])) thin organic films is investigated using picosecond pulses on rigid glass as well as on flexible barrier substrates.

6.1 Introduction

The nanosecond laser pulses have the major problem of thermal damage (heat affected zone) and edge quality of the patterned grooves. In case of such longer pulses, there is sufficient time for thermal diffusion to melt the material rather than to vaporize, however it is not the case with shorter pulses or ultrafast pulses. The benefits of using ultrafast pulses (picosecond or famtosecond) over longer pulses (nanonsecond)

are reduction of laser fluence, improvement of the contour sharpness of laser generated structures and very low collateral heat effects [1].

The picosecond laser ablation of optically transparent materials is assumed to be a combination of photochemical induced dissociation and photothermal process due to relaxation of excited polymer [2]. As compared to nanosecond pulses lower ablation thresholds are obtained with picosecond pulses, which can be attributed to the higher intensities of shorter pulses. The application driven towards organic electronics needs not only the ablation of polymer thin films but the selective patterning without damaging the underneath layer. Picosecond and nanosecond laser structuring of thin films (TCOs, organic layers and metal layers) for the organic electronics are studied by A. Schoonderbeek et al.[3]. An economical feasible processing speed and reproducibility is necessary for the industrial applications. In particular, the picosecond laser patterning of OLED layers on flexible substrates for solid state intelligent lighting applications has been reported [4]. In their investigation, a stress induced photomechanical ablation mechanism was assumed to be responsible for the selective removal of thin films on a barrier stack. On the same vein, selective patterning of thin organic layers using Ti:Sapphire, 150 fs laser with pulse repetition rate of 1 kHz on a flexible substrate has been studied [5]. It is interesting to mention that the layer removal is not partial, either a complete layer has been removed or no ablation is observed, which they call "almost digital" removal and the mechanism is termed as "step like ablation". The selective ablation studies on multilayer systems (150 nm thin indium tin oxide (ITO), 200 nm thin polyaniline (PANI) on 1 µm thick photo resist; and 280 nm Poly(p-phenylene vinylene)(PPV)/ PEDOT layer-combination on 150 nm thin ITO) at different wavelength and pulse duration combinations have been reported [6]. From this study, a strong pulse duration dependence on the ablation threshold has been noticed, which is an indication for the observed difficulties using nanosecond laser pulses. Comparative studies at different wavelengths demonstrate that laser pulses in the UV are not necessarily always a first choice to achieve a precise removal of the optically transparent top layer. The picosecond laser pulses are successfully used for patterning of the thin film solar cells based on Copper Indium Gallium Selenide (CIGS) technologies[7], i.e. inorganic materials. However, the present interest is not only in picosecond pulses but also organic thin films, which is a relatively difficult task. Moreover, the patterning of inorganic material on organic substrates with picosecond pulses has been very

successful. For instance, the pulsed picosecond laser ablation of indium tin oxide (ITO) coated on a flexible polyethylene terephthalate (PET) substrate has been investigated[8]. They compared the ablation results with picosecond pulses at different wavelengths, 355 nm, 532 nm and 1064 nm, and it has been observed that the fundamental 1064 nm wavelength with back-side irradiation demonstrates better performance compared to second harmonic (532 nm) and third harmonic (355 nm) wavelengths. A similar comparative study of picosecond laser patterning of ITO thin films for OLED applications using 355 nm, 532 nm and 1064 nm irradiation has been carried out, in which the better groove quality was obtained for 1064 nm wavelength [9]. Therefore, from these studies it has been concluded that 1064 nm wavelength with picosecond pulses shows better results for inorganic material as compared to its harmonics. To summarize, the organic thin films patterning for OLED / OPV applications with picosecond pulses has not been explored much, hence it needs more investigation to understand the mechanisms and to optimize the ablation process.

In this chapter, thin organic films like PEDOT:PSS and Plexcore are investigated on glass / flexible barrier foil substrates. PEDOT:PSS has been discussed in the previous chapters, but Plexcore is a new material to be introduced in this study. Plexcore (poly(thiophene-3-[2[(2-methoxyethoxy)ethoxy]-2,5-diyl)) is an organic conductive ink developed by Plextronics[10], which is used as hole injection layer (HIL) in organic electronics devices. In this investigation, a picosecond laser with 355 nm, 532 nm and 1064 nm wavelengths is used. The ablation thresholds for the thin films are determined at different wavelengths. The primary object is to develop the selective ablation processes for patterning the films. The optimization of the ablation process at a particular wavelength is very critical and highly required. The process has been optimized by varying the number of pulses per location, fluence and wavelength of operation. Since Silicon Nitride is widely used as a barrier layer or passivation layer in organic electronics devices, it has been also considered for investigation with picosecond laser pulses. As a result, the thin film selective patterning of Silicon Nitrides on an Indium Tin Oxide (ITO) substrate using 355 nm and 1064 nm picosecond laser has been summarized at the end. The substrate chosen in this case is ITO, as it is a transparent conducting oxide very suitable for anode contacts.

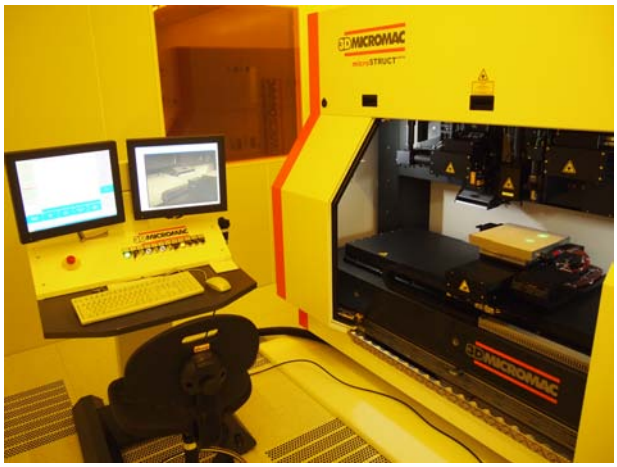

Figure 6.1: Ultrafast laser system used for thin film patterning equipped with automated software and controlling units.

6.2 Picosecond Ablation Set-up

The experiments were conducted with an industrial picosecond laser system provided by 3D-Micromac Aktiengesellschaft, Germany. This workstation is equipped with the Time Bandwidth picosecond laser source. It offers a new level of precision and versatility. This laser source can ablate a wide variety of materials with minimum thermal side effects and with high precision. This picosecond system can provide three wavelengths: 355 nm, 532 nm and 1064 nm. The pulse duration is less than 12 ps, pulse repetition rate of 50 kHz to 8 MHz and pulse energies upto 200 µJ can be reached. The picture of the ultrafast laser system is shown in the Figure 6.1 and a more detailed picture is shown in Figure 6.2. As shown in the Figure 6.2(a), three picosecond laser wavelengths can be obtained: 355 nm, 532 nm, and 1064 nm (Duetto, Time Bandwidth). However, in this system there is an integration of the femtosecond laser which provides 1030 nm wavelength with femtosecond pulses (Amplitude Systems). On the right, Figure 6.2(b) shows three cabinets, at the top is the power supply for the picosecond laser system, the middle cabinet is the power supply for the femtosecond system and the bottom cabinet is the chiller (cooling system). The detailed specifications of these ultafast laser systems can be found in the Chapter 2, Table 2.2.

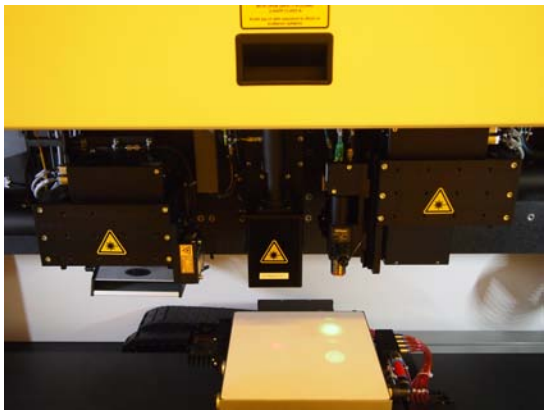

(a) Left: 355 nm, Center: 1030 nm, Right: 532 nm / 1064 nm scanners

(b) Top: Time Bandwidth, Middle: Amplitude Systems, Bottom: Chiller

Figure 6.2: Ultrafast (ps/fs) laser heads, power supplies and chiller.

6.3 Methodology

6.3.1 Sample preparation

Samples of PEDOT:PSS and Plexcore thin films are prepared at Holst Center, the Netherlands; both on rigid glass and flexible barrier substrates. First, the glass substrates (sodalime) were cleaned with standard cleaning procedures (pre-clean, scrub, shower, ultrasonic bath, rinsing and drying in an oven). After cleaning of the glass substrate, samples are prepared with spin coating of the wet materials and followed by drying in an oven. The thicknesses of the PEDOT:PSS and Plexcore thin films after spinning were 100 nm and 60 nm respectively. In the other set of samples, a multilayered barrier is prepared with Plasma Enhanced Chemical Vapor Deposition (PECVD) technique which consists of three layers: (1) Inorganic Silicon Nitride (150 nm) layer, (2) An optical coating for planarization (20 µm), and (3) Silicon Nitride (150 nm) inorganic layer. On top of the multilayer barrier foil, the thin films of PEDOT:PSS and Plexcore were spin coated as in previous case.

6.3.2 Absorption characteristics

In order to understand the ablation mechanisms and selective processing on glass and barrier substrates, the absorption spectra of the thin films were characterized. The absorption characteristics were measured with a LAMBDA 35 UV/Vis Systems (Perkin Elmer) instrument at the Liquid Crystal Display (LCP) Research Group of the Ghent University.

6.3.3 Analysis

Analysis of the ablated regions is carried out with an optical microscope, SEM and non-contact optical profiler. The equipment details has been given in the previous chapters.

6.4 PEDOT:PSS Thin Films

We have started experiments with PEDOT:PSS thin films. In the first part the patterning is performed on a glass substrate, and later the identical experiments were carried out on flexible barrier substrates. The absorption spectrum of the thin film of PEDOT:PSS obtained with the UV-Vis instrument is shown in Figure 6.3. The spectrum indicates clearly that at UV wavelengths there is higher absorption compared to the visible and near IR wavelengths. This is the reason that UV excimer lasers are very successful in the selective patterning of thin organic films [11–13].

A picosecond laser with 355 nm wavelength and 200 kHz pulse repetition rate was used to selectively pattern PEDOT:PSS on glass substrates. The optical microscopic pictures of the selective removal of thin films are shown in Figure 6.4. This figure shows first the onset of thin film removal (Figure 6.4(a)), where the film is not removed completely but ablation is about to start. However on the right image (Figure 6.4(b)), the selective removal of the thin film with the single pulse is clearly visible.

This onset of ablation was observed (Figure 6.4(a)) at the peak fluence of $0.480\,\mathrm{J/cm^2}$ with single pulse rough power scan experiments. The experiments were tuned further with a fine power scan to obtain a suitable range of fluence needed for patterning. The single pulse ablation result as shown in Figure 6.4(b) was obtained at a peak fluence of $1.010\,\mathrm{J/cm^2}$. If we analyze these images, it is inferred that single pulse selective removal of thin film is very clean and

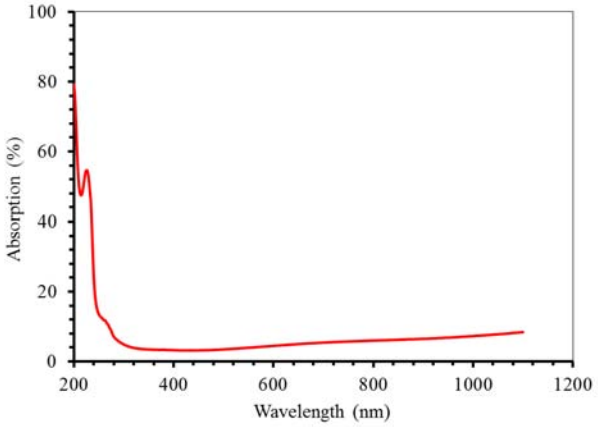

Figure 6.3: PEDOT:PSS thin films absorption spectrum obtained with LAMBDA 35 UV/Vis System on a quartz substrate.

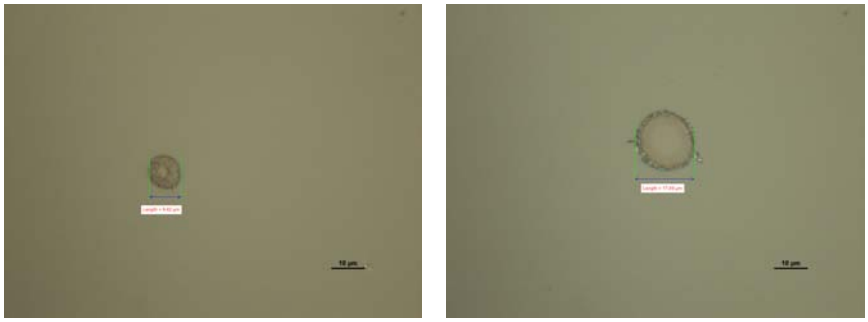

(a) Onset of ablation (b) Single pulse

Figure 6.4: Selective patterning of PEDOT:PSS thin films with picosecond pulses. The spot diameter in (a) is 9 µm and in the part (b) is 17µm.

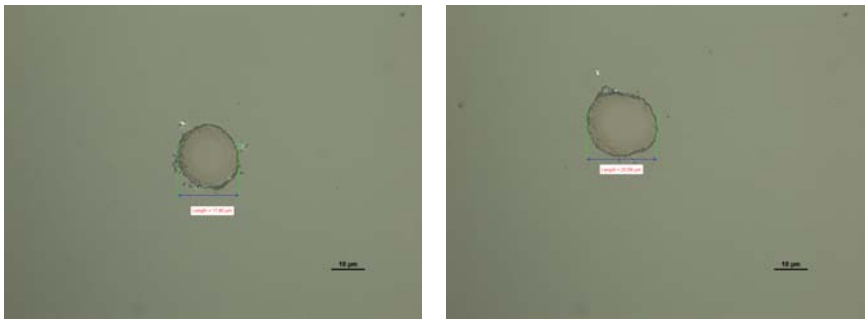

(a) Two pulses (b) Five pulses

Figure 6.5: Multiple static pulse experiment; the diameter of spot: (a) 17 µm with 2 pulses (b) 20 µm with 5 pulses.

debris free. No visible contamination or damage on the substrate is noticed. After determining the fluence range for selective patterning, the multiple pulse static experiments were performed, resulting in no additional information as illustrated in Figure 6.5. At a fixed peak fluence of 1.178 J/cm^2, the experiments were conducted for 1 pulse to 5 pulses per location. The optical microscopic images show that there is only change in the spot diameter, which increases from 17 µm (2 pulses) to 20 µm (5 pulses).

Now, with pulse overlapping it is possible to scribe the lines. Different line patterns were obtained by varying the pulse overlap from 10 % to 50 %. The selective line patterning on a glass substrate was successful and is depicted in Figure 6.6. The peak fluence in this case is 1.178 J/cm^2 and the pulse overlap is 50 %. The first optical microscopic image shows the impression of the laser pulse on the ablated line track, which indicates the re-deposition of debris during the ablation process. The higher fluence could be more effective to remove the complete material from the substrate. On the other hand, the dark field image shows layered removal of the thin films from the substrate. The ablation mechanism is driven by photochemical processes.

Now, changing the wavelength from 355 nm to 532 nm and carrying out the similar experiments for the PEDOT:PSS thin films on a glass substrate. The ablation thresholds are determined with rough and fine power scans with static single pulse experiments at 300 kHz pulse repetition rate. The selective removal of the thin film was successful with single pulse and the results obtained are illus-

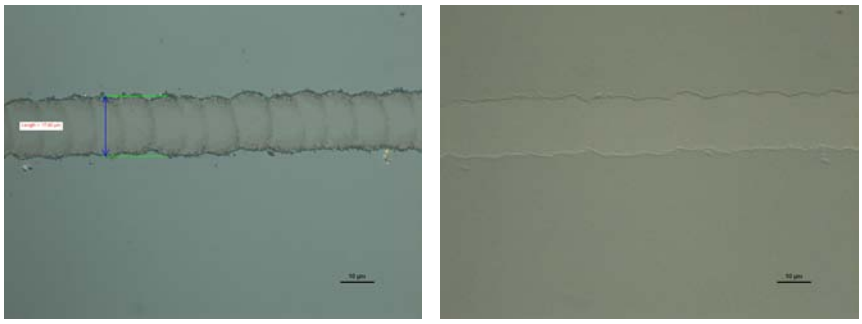

(a) Line patterning (width: 17 µm) (b) Image with dark field

Figure 6.6: Selective line patterning of the PEDOT:PSS thin films with picosecond pulses.

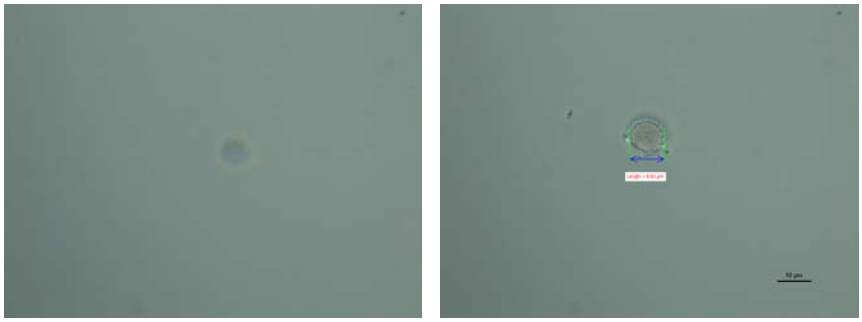

(a) Onset of ablation (b) Selective removal (diameter = 10 µm)

Figure 6.7: The PEDOT:PSS ablation on glass with 532 nm picosecond pulses, indicating onset of the ablation and selective removal with single pulse.

trated in Figure 6.7. The onset of ablation (6.7(a)) was determined with the different power scan experiments, and found at peak fluence of 0.401 J/cm^2, but the actual thin film removal as shown in Figure 6.7(b) is occurred at the fluence of 0.592 J/cm^2. It can be easily noticed that there is a small circular ring shape region around the ablated spot, which is not ablated but a change in the material properties. This particular ring shape has not been observed in case of the 355 nm wavelength experiments (Figure 6.4).

In fact, the optical microscopic images show the layer removal

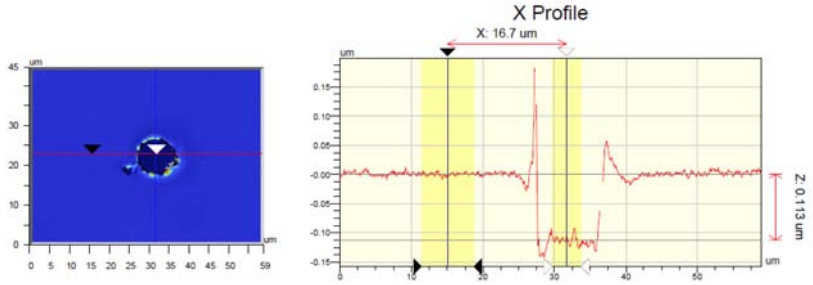

(a) Wyko profile (b) Depth = 113 nm

Figure 6.8: The Wyko NT3300 depth measurement after PEDOT:PSS thin film removal with 532 nm picosecond pulses.

although it is necessary to measure the depth of the ablated regions. One of the depth measurements for such thin films removal has been illustrated in Figure 6.8. The depth measured with a non-contact optical profiler is approximately 113 nm, although the actual thickness of the PEDOT:PSS thin film is about 100 nm. Besides, there are some peaks at the periphery of the crater, which can be attributed to flakes of the thin film after ablation.

After knowing the fluence range for selectively ablating PEDOT:PSS with single pulse experiments, it is the right time to focus on patterning. In this vein, different pulse overlaps with various fluences were applied. It is interesting to visualize the pattern obtained with 532 nm wavelength, one of the such patterned line is shown in Figure 6.9. In these observations, the applied peak fluence is 0.594 J/cm^2 with pulse overlaps 10 % (6.9(a)) and 50 % (6.9(b)).

These results show that there is not a complete removal of thin film at overlapping regions. This is due to the change in material properties with lower energy side-tail of the Gaussian beam. Once the material has been modified or changed with the first pulse, it responds differently for next incoming laser pulses. Therefore, it is possible to observe the complete removal with a single static pulse at the center of the spot, however at the edges there is a deformation of material which is not suitable for patterning applications.

Finally, 1064 nm wavelength is chosen for selective patterning of PEDOT:PSS thin films on glass substrates. A pulse repetition rate of 1000 kHz was found suitable to perform these experiments. The single shot selective ablation of thin film was successful, however at the outer periphery of the ablated region, some area has been deformed

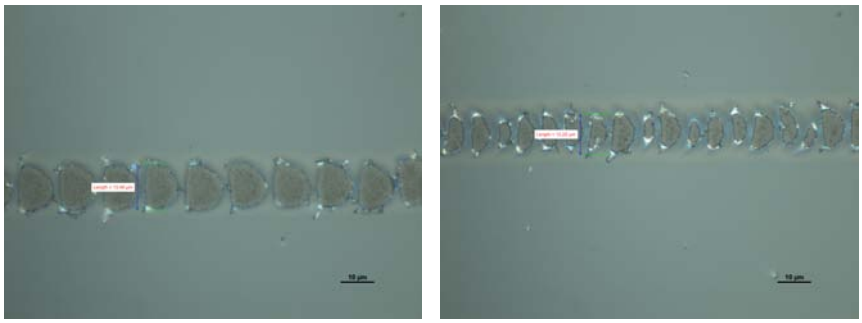

(a) Pulse overlap = 10 % (b) Pulse overlap = 50 %

Figure 6.9: Comparison of the line patterns with different pulse overlaps at 532 nm picosecond pulses.

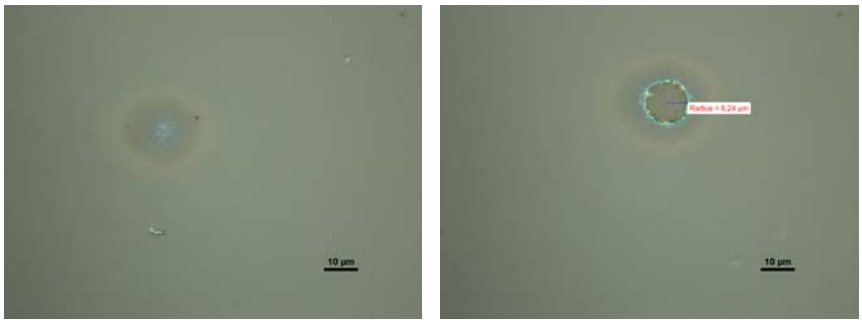

(a) Onset of ablation (b) Single pulse removal (spot = 6 µm)

Figure 6.10: Onset of the ablation and single pulse removal of the PEDOT:PSS thin film on a glass substrate, with 1064 nm picosecond pulses.

or modified after interaction with the laser pulse. This behavior has been already noticed for 532 nm wavelength but in that case the deformed area was comparatively smaller. It has been assumed that the laser beam shape is responsible for this deformation of material, as lower energy of Gaussian beam at both sides is not sufficient to remove the material completely. In addition to this, it was interesting to notice that there is no material removal when the pulses were overlapped more than 50 %, and no line patterning was possible in this case. Consequently, the targeted ablation region was only modified or deformed with laser pulses. In order to investigate the deformation of material, another series of experiments was separately carried out. The PEDOT:PSS samples were prepared on a quartz substrate and experiments were conducted with 1064 nm wavelength picosecond pulses. The thickness of the PEDOT:PSS layer for this study is about 110 nm deposited by spin coating. However, the similar results were obtained on the quartz substrates, as in case of the glass substrates. As mentioned earlier that single pulse selective ablation was possible with these laser parameters, although line patterning and area ablation seems difficult. The single pulse ablation results with 1064 nm wavelength at 1000 kHz are depicted in Figure 6.11. The depth of the crater measured is about 110 nm, which is the same as the thickness of the PEDOT:PSS layer. There are some peaks at the edges which are primarily attributed to the flakes after ablation and also to mention here that the surface roughness of such thin films via spin coating is higher. However, the deep spikes in the depth profiles are associated with artifacts of the measuring device.

During the experiments of thin films patterning at 1064 nm wavelength with picosecond pulses, the deformation / modification of organic material was an important observation for line or area patterns. Some of the deformation results are illustrated in Figure 6.12. From Figure 6.12(a) it is important to deduce that the first pulse has removed the thin film completely at the beginning of the line trace, and as the pulses overlapped the film removal became difficult. In order to evaluate the properties of deformed material, a conductivity (or resistivity) measurement experiment was planned. With the single static pulse, there is material removal at the center of the ablated spot, however only deformation of material was noticed at the edges; so a design was created to make 90 % overlap between pulses. An area was isolated by scanning lines with 1064 nm wavelength and 90 % overlapping of pulses. The pattern for such kind of measurement is shown in the Figure 6.12. The area was isolated with one line scan

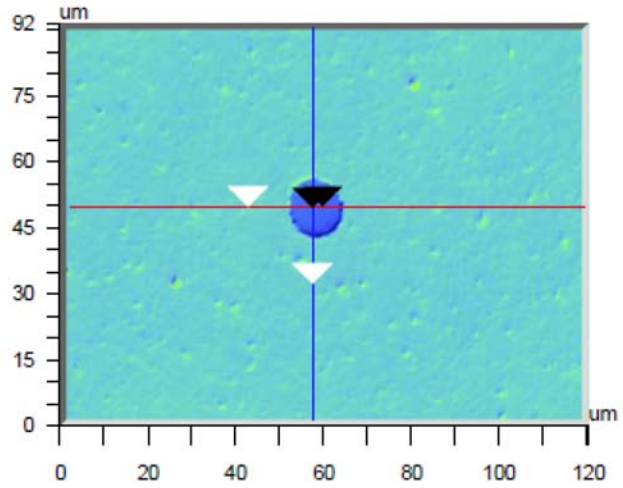

(a) Wyko profile

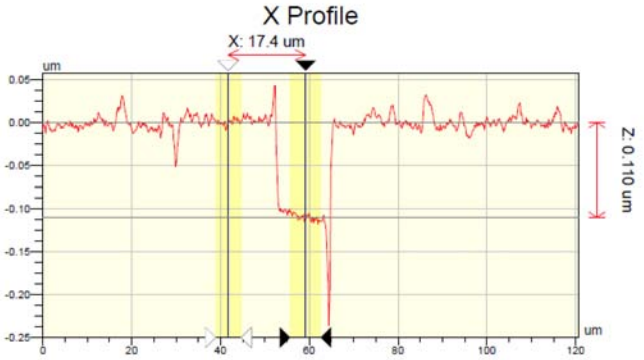

(b) X profile

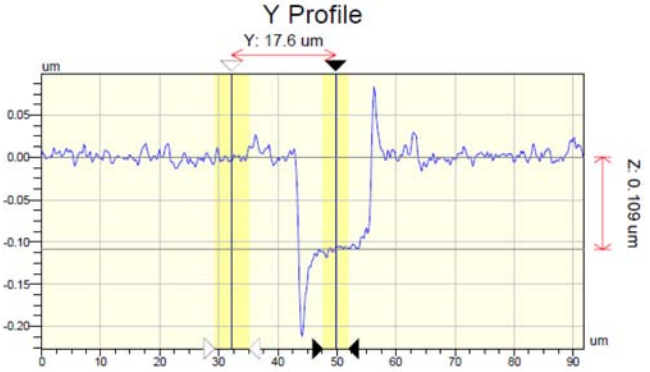

(c) Y profile

Figure 6.11: Selective ablation of PEDOT:PSS on a quartz substrate, with 1064 nm wavelength at 1000 kHz.

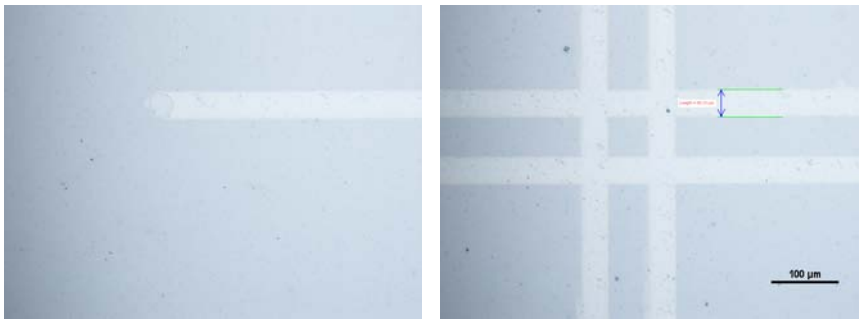

(a) Line trace (width = 40 µm) (b) Isolated area for conductivity measurement

Figure 6.12: (a) Line pattern traces with 1064 nm wavelength at 1000 kHz picosecond pulses. (b) A line pattern design for the isolation of area to measure conductivity / resistance.

and two parallel line scans, in separate experiments. This particular picture is shown for two lines isolation. The resistivity of the deformed area was measured. With a peak fluence of 0.591 J/cm^2 and one line scan, the measured value of resistance is 2.5 MΩ. Moreover, when two lines in parallel were scanned for deformation and isolation of areas i.e. two resistances in series ideally, the measured value of resistance was 4.0 MΩ. When the peak fluence is increased from 0.591 J/cm^2 to 2.105 J/cm^2, the values of resistance were 4.0 MΩ (one line isolation) and 12.0 MΩ (two line isolation). Hence, the material is no more conductive as PEDOT:PSS, it is deformed and possibly can attract some other applications in future.

The ablation thresholds for 355 nm, 532 nm and 1064 nm wavelengths are determined and corresponding plots are shown in Figure 6.13. The values of ablation thresholds from these plots at 355 nm, 532 nm and 1064 nm are 0.297 J/cm^2, 0.431 J/cm^2 and 0.509 J/cm^2 respectively.

After successful patterning of thin films on glass substrates, the experiments were conducted on flexible barrier / foil substrates in a similar fashion. With 355 nm wavelength at 200 kHz single pulse it was difficult to selectively remove the thin PEDOT:PSS film from the barrier foil. At a peak fluence of 0.136 J/cm^2, the single pulse results show only melting of the thin film with foil substrate. The similar investigation results were obtained with 532 nm and 1064 nm wavelengths. Therefore, it is realized that in the picosecond regime

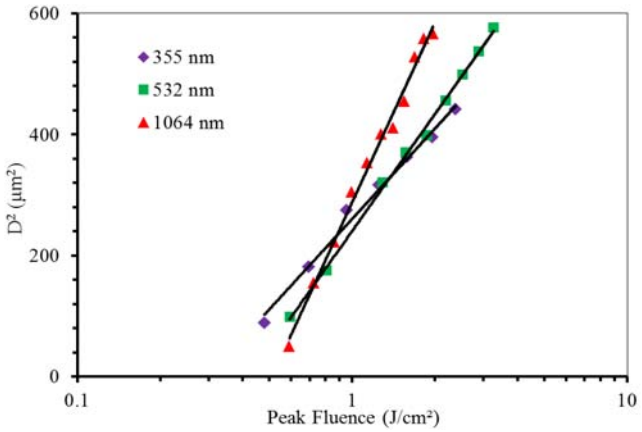

Figure 6.13: Comparison of ablation thresholds of PEDOT:PSS thin film at 355 nm, 532 nm and 1064 nm wavelengths; picosecond pulses.

these wavelengths are not very suitable for thin film patterning on flexible barrier substrates.

6.5 Plexcore Thin Films

Plexcore thin films are commonly used in organic electronics as hole injection layer (HIL), particularly in Organic Light Emitting Diodes or Organic Photovoltaics stacks. The absorption spectrum of the Plexcore thin film as obtained by UV-Vis measurements, is shown in Figure 6.14. The absorption curve shows the higher absorption at UV wavelengths, whereas lower absorption at higher wavelengths.

As in case of PEDOT:PSS thin films, the experiments were performed for Plexcore thin films at three different wavelengths, pulse repetition rates and with static single pulse as well as dynamic patterning. This discussion starts with the results obtained for Plexcore patterning on glass substrates, and later on the investigation on the flexible foil substrates will be discussed. A picosecond laser with 355 nm wavelength at a pulse repetition rate of 200 kHz was used for the thin film ablation on a glass substrate. The onset of ablation occurs at a fluence of 0.460 J/cm^2 with single pulse experiments. A clean removal of thin Plexcore film was obtained with fine power scan tests at a peak fluence of 1.480 J/cm^2. The optical images for

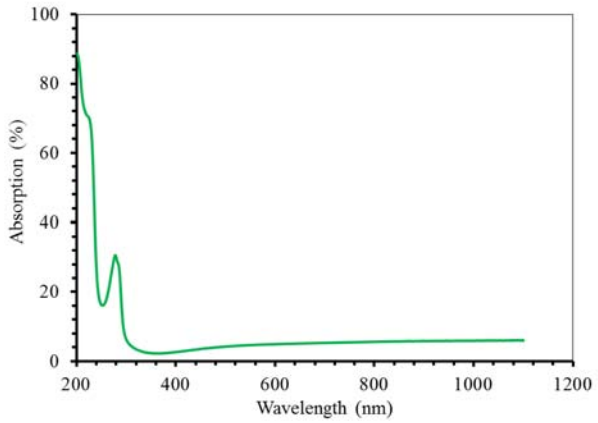

Figure 6.14: Plexcore thin film absorption spectrum obtained with LAMBDA 35 UV/Vis System on a quartz substrate.

the onset and single pulse removal are shown in Figure 6.15. The single pulse selective removal is clean and debris free.

Thereafter, the dynamic line patterning is carried out with different pulse overlap. As with a peak fluence of $1.480\,\mathrm{J/cm^2}$, there is a successful single pulse ablation. Hence, three different fluences $1.217\,\mathrm{J/cm^2}$ (lower), $1.480\,\mathrm{J/cm^2}$ and $1.769\,\mathrm{J/cm^2}$ (higher); are considered and pulse overlaps of 10 %, 20 %, 30 %, 40 % and 50 %; are used for patterning lines. The line patterning results were very successful and a typical patterned line is shown in Figure 6.16. This particular line is patterned at a fluence of $1.480\,\mathrm{J/cm^2}$ with 50 % pulse overlap and pulse repetition rate of 200 kHz. From the optical microscopic image, it can be noticed that the ablated track is clean and debris free. Whereas in the non-contact optical depth profile, the measured depth is approximately 64 nm, which is close to the actual thickness of Plexcore thin film (60 nm). Besides, it is known that the surface roughness is usually high in case of such thin films, deposited via the spin coating method.

In order to have a better visualization of debris and damage on the substrate the SEM micrographs were inspected. For the single pulse (Figure 6.15(b)) and patterned line (Figure 6.16(a)) the SEM micrographs are illustrated in Figure 6.17. From this figure, it is observed that there might be a little damage at the center of the ablated region with single pulse. There are some very tiny particles visible on the ablated region (might be some debris), which is really

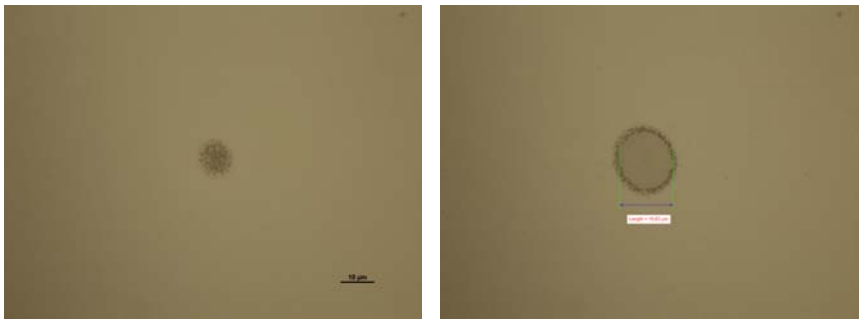

(a) Plexcore: onset of ablation (b) Selective ablation: single pulse

Figure 6.15: Plexcore thin film selective ablation with 355 nm wavelength at 200 kHz picosecond pulses, spot diameter in (b) is 15 µm.

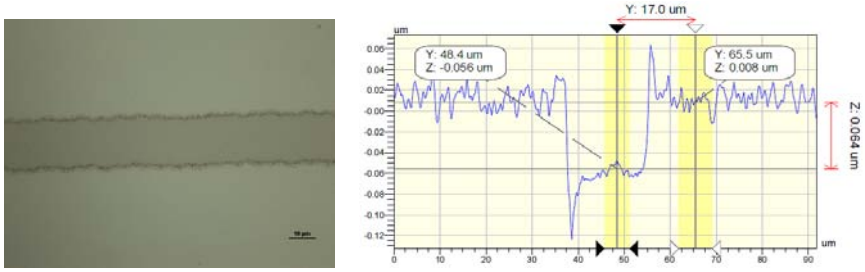

(a) Plexcore: line patterning (b) Depth profile (depth = 64 nm)

Figure 6.16: Plexcore thin film patterning with 355 nm wavelength at 200 kHz picosecond pulses.

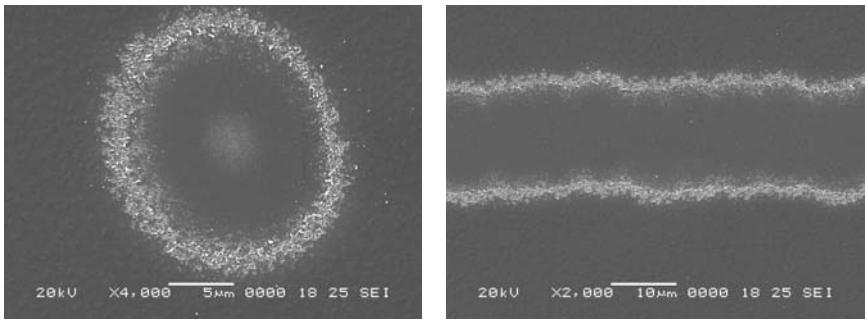

(a) (b)

Figure 6.17: SEM micrographs of Plexcore thin film ablation (a) Single pulse (b) Line patterning.

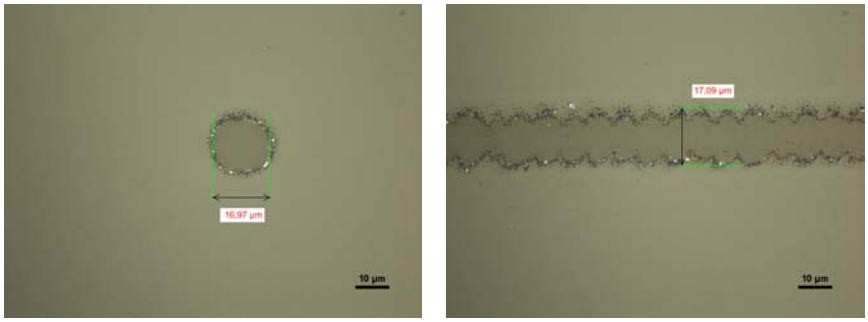

(a) Single pulse (diameter = 17 µm) (b) Line patterned (width = 17 µm)

Figure 6.18: Selective patterning of Plexcore thin film on glass substrate with 532 nm wavelength at 300 kHz picosecond pulses.

very small as the scale bar is only 5 µm. On the other hand, the SEM image of the patterned line does not show any damage on the substrate, albeit there are some tiny particles in this case also. Hence, a peak fluence of 1.480 J/cm^2 with 200 kHz pulse repetition rate and 50 % pulse overlap is found suitable for the patterning of the Plexcore thin films on the glass substrate.

The next stage of experiments were conducted with 532 nm wavelength and 300 kHz pulse repetition rate. The ablation experiments were successful and some of the results are depicted in Figure 6.18.

Finally, Plexcore thin film patterning was investigated with 1064 nm wavelength and at 1000 kHz pulse repetition rate. In case of the

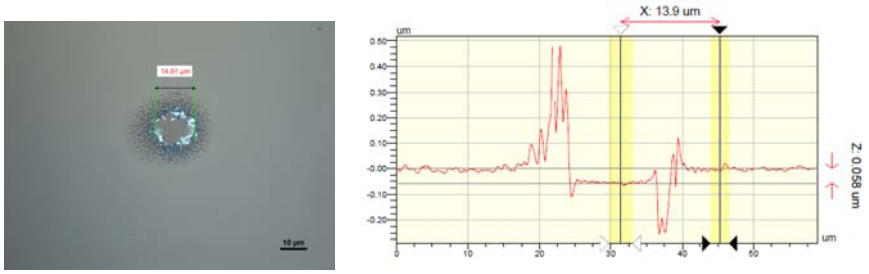

(a) Single pulse (spot = 15 µm) (b) Depth profile (depth= 58 nm)

Figure 6.19: Selective patterning of Plexcore thin film on glass substrate with 1064 nm wavelength at 1000 kHz picosecond pulses.

PEDOT:PSS thin films, only single pulse selective removal were successful with 1064 nm wavelength, similar results were obtained for the Plexcore thin films. The single pulse selective ablation with 1064 nm picosecond pulse was successful and one of the results is shown in Figure 6.19. In this case, the fluence applied is 4.216 J/cm^2, the ablated region is debris free and the depth measured is approximately 58 nm. When the dynamic patterning was used to scribe lines, there was no removal of material. This behavior is also seen in case of the PEDOT:PSS thin films. A comparison of the ablation thresholds for 355 nm, 532 nm and 1064 nm wavelengths is plotted in Figure 6.20. From these plots, the threshold values obtained are 0.454 J/cm^2, 0.376 J/cm^2 and 2.382 J/cm^2 ; for 355 nm, 532 nm and 1064 nm respectively.

The experiments on barrier foil were conducted in the identical manner, but it needs more process optimization to selectively remove the thin organic film from the flexible barrier.

6.6 Silicon Nitride Thin Films

In the next step, we have investigated inorganic Silicon Nitride thin films patterning on ITO substrates. These experiments were conducted at Holst Center, The Netherlands and the results are included here for discussion. The Silicon Nitride thin films act as a barrier, encapsulation layer or passivation layer in organic electronics devices. Silicon Nitride patterning is carried out on ITO substrate with 355 nm and 1064 nm picosecond laser pulses. Unlike the organic Plexcore

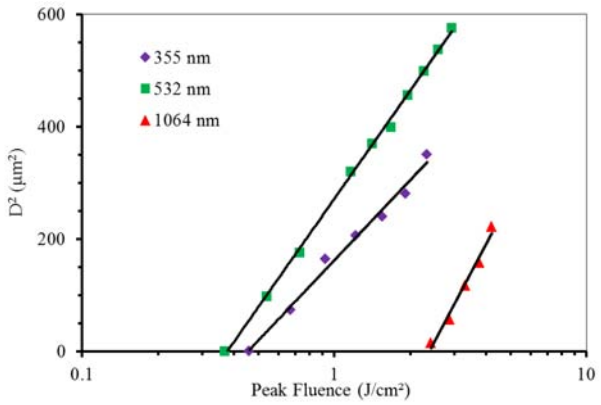

Figure 6.20: Comparison of ablation thresholds of Plexcore thin film at 355 nm, 532 nm and 1064 nm wavelengths with picosecond pulses.

thin films, in this case 1064 nm wavelength picosecond pulses were able to selectively pattern the Silicon Nitride thin film on the ITO substrate. Some of the results are depicted in Figure 6.21(a) (single pulse removal) and Figure 6.21(b) (line patterning), in which the patterned regions are clean and debris free. In this case, the ablation mechanism assumed to be photomechanical in nature. On the other hand, the 355 nm picosecond pulses can not provide the better results for Silicon Nitride patterning on ITO substrate. The successful ablation of Silicone Nitride thin film with 1064 nm can be attributed to the substrate influence on patterning, as the absorption of ITO plays an essential role in this case. Hence, this selective patterning is substrate assisted and it is not always a condition to have higher absorption of the top layer compared to underneath substrate. The single pulse removal is possible with a peak fluence of $0.384\,\mathrm{J/cm^2}$ at a pulse repetition rate of 200 kHz, and the line has been patterned with $0.351\,\mathrm{J/cm^2}$ at the same repetition rate.

6.7 Conclusions

A detailed investigation of thin films patterning at different wavelengths with picosecond pulses was carried out. The ablation thresholds on glass substrates were determined and the process for selective patterning was discussed. The ablation mechanism was driven by a

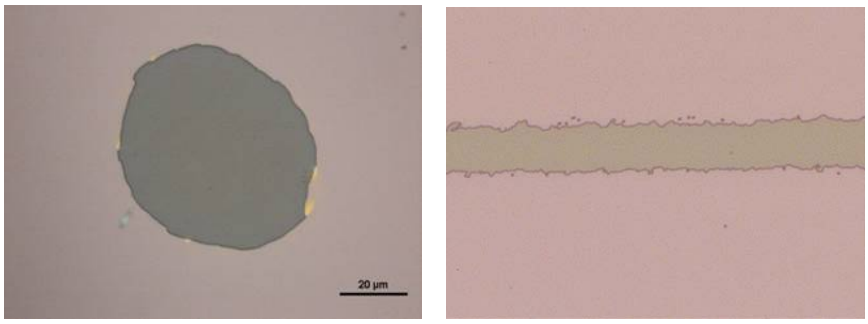

(a) Silicon Nitride single pulse removal (spot size = 70 µm)

(b) Silicon Nitride patterning on ITO

Figure 6.21: Silicon Nitride thin film patterning on ITO substrate with 1064 nm picosecond pulses.

combination of photochemical and photothermal processes in case of organic thin films. In addition, the experiments were also performed for thin films on a flexible barrier foil, however the results were not very encouraging to discuss. The selectivity is a challenging issue in this case and the process still needs further optimization. Amongst three wavelengths, the 355 nm selective patterning was very successful for the PEDOT:PSS as well as for Plexcore thin films. The results with higher wavelength 1064 nm were limited to single pulse selective removal and a deformation behavior was noticed while overlapping the pulses to scribe lines or areas. The inorganic Silicon Nitride thin films were successfully patterned on a ITO substrate with 1064 nm wavelength and the nature of ablation mechanism was assumed to be stress assisted photomechanical. These results are a benchmark for the further process optimization with ultrafast laser systems, in particular to structure and pattern the OLED / OPV stack for industrial mass production integrated with roll-2-roll laser processing.

References

[1] J. Kruger and W. Kautek, "Ultrashort Pulse Laser Interaction with Dielectrics and Polymers", in *Polymers and Light*, ser. Advances in Polymer Science, T. K. Lippert, Ed., vol. 168, Springer Berlin Heidelberg, 2004, pp. 247–290. [Online].

[2] A. Serafetinides, C. Skordoulis, M. Makropoulou, and A. Kar, "Picosecond and subpicosecond visible laser ablation of optically transparent polymers", *Applied Surface Science*, vol. 135, no. 1, pp. 276–284, 1998. [Online].

[3] A. Schoonderbeek, L. Richter, and R. Kling, "Laser Structuring of Thin-Films in Organic Electronics", in *International Exhibition and Conference for Printed Electronics Industry*, Organic and Printed Electronics Association, 2009.

[4] D. Karnakis, A. Kearsley, and M. Knowles, "Ultrafast Laser Patterning of OLEDs on Flexible Substrate for Solid-state Lighting", *Journal of Laser Micro/Nanoengineering*, vol. 4, no. 3, pp. 218–223, 2009. [Online].

[5] R. Mandamparambil, H. Fledderus, G. Van Steenberge, and A. Dietzel, "Patterning of Flexible Organic Light Emitting Diode (FOLED) stack using an ultrafast laser", *Optics Express*, vol. 18, no. 8, pp. 7575–7583, 2010. [Online].

[6] D. Ashkenasi and A. Rosenfeld, in *Processing multilayer systems using femtosecond, picosecond, and nanosecond laser pulses at different wavelengths*, vol. 4637, Proc. SPIE, 2002, pp. 169–179. [Online].

[7] P. Gecys, G. Raciukaitis, E. Miltenis, A. Braun, and S. Ragnow, "Scribing of Thin film Solar Cells with Picosecond Laser Pulses", *Physics Procedia*, vol. 12, Part B, pp. 141–148, 2011. [Online].

[8] S. Xiao, S. A. Fernandes, and A. Ostendorf, "Selective Patterning of ITO on flexible PET Substrate by 1064 nm picosecond Laser", *Physics Procedia*, vol. 12, Part B, pp. 125–132, 2011, Lasers in Manufacturing 2011 - Proceedings of the Sixth International WLT Conference on Lasers in Manufacturing. [Online].

[9] A. Risch and R. Hellmann, "Picosecond Laser Patterning of ITO Thin Films", *Physics Procedia*, vol. 12, Part B, pp. 133–140, 2011. [Online].

[10] "www.plextronics.com", 2014. [Online].

[11] S. Naithani, R. Mandamparambil, F. van Assche, D. Schaubroeck, H. Fledderus, *et al.*, "Influence of barrier absorption properties on laser patterning thin organic films", in *Photonics Europe*, Brussels, Belgium: SPIE, 2012, pp. 843 505–843 509. [Online].

[12] S. Naithani, D. Schaubroeck, Y. Vercammen, R. Mandamparambil, I. Yakimets, *et al.*, "Excimer laser patterning of PEDOT:PSS thin-films on flexible barrier foils: A surface analysis study", *Applied Surface Science*, vol. 280, pp. 504–511, 2013. [Online].

[13] S. Naithani, R. Mandamparambil, H. Fledderus, D. Schaubroeck, and G. V. Steenberge, "Fabrication of a laser patterned flexible organic light emitting diode on an optimized multilayered barrier", *Applied Optics*, vol. 53, no. 12, pp. 2638–2645, 2014. [Online].

7 Mid-infrared Ablation

In the previous chapters, the focus was on the selective patterning of thin organic films with UV (248 nm, 355 nm), visible (532 nm) and near-IR (1064 nm) wavelengths. In this chapter, Resonant mid-Infrared Ablation (RIA) has been introduced as an alternative and promising approach, in which the laser wavelength is tuned to one of the molecular vibrational transitions of the organic material to be ablated. Consequently, the technique is selective in respect of processing a diversity of organic materials which usually have different infrared absorption bands.

7.1 Introduction

Laser ablation proved to be a reliable microfabrication technique for patterning and structuring of both thin film and bulk polymer materials. As most of the polymers absorb very well in the UV and as shorter wavelengths correspond to a better optical resolution of the beam delivery system, UV excimer lasers are very suitable for patterning with micron and even submicron resolution [1, 2]. This is in particular the case when the machined substrate is a polymer since this material features a low thermal conductivity, extremely high UV absorption, and the ability to decompose photochemically. During this photochemical ablation process, the incident photons have suffi-

ciently high energy to directly break main chain bonds, restricting the temperature rise, and the extent of thermal damage to the substrate [3]. These UV lasers are suitable for structuring and patterning of thin films and particularly relevant for organic electronics. Ultraviolet lasers have proven their full potential for patterning single organic layers [4], but in a multilayer organic device the obtained layer selectivity is limited as all organic layers show high UV absorption. That a purely thermal process can produce effective polymer ablation has been confirmed by a number of investigations using long wavelength CO_2 lasers, in which the photons couple to vibrational modes of the molecule [5].

A promising approach named resonant infrared laser ablation (RIA) was introduced at the beginning of the 21st century [6]. This method uses a short pulse mid-infrared laser system, which can be wavelength tuned to one of the molecular vibrational transitions of the polymer to be ablated. As a result, the technique is selective in respect of ablating a diversity of polymers, which usually have different infrared absorption bands. So far most of the studies have been carried out using a free electron laser (FEL), providing picosecond pulses tunable between 2 µm to 10 µm [6, 7]. However, in most applications, FELs are not practical since they are coupled to huge and expensive accelerators. Therefore, new technologies are being developed to replace FELs by bench-top solid-state photonic sources[8, 9]. Most of the resonant infrared ablation (RIA) studies have been focused on the applications in thin film deposition [10, 11] and matrix-assisted laser desorption/ ionization mass spectroscopy [12, 13]. However, the utilization of RIA in the patterning of thin films has not been reported so far. Moreover, RIA can be integrated with roll-to-roll (R2R) processes for patterning organics electronics.

In this chapter, we present mid-infrared resonant ablation of Poly (methyl methacrylate)(PMMA) employing nanosecond laser pulses tunable between 3 µm and 4 µm. The material PMMA has been chosen due to its versatile applications in science and technology. Knowing the importance of PMMA, it has been investigated significantly using different laser wavelengths and pulse-lengths[14–17]. The RIA nanosecond laser set-up used in this study is based on a commercial laser at 1064 nm pumping a singly resonant Optical Parametric Oscillator (OPO) built around a Periodically-Poled Lithium Niobate (PPLN) crystal with several Quasi Phase Matching (QPM) periods. This source delivers more than 0.30 W of mid-IR power, corresponding to 15 µJ pulses. Furthermore, mid-IR resonant ablation has been

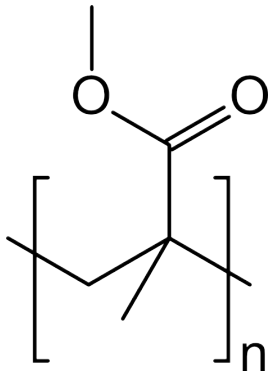

Figure 7.1: Chemical structure of PMMA:$(C_5O_2H_8)n$.

successfully implemented for patterning thin films of PMMA on a glass substrate, which provides a base of using this technique for patterning applications, where selective removal is very crucial. This study is the proof-of-concept of using RIA as a pattering technique for organic material, and the concept will be utilized in the next chapter (Chapter 8) for patterning OPV thin films.

7.2 Poly(methyl methacrylate):PMMA

Poly(methyl methacrylate) is a synthesized transparent thermoplastic, which is durable and lightweight. It has a wide range of applications such as a transparent glass, medical implants [18–20], microfluidics[21–24], optical media (CDs and DVDs), semiconductor industry (as resist) and in day-light reflection panels. The chemical formula of PMMA (IUPAC:Poly(methyl 2-methylpropenoate)) is $(C_5O_2H_8)$n and its structure is shown in Figure 7.1. PMMA has a density varying from 1.17 mg/cm^3 to 1.20 mg/cm^3, and its glass transition temperature is 105 °C[25]. The transmission of a 3 mm thick PMMA sheet is up to 92 % for the visible light, and surface reflection is about 4 % due to its refractive index (1.4905 at 589.3 nm) [26].

7.3 Tunable Mid-IR Ablation Set-up

The experimental mid-IR laser set-up, as schematically shown in Figure 7.2, is based on a commercial laser at 1064 nm, pumping with 15 ns pulses a singly resonant Optical Parametric Oscillator (OPO)

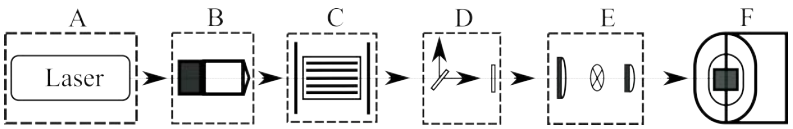

Figure 7.2: Schematic diagram of the mid-IR ablation set-up consisting of six sub-divisions: (A) pump laser (B) attenuator / isolator (C) OPO / wavelength conversion unit (D) filtering section (E) beam delivery unit (F) motorized sample stage.

built around a Periodically-Poled Lithium Niobate (PPLN) crystal with several Quasi Phase Matching (QPM) periods. In the OPO cavity, the signal can oscillate between 1500 nm to 1650 nm, corresponding to idler wavelengths from 3660 nm to 3000 nm. Coarse wavelength tuning can be obtained by translating the PPLN crystal, thus changing the QPM periods. Moreover, wavelength fine tuning is achieved by heating the crystal, which allows us to achieve a continuous wavelength tuning between 3000 nm and 3660 nm, by combining both (coarse and fine) wavelength tunings. Taking into account the various filters used after the OPO cavity to remove the remaining pump and signal photons, this OPO delivers more than 0.30 W of mid-IR power at 20 kHz repetition rate, which corresponds to 15 µJ pulses.

The laser source was delivered from Thales Research and Technology and the processing set-up was build at our laboratory. The photograph of the bench top mid-IR laser ablation set-up used in these experiments is shown in Figure 7.3, in which the beam path is represented by an arrow. The signal wavelength is projected to a free space fiber coupler, which is eventually connected to an Optical Spectrum Analyzer (OSA). The signal wavelength is measured using an OSA and the corresponding idler wavelength is calculated. In the ablation set-up, the laser beam was focused on the target sample by a beam delivery system consisting of an IR microscopic objective (Edmund Optics, 3.75 µm CWL, 6 mm FL ZnSe). The samples were mounted on a motorized rotational stage, allowing a controlled amount of laser shots per spot. The ablation experiments for the bulk PMMA sheets were conducted for non-resonant wavelength (3.20 µm) and resonant (3.34 µm, 3.39 µm) wavelengths. In case of PMMA thin film patterning on a glass substrate, the resonant (3.39 µm) wavelength was selected. A pulse repetition rate of 20 kHz, 165 mW output power, with different ablation speeds of 1 mm/s to 50 mm/s, were

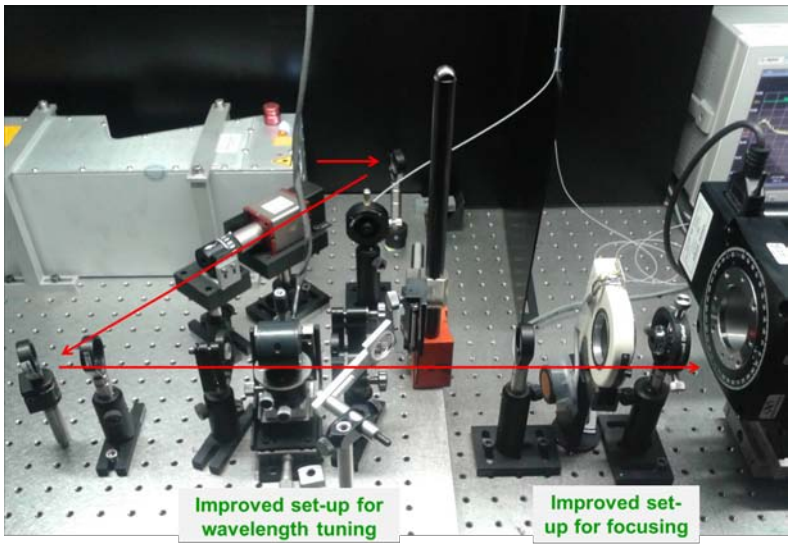

Figure 7.3: Photograph of the bench-top mid-IR tunable high power nanosecond ablation set-up (schematic is illustrated in Figure 7.2).

used during these experiments.

7.4 Methodology

7.4.1 Sample preparation

Bulk sheets and thin films of PMMA were prepared for resonant and non-resonant mid-infrared ablation experiments. First, bulk sheets of PMMA (Good fellow, PMMA Acrylic sheet, 750 µm) were used for the demonstration of the Resonant Infrared Ablation technique. These PMMA sheets are pure and acrylic rubber modified. Next, in order to investigate selective laser patterning of thin films, samples with thicknesses of 650 nm and 1300 nm were prepared. For this application, a specific PMMA solution in anisole (950 PMMA A resist) was purchased from MICROCHEM technology (Germany). It is pure PMMA (molecular weight Mw 950,000 g / mol.) dissolved in Anisole. The thin films were obtained by spin coating on a glass substrate (2 inch × 2 inch). Anisole (Bp 154 °C) has been removed by evaporation at high temperature (180 °C, 90 second) on a hot plate immediately after spin coating.

7.4.2 Infrared spectral characterization

The infrared (IR) absorption spectra of the PMMA materials were obtained by ATR-IR (Attenuated Total Reflection InfraRed) spectroscopy, using a Bio-Rad 575c FT-IR spectrometer equipped with a golden gate module. The spectrum consists of 32 scans with a resolution of $4\,cm^{-1}$. These measurements were carried out in the department of Chemistry, at Ghent University.

7.4.3 Analysis

The ablated craters were first inspected with an optical microscope. Thereafter, the crater depths were measured with a non-contact optical profiler (Wyko NT3300) and a mechanical profiler (Dektak 150). Scanning electron microscope (SEM) analysis was performed on a JEOL JSM-5600. The apparatus was used in the secondary electron mode. Prior to analysis, all samples were coated with a thin gold layer (20 nm) via plasma magnetron sputter coating.

7.5 Results and Discussion

A detailed mid-IR absorption spectrum of PMMA obtained by ATR-IR spectroscopy is illustrated in Figure 7.4. It is observed from this figure that there is a maximum peak of absorption at wavelength 3.39 µm which corresponds to the C-H asymmetric stretch in CH_3. Next, a medium absorption peak at 3.34 µm (C-H asymmetric stretch in CH_2) is also noticed. Given the tunability of the laser, we are able to address both peaks, as well as a wavelength of 3.20 µm which corresponds to minimum absorption in this specific mid-IR range of PMMA.

7.5.1 Bulk sheets

Experiments on bulk PMMA sheets at the above mentioned resonant and non-resonant absorption wavelengths were performed with various amounts of laser shots. A comparative and qualitative study at three wavelengths has been carried out keeping all other laser parameters (fluence, pulse energy, focusing conditions) fixed.

The quality of the grooves obtained after mid-IR experiments at different wavelengths is illustrated in Figure 7.5. After ablation at the lowest absorption wavelength (3.20 µm), it is observed that

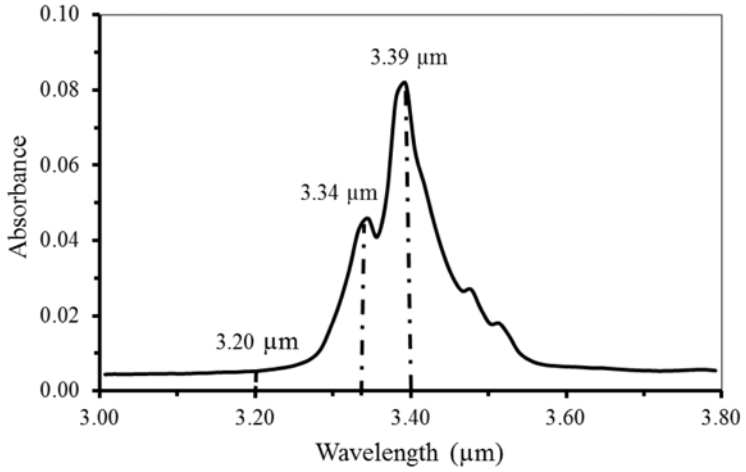

Figure 7.4: Mid-infrared absorption spectrum of PMMA indicating a highest peak of absorption at 3.39 µm, a lower peak at 3.34 µm and minimum absorption at 3.20 µm.

the rim width is more pronounced and the ablated crater depth is shallow (See Fig. 7.5 (a)). As the wavelength is tuned to the medium absorption wavelength (3.34 µm), the width and depth of the ablated crater increases (Fig. 7.5 (b)). Interestingly, few tiny particles in the ablated region are present which are attributed to trapped air bubbles during the resolidification of material from the molten state. Finally, at the resonant wavelength (3.39 µm), it can be clearly noticed (Fig. 7.5 (c)) that the ablated grooves width increases further. Moreover, the region is free of debris and / or redeposited particles.

By plotting the ablation depth versus translation speed, or amount of pulses, the ablation behavior of PMMA can be quantified. Results are summarized in Figure 7.6 and Figure 7.7 for the three different wavelengths of operation. Indeed, as expected, the influence of the wavelength on ablation is significant.

Now, if we compare the slopes in the Figure 7.7, the influence of the laser wavelength on the ablation rate (amount of material removed per laser pulse) is clearly noticeable. The ablation rate varies from 54 nm per laser pulse at non-resonant ablation to 77 nm per laser pulse at resonant ablation. Furthermore, the influence of laser wavelength on the incubation effect is pronounced. In general, incubation occurs when a weakly absorbing polymer material is converted

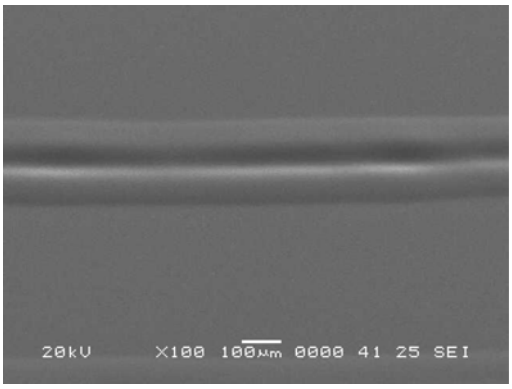

(a) 3.20 µm

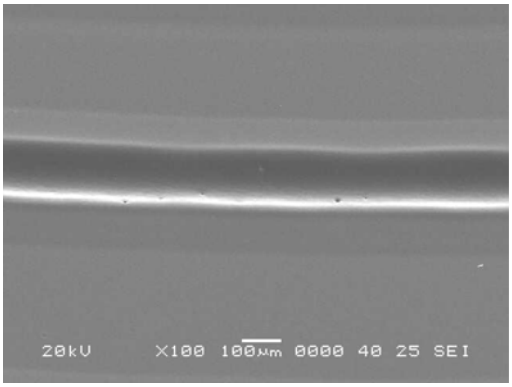

(b) 3.34 µm

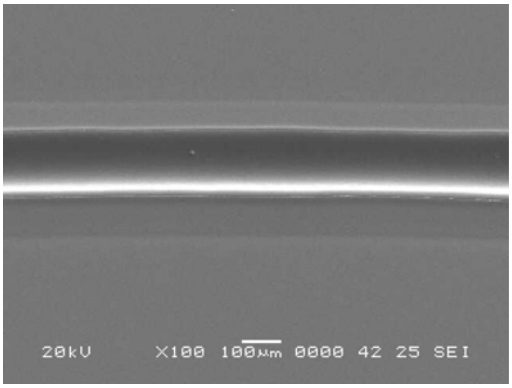

(c) 3.39 µm

Figure 7.5: SEM micrographs of PMMA mid-IR ablation at three wavelengths (a) 3.20 µm (b) 3.34 µm and (c) 3.39 µm.

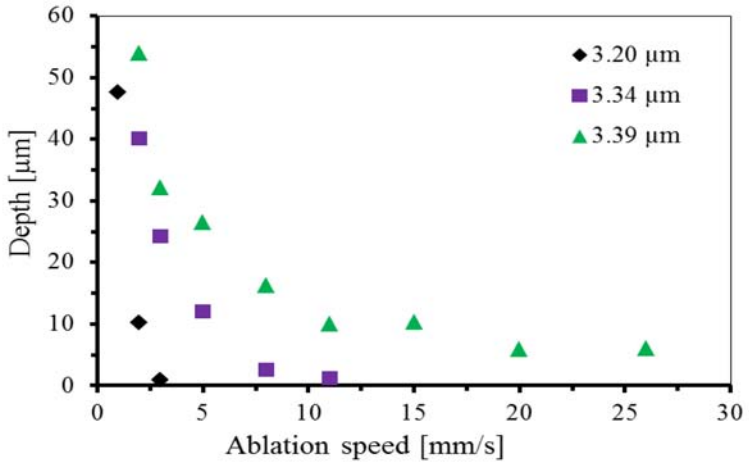

Figure 7.6: Ablation depth plots for PMMA at three different wavelengths: 3.20 µm, 3.34 µm and 3.39 µm.

to a material with a higher absorption cross-section after repetitive exposure through photochemical and/or photothermal reactions.

For the resonant ablation the incubation effect is very limited, however in case of non-resonant wavelengths it is more pronounced. For instance from Figure 7.7, at 3.20 µm wavelength with 430 shots per location the ablation depth is almost negligible compared to ablation depths of 24 µm and 32 µm, at 3.34 µm and 3.39 µm respectively. This behavior of incubation and the given tunability of the RIA source can be exploited in case of selective laser patterning of a polymer on another polymer. For selective ablation, it is very important to remove the top layer without damaging the underneath layer.

7.5.2 Thin films patterning

For the patterning applications, experiments were conducted at 20 kHz, 165 mW and the output wavelength was tuned to the resonant peak (3.39 µm) of absorption. In this case, the laser fluence has been maximized by using a mid-IR microscopic objective (focal length 6 mm). The laser spot size was not measured exactly, but estimated from the crater depth profile as indicated in Figure 7.8 . The calculated fluence for thin films patterning with this mid-IR ablation set-up and estimated spot size of 17.1 µm (Full Width Half Maximum) is ap-

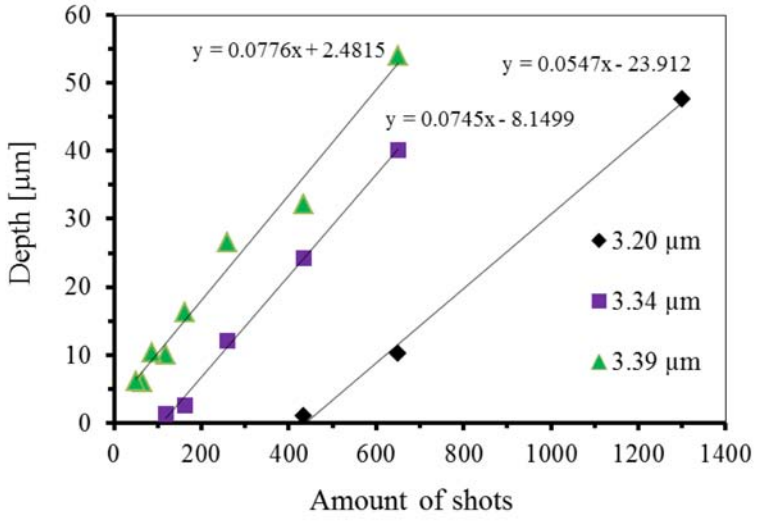

Figure 7.7: Ablation rate plots for PMMA at three different mid-IR wavelengths of absorption: 3.20 µm, 3.34 µm and 3.39 µm.

proximately 6.5 J/cm^2. The thin film patterning results of 650 nm and 1300 nm PMMA films on glass substrate are illustrated in Figure 7.9. The optical microscopic inspection in Figure 7.9(a) and Figure 7.9(c) represents a clean and debris free ablation.

If we look at the depth profiles, it can be observed from Figure 7.9(b) and Figure 7.9(d) that there are ridges at the edges of the ablated area. There are two possible reasons for these ridges. First, the molecular weight of PMMA plays a significant role in the formation of ridges. It has been reported that there is bulge formation on rims for lower molecular weight PMMA, whereas no bulge formation for higher molecular weights [27]. Secondly, the laser beam profile is also responsible for ridges, which is a Gaussian profile in this case. The energy content at the sides of Gaussian beam is lower compared to the energy at beam axis and is also below the threshold value to ablate the material. This energy is absorbed near the surface, modifying surface chemistry, crystal structure, and /or multiscale morphology without altering the bulk. These modifications at the surface are followed by a re-solidification process, which leads to edges after laser patterning [28].

The SEM micrographs (Figure 7.10) of the ablated regions with higher magnification (×1000) are clean and there is no visible rede-

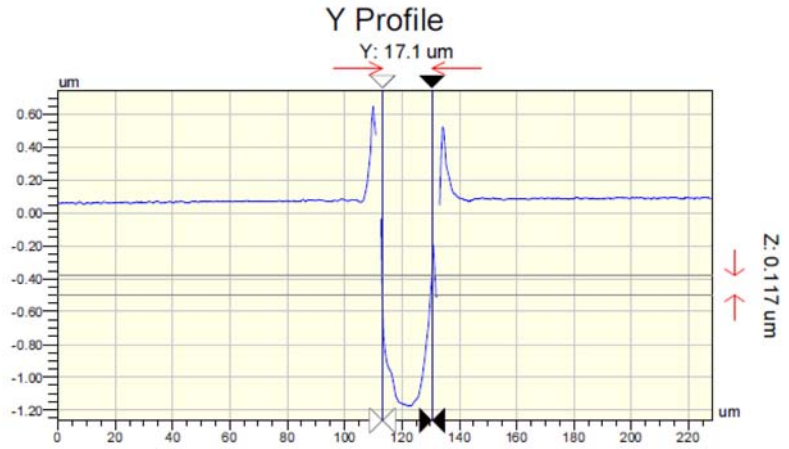

Figure 7.8: Cross-section profile of an ablated structure indicating a spot size of 17.1 µm at full-width-half-maximum (FWHM).

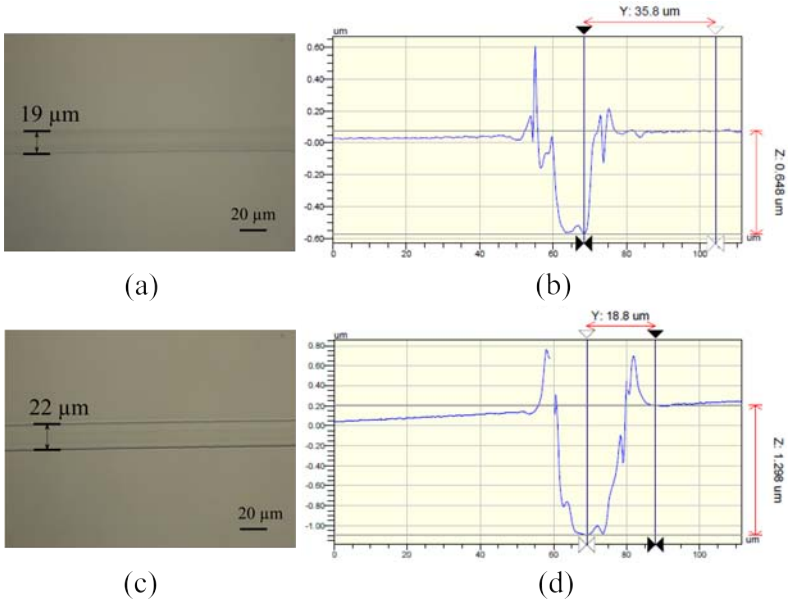

Figure 7.9: Optical microscopic images: (a) and (c), of RIA patterned 650 nm and 1300 nm thin films of PMMA on a glass substrate. On the right: (b) and (d) are the corresponding depth profiles, indicating the removal of 648 nm and 1298 nm of PMMA thin films.

position or debris on the ablated tracks. It is inferred from these observations that the ablation is likely to be driven by photothermal mechanisms. The laser energy deposited into PMMA target is transformed into heat. Resonant infrared (3.39 µm) excitations of localized molecular-vibrations couple to the phonon within hundreds of femtoseconds to picoseconds. This leads to heat accumulation in the material. The thermal energy can be diffused from the localized volume in its thermal confinement time. When the spot size of the laser beam is much larger than the absorption length of the material to be ablated, one dimensional thermal diffusion can be assumed. In such a case, the thermal confinement time can be calculated by using the following equation [29]:

$$\tau_{th} = \frac{c_p \rho}{\alpha^2 \kappa}$$

where τ_{th} is the thermal confinement time, c_p is the specific heat, ρ is the material density, α is the absorption coefficient and κ is the thermal conductivity. Plugging in some numerical values into this formula for PMMA, as $c_p \approx 1466\,\mathrm{J/(kg\,K)}$, $\rho \approx 1.18\,\mathrm{g/cm^3}$, $\alpha \approx 1730\,\mathrm{cm^{-1}}$ and the thermal conductivity of PMMA varies from $0.167\,\mathrm{W/(m\,K)}$ to $0.251\,\mathrm{W/(m\,K)}$. This calculation leads to a thermal confinement time of $\approx 0.29\,\mathrm{ms}$ (for $\kappa = 0.200\,\mathrm{W/(m\,K)}$, which is much higher than the laser pulse duration (about 15 nanoseconds). Since the time required for the heat to diffuse out of the localized volume is much higher than the laser pulse length, this RIA ablation mechanism for PMMA is assumed to be photothermal in nature.

7.6 Conclusions

A qualitative and quantitative analysis of the resonant mid-IR laser ablation (RIA) of bulk PMMA has been successfully demonstrated using a recently developed mid-IR tunable source. Higher ablation rates were observed at the resonant wavelength of operation and the ablated crater was free of debris. A proof-of-concept of thin film PMMA patterning using RIA on a glass substrate has been provided. The possibilities of patterning a thin organic film on a flexible substrate is a part of future work in this mid-IR region. The absorption spectra show that there are significant peaks of polymer absorption around 4.5 µm; and in the range of 6 µm to 7 µm, which can be exploited in further studies.

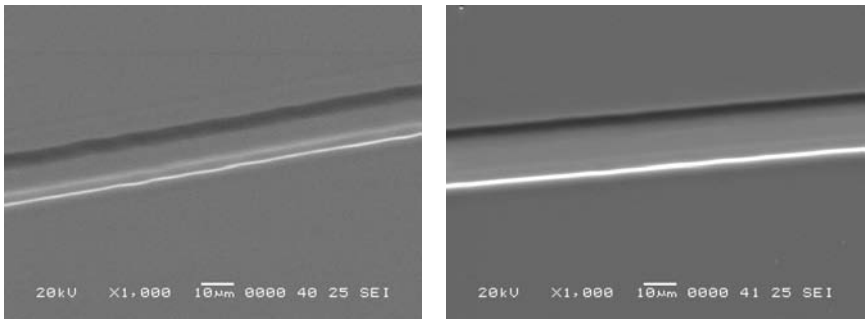

(a) (b)

Figure 7.10: SEM micrographs of the patterned PMMA thin films (a) 650 nm (b) 1300 nm. The micrographs are taken with 45 degree tilt and 1000 magnification.

References

[1] K. Naessens, H. Ottevaere, P. V. Daele, and R. Baets, "Flexible fabrication of microlenses in polymer layers with excimer laser ablation", *Applied Surface Science*, vol. 208, pp. 159–164, 2003, Physics and Chemistry of Advanced Laser Materials Processing. [Online].

[2] M. Schaefer, J. Holtkamp, and A. Gillner, "Ablation of PEDOT/PSS with excimer lasers for micro structuring of organic electronic devices", *Synthetic Metals*, vol. 161, no. 11, pp. 1051–1057, 2011. [Online].

[3] R. Srinivasan and W. Leigh, "Ablative photodecomposition: action of farultraviolet (193 nm) laser radiation on poly(ethylene terephthalate) films", *Journal American Chemical Society*, vol. 104, no. 24, pp. 6784–6785, 1982. [Online].

[4] S. Naithani, D. Schaubroeck, Y. Vercammen, R. Mandamparambil, I. Yakimets, *et al.*, "Excimer laser patterning of PEDOT:PSS thin-films on flexible barrier foils: A surface analysis study", *Applied Surface Science*, vol. 280, pp. 504–511, 2013. [Online].

[5] J. H. Brannon and J. R. Lankard, "Pulsed CO2 laser etching of polyimide", *Applied Physics Letters*, vol. 48, no. 18, pp. 1226–1228, 1986. [Online].

[6] D. M. Bubb, J. S. Horwitz, J. H. Callahan, R. A. McGill, E. J. Houser, *et al.*, "Resonant infrared pulsed-laser deposition of polymer films using a free-electron laser", *Journal of Vacuum Science and Technology A*, vol. 19, no. 5, pp. 2698–2702, 2001. [Online].

[7] D. M. Bubb, J. S. Horwitz, R. A. McGill, D. B. Chrisey, M. R. Papantonakis, *et al.*, "Resonant infrared pulsed-laser deposition of a sorbent chemoselective polymer", *Applied Physics Letters*, vol. 79, no. 17, pp. 2847–2849, 2001. [Online].

[8] *The European commission FP7 IMPROV project*, 2013. [Online].

[9] M. Duering, R. Haglund, and B. Luther-Davies, "Resonant Infrared Pulsed Laser Ablation of Polymers with Single Picosecond Pulses Generated by an Optical Parametric Amplifier", in *Conference on Lasers and Electro-Optics 2010*, Optical Society of America, 2010, CMH3. [Online].

[10] S. Chaudhuri, M. Nevala, T. Hakkarainen, T. Niemi, and I. Maasilta, "Infrared Pulsed Laser Deposition of Niobium Nitride Thin Films", *IEEE Transactions on Applied Superconductivity*, vol. 21, no. 3, pp. 143–146, 2011. [Online].

[11] D. Bubb, B. Toftmann, R. Haglund Jr., J. Horwitz, M. Papantonakis, *et al.*, "Resonant infrared pulsed laser deposition of thin biodegradable polymer films", *Applied Physics A*, vol. 74, no. 1, pp. 123–125, 2002. [Online].

[12] W. P. Hess, H. K. Park, O. Yavas, and R. H. Jr., "IR-MALDI of low molecular weight compounds using a free electron laser", *Applied Surface Science*, vol. 127, pp. 235–241, 1998. [Online].

[13] M. Sadeghi, Z. Olumee, X. Tang, A. Vertes, Z.-X. Jiang, *et al.*, "Compact tunable Cr:LiSAF laser for infrared matrix-assisted laser desorption/ionization", *Rapid Ccommunications in Mass Spectroscopy*, vol. 11, pp. 393–397, 1997. [Online].

[14] R. Srinivasan, B. Braren, D. E. Seeger, and R. W. Dreyfus, "Photochemical cleavage of a polymeric solid: details of the ultraviolet laser ablation of poly(methyl methacrylate) at 193 nm and 248 nm", *Macromolecules*, vol. 19, no. 3, pp. 916–921, 1986. [Online].

[15] Z. Liu, Y. Feng, and X.-S. Yi, "Coupling effects of the number of pulses, pulse repetition rate and fluence during laser PMMA ablation", *Applied Surface Science*, vol. 165, no. 4, pp. 303–308, 2000. [Online].

[16] J.-S. Koo, P. G. Smith, R. B. Williams, C. Riziotis, and M. C. Grossel, "UV written waveguides using crosslinkable PMMA-based copolymers", *Optical Materials*, vol. 23, no. 3, pp. 583–592, 2003. [Online].

[17] G. Davis, M. Gower, C. Fotakis, T. Efthimiopoulos, and P. Argyrakis, "Spectroscopic studies of ArF laser photoablation of PMMA", *Applied Physics A*, vol. 36, no. 1, pp. 27–30, 1985. [Online].

[18] W. F. Mousa, M. Kobayashi, S. Shinzato, M. Kamimura, M. Neo, *et al.*, "Biological and mechanical properties of PMMA-based bioactive bone cements", *Biomaterials*, vol. 21, no. 21, pp. 2137–2146, 2000. [Online].

[19] J. H. Levy and A. M. Pisacano, "Initial clinical studies with silicone intraocular implants", *Journal of Cataract and Refractive Surgery*, vol. 14, no. 3, pp. 294–298, 1988. [Online].

[20] P. L. Davis, P. Hill, and A. Coffey, "Convex Posterior PMMA Implants: Do PMMA vs Prolene Haptics Alter Capsular Opacity?", *European Journal of Implant and Refractive Surgery*, vol. 3, no. 2, pp. 127–130, 1991. [Online].

[21] J. M. Li, C. Liu, X. D. Dai, H. H. Chen, Y. Liang, *et al.*, "PMMA microfluidic devices with three-dimensional features for blood cell filtration", *Journal of Micromechanics and Microengineering*, vol. 18, no. 9, pp. 1–7, 2008. [Online].

[22] T.-F. Hong, W.-J. Ju, M.-C. Wu, C.-H. Tai, C.-H. Tsai, *et al.*, "Rapid prototyping of PMMA microfluidic chips utilizing a CO2 laser", *Microfluidics and Nanofluidics*, vol. 9, no. 6, pp. 1125–1133, 2010. [Online].

[23] A. Mathur, S. Roy, M. Tweedie, S. Mukhopadhyay, S. Mitra, *et al.*, "Characterisation of PMMA microfluidic channels and devices fabricated by hot embossing and sealed by direct bonding", *Current Applied Physics*, vol. 9, no. 6, pp. 1199–1202, 2009. [Online].

[24] M. Haiducu, M. Rahbar, I. G. Foulds, R. W. Johnstone, D. Sameoto, *et al.*, "Deep-UV patterning of commercial grade PMMA for low-cost, large-scale microfluidics", *Journal of Micromechanics and Microengineering*, vol. 18, no. 11, pp. 115 029–7, 2008. [Online].

[25] "www.matbase.com", 2014. [Online].

[26] "http://refractiveindex.info", 2014. [Online].

[27] N. C. Nayak, Y. C. Lam, C. Y. Yue, and A. T. Sinha, "CO2 -laser micromachining of PMMA: the effect of polymer molecular weight", *Journal of Micromechanics and Microengineering*, vol. 18, no. 9, 2008. [Online].

[28] M. Brown and C. B. Arnold, "Fundamentals of laser-material interaction and application to multiscale surface modification", in *Laser Precision Microfabrication*, ser. Springer Series in Materials Science, K. Sugioka, M. Meunier, and A. Pique, Eds., vol. 135, Springer Berlin Heidelberg, 2010, pp. 91–120. [Online].

[29] S. Johnson, D. Bubb, and J. Haglund R.F., "Phase explosion and recoil-induced ejection in resonant-infrared laser ablation of polystyrene", *Applied Physics A*, vol. 96, no. 3, pp. 627–635, 2009. [Online].

8

Thin Film Resonant Mid-IR Patterning

In this chapter, thin film patterning using RIA technique is carried out for a more specific application in Organic Photovoltaics (OPVs). The focus is on the OPV substrate materials, transparent conductive materials, hole transport materials, and absorber materials. The process has been successfully demonstrated for selective thin film patterning and the influence of the various laser parameters is discussed.

8.1 Introduction

A wide range of large area deposition and patterning techniques can be used for organic and printed electronics. However, this chapter describes the use of laser technology for patterning organic photovoltaic thin film materials. By laser patterning, very fine feature sizes can be obtained with high process speeds from homogeneously deposited layer sequences. Proper power density adjustment, wavelength and pulse width selection of the laser beam have to be optimized for selective removal of different thin organic layers. Ultraviolet lasers have proven their full potential for patterning single organic layers, but in a multilayer organic device the obtained layer selectivity is limited as all organic layers show high UV absorption.

We introduce mid-infrared resonant ablation as an alternative approach, in which a short pulse mid-infrared laser can be wavelength

tuned to one of the molecular vibrational transitions of the organic layer to be ablated. In this wavelength region, the absorption of the material is linked to vibrational transitions of the molecular chain rather than resonant electronic transitions. As a result, the technique is selective in respect of processing a diversity of organic materials, which usually have different infrared absorption bands. Mid-infrared lasers have already been tested and validated for material processing. Most of the studies [1] employing long wavelength CO_2 lasers revealed that the chemical structures and compositions of the ablated polymers were strongly dependent on the wavelength of ablation. The laser pulse duration in these studies was in the range of a few hundreds of nanoseconds. More recent works employed a Free Electron Laser (FEL) for studying the wavelength influence on polymer Pulsed Laser Deposition (PLD) over a large infrared region. After evaluating the position and intensity of the vibrational absorption bands of the polymers in the IR spectrum, the laser wavelength can be matched to a maximum of absorption of the polymer target. The results show that PolyStyrene (PS) has relatively high absorption coefficients in some specific IR absorption bands e.g. at 3.31 µm, and at 3.43 µm, corresponding to aromatic ring C−H stretching modes, and aliphatic C−H asymmetric stretching modes, respectively. However, in most of the applications, FELs are not practical since they are coupled to huge and expensive accelerators. Therefore, new technologies are being developed to replace FELs with bench-top solid-state photonic sources [2, 3]. In our previous study [4], resonant ablation of Polymethylmethacrylate) (PMMA) on glass has been successfully demonstrated.

In this chapter, the mid-IR resonant ablation for a variety of organic thin-films, employing both nanosecond (15 ns) and picosecond (250 ps) laser pulses tunable between 3 µm to 4 µm are discussed. The nanosecond experimental set-up is based on a commercial laser at 1064 nm pumping a singly resonant Optical Parametric Oscillator (OPO) built around a Periodically-Poled Lithium Niobate (PPLN) crystal with several Quasi-Phase Matching (QPM) periods, delivering more than 0.30 W of mid-IR power at 20 kHz, corresponding to 15 µJ pulses. The picosecond laser set-up is based on an Optical Parametric Amplifier (OPA) in a similar crystal, allowing for a direct comparison between both pulse length regimes. The wavelength of the mid-infrared laser can be tuned to one of the molecular vibrational transitions of the organic material to be ablated. For that reason, the IR absorption spectra of the organic materials used in a

typical organic photovoltaic device were characterized in the wavelength region that can be reached by the laser setups. This study is focused on three types of materials prototypical for organic solar cells (OSCs): as a planarization layer, the polymer PEDOT:PSS (poly(3,4-ethylene dioxythiophene) poly(styrenesulfonate)); as hole transport layer two typical materials that can be used alternatively in the organic solar cells, BPAPF (9,9-bis[4-(N,N-bis-biphenyl-4-yl-amino)phenyl]-9H-fluorene) and α-NPB (N,N'-diphenyl-N,N'-bis(1-naphthyl)-1,1'-biphenyl-4,4"-diamine); and as typical high-efficiency absorber materials, like Heliatek's [5] HDR014 (an oligothiophene derivative with non-disclosed structure), and DCV4T-Et2 (2,2'-[(3,3"'-diethyl [2,2': 5': 2": 5", 2"'-quaterthiophene]-5,5"'-diyl) dimethylidyne] bis- Propanedinitrile) [6]. BPAPF and α-NPB are widely used as hole transport materials in organic solar cells (OPVs) and organic light-emitting diodes (OLEDs) [7, 8]. HDR014 is a donor material with strong absorption in the red spectral region. At the end of this chapter, a short investigation of thin film patterning of DCV4T-Et2 and HDR014 with 4.50 µm wavelength is illustrated. To summarize, the ablation process is successfully demonstrated for selective thin film patterning, and the influence of the various laser parameters is discussed.

8.2 Organic Photovoltaics

The Organic Photovoltaics (OPV) or Organic Solar Cell (OSC), is based on organic materials such as polymer thin film or small molecules. The schematic layered structure of the a typical OPV is shown in Figure 8.1. In case of an OPV the input is solar light and the output is electrical energy in the form of Direct Current (DC). As shown in the schematic figure, this device consists of thin films in between two electrodes, one is a metallic cathode and another electrode must be a transparent material. The role of hole transport layer or hole blocking layer is to enhance the movement of charge carriers in one direction to build up the opposite electric charge potential on the electrodes. The key elements in any OPV design are two materials, donor layer and acceptor layer. The working principle of an OPV relies on three phenomena: absorption of light by the donor layer, which creates an exciton (electron-hole pair); separation of the charge carriers and finally extraction of the charge carriers to an external circuit. Therefore, the working principle of an OPV can be summarized in 4 steps:

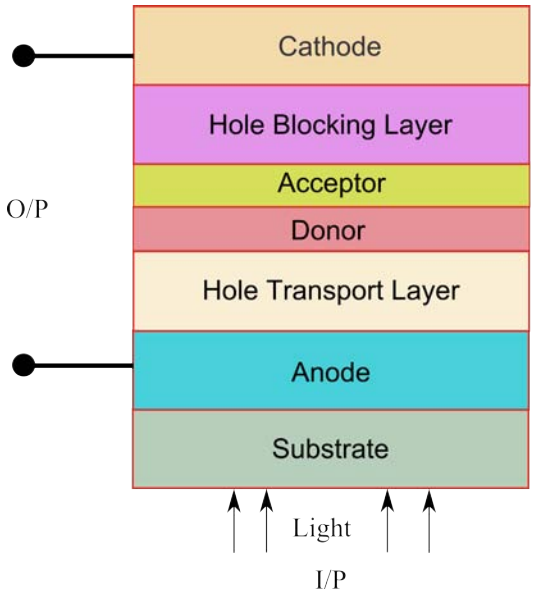

Figure 8.1: A typical and general schematic layered structure of organic photovoltaics (OPV) consisting of different organic thin films.

1. Absorption of sun light by organic material.
2. Exciton creation and diffusion.
3. Charge separation (generation of electron hole pair).
4. Charge extraction by effective fields (electrons and holes move in opposite directions).

The energy bands of organic materials are Highest Occupied Molecular Orbital (HOMO) and Lowest Unoccupied Molecular Orbital (LUMO), which are analogous to the valence and conduction band of inorganic semiconductor materials. When the light falls on the donor material, the exciton is created in the donor layer. The exciton eventually breaks in a free electron-hole pair due to the effective fields set up by the dissimilar material hetero-junction. The free electrons travel from donor LUMO to the acceptor LUMO orbital band. This movement of carriers is supported by the hole blocking layer or electron transport layer and is only in one direction. This process of charge separation builds up the potential across the

electrodes. In general, the cathode is made of low work function materials like Calcium, Magnesium or Aluminum, however the anode is of high work function conducting transparent material such as Indium Tin Oxide (ITO). The hole transport layer is usually made of PEDOT:PSS material and the hole blocking layer is of Tris(8-hydroxyquinolinato)aluminium (Alq_3) or bathocuproine (BCP). The typical example material for the donor is poly(3-hexylthiophene) (P3HT) and for the acceptor is phenyl-C61-butyric acid methyl ester(PCBM). In order to improve the efficiency of a solar cell, different architectures have been proposed with various kinds of materials. As mentioned in the previous section, our focus is on three different kinds of layers of OPV: planarization layer (PEDOT:PSS), hole transport material (BPAPF, α-NPB) and absorber / donor material (DCV4T-Et2, Heliatek's HDR014).

8.3 Methodology

8.3.1 Sample preparation

Thin films of PEDOT:PSS (poly(3,4-ethylenedioxythiophene) poly (styrenesulfonate)) on both glass (Prinz Optics) and PET (polyethylene terephthalate) (DuPont) substrates with nominal thicknesses of 70 nm, 140 nm, and 210 nm were produced via spin-coating. PEDOT:PSS layers were produced using a commercial aqueous solution (Heraeus) with a PEDOT:PSS ratio of 1:6 (by weight) and solid content of 1.3 % to 1.7 %. The nominal thickness of the PEDOT:PSS layer was reached after a multi-step spin-coating process. The thickness of the layers after a single step at rotation speed of 1500 rpm and acceleration of 500 rpm/s corresponds to about 70 nm. After each coating step, the PEDOT:PSS layers were annealed for 15 minutes at 120 °C to remove the solvent.

BPAPF, α-NPB, DCV4T-Et2 and HDR014 films with nominal thickness of 140 nm were deposited on glass substrates (Prinz Optics or Glas-Meyer) via thermal evaporation in a Ultra High Vacuum (UHV) chamber (Kurt J. Lesker) at a deposition rate of 0.3 Å/s. HDR014 , DCV4T-Et2 (both from Heliatek) and BPAPF (Lumtec) were purified by vacuum sublimation prior to thin film preparation. The hole transport material α-NPB (Sensient) was used as synthesized. The film thickness was controlled by a quartz crystal microbalance (QCM). The samples were prepared and supplied by Heliatek under the EU FP-7 project "IMPROV" [2].

8.3.2 Mid-infrared absorption spectra

The IR absorption spectra of the prototypical materials used in the OPV stack were obtained in the wavelength regions of interest. Attenuated Total Reflectance Infrared Spectroscopy (ATR-IR) was employed to characterize the substrate foils, since a measurement in transmission requires a sample thickness limited to a few tens of microns. The thin-film materials were deposited on an IR transparent substrate material (e.g.CaF_2), to avoid overlap in the spectra of thin-film coating versus substrate material. Reliable spectra could be obtained using measurements in transmission and in reflection. Further, powder spectra in KBr pellets were collected for comparison with thin-film measurements.

8.3.3 Ablation set-up

The mid-IR ablation experiments were performed using two set-ups, providing nanosecond and picosecond pulses. The nanosecond laser (build up at Optics Lab, Imec/ UGent with the help of Thales Research and Technology, France for the OPO section) is based on a commercial laser at 1064 nm wavelength, pumping with ≈ 15 ns pulses at a repetition rate of 20 kHz singly resonant Optical Parametric Oscillator (OPO) build around a PPLN crystal with several Quasi-Phase Matching (QPM) periods is used in this configuration[9]. In the OPO cavity, the signal can oscillate between 1500 nm and 1650 nm wavelengths, corresponding to idler wavelengths from 3660 nm to 2996 nm. The coarse tuning can be obtained by translating the PPLN crystal, thus changing the QPM period. Besides, the wavelength fine tuning is achieved by heating the crystal, which allows us to achieve continuous wavelength tuning between 3000 nm and 3600 nm. This means that by combining coarse and fine wavelength tuning, it is possible to address the IR absorption bands in the range of 3 µm to 4 µm. The picture of the nanosecond laser patterning set-up is shown in Figure 8.2.

After the OPO and filtering section (designated to remove residual pump and signal), the laser beam is loosely collimated by a Si plano-convex lens (100 mm focal length), and focused by a mid-IR microscopic objective (6 mm focal length) on the sample. The samples were mounted on an automatic translational stage to allow for a controlled amount of laser shots, a key parameter in thin-film patterning. During the experiments, the influence of scanning speed, pulse energy and mid-IR wavelength was studied. Scanning speeds

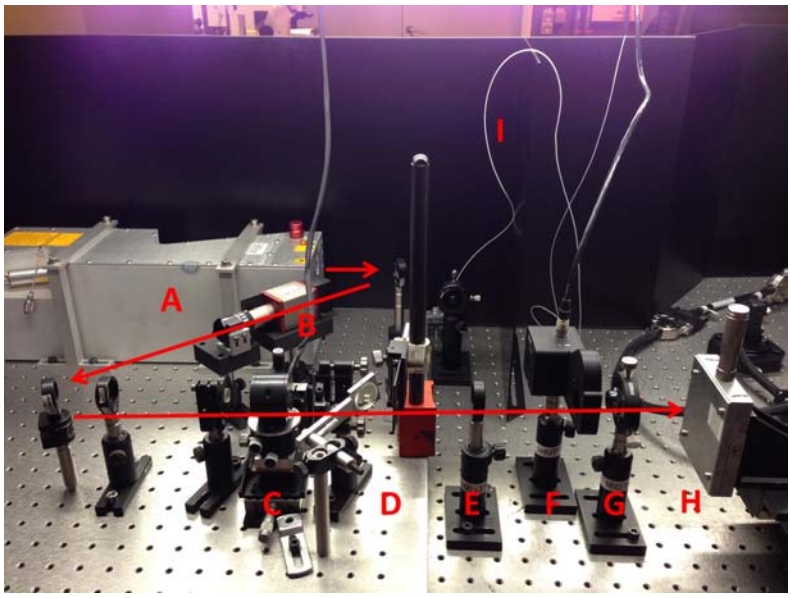

Figure 8.2: Mid-IR nanosecond ablation set up:

(A) Pump Laser
(B) Attenuator-Isolator
(C) OPO - Wavelength conversion unit
(D) Filtering section
(E) Focusing lens
(F) Shutter
(G) mid-IR objective
(H) Sample stage
(I) Fiber to OSA

were widely varied from 0.01 mm/s to 300 mm/s, pulse energies were adjusted by varying the power (attenuator unit) while keeping the pulse repetition rate fixed at 20 kHz. The average power was varied from 120 mW to 170 mW, resulting in corresponding pulse energies of 6 µJ to 8.5 µJ. All thin-film organic materials were investigated for two wavelengths, allowing for a comparison of resonant versus non-resonant absorption. The signal wavelengths (around 1500 nm) were measured by an optical spectrum analyzer (OSA), whereas the corresponding idler wavelengths (around 3 µm) were calculated by using the following relationship:

$$\frac{1}{\lambda_{pump}} = \frac{1}{\lambda_{idler}} + \frac{1}{\lambda_{signal}}$$

The PPLN crystal output wavelengths are temperature dependent and the relationship is shown in Figure 8.3. By varying the crystal temperature the output wavelengths can be tuned to the desired value. The signal wavelengths are measured by using an OSA, and one of the measurements is shown in Figure 8.4.

On the other hand, the picosecond laser set-up was built up at Multitel (Belgium) and the picosecond laser experiments were conducted at "Multitel lab", while the analysis is conducted at Imec / UGent together with Heliatek (Germany). This set-up is based on a commercial laser (Amplitude Systems, France) emitting at 1028 nm and modified to have 250 ps pulse duration at the output. The repetition rate has been fixed to 25 kHz and the maximum power at 4 W corresponds to a pulse energy of 160 µJ. A multi-grating PPLN crystal has been used for the experiments in a double pass OPA configuration [10]. The signal source (CW, 5 mW) to be amplified is tunable between 1460 nm and 1580 nm, making it possible to have an idler wavelength from 2.94 µm to 3.47 µm. The maximum output power obtained at 3.03 µm and 3.37 µm is 80 mW and 160 mW respectively (see the results on mid-IR spectra as a motivation for these two particular wavelengths). An aspherical lens has been used to focus the beam on the sample to process. The M^2 of the beam is unknown but for a perfect beam ($M^2 = 1$) the spot diameter is estimated to be around 12 µm in the focal plane. The schematic diagram of the picosecond laser set-up is shown in the Figure 8.5.

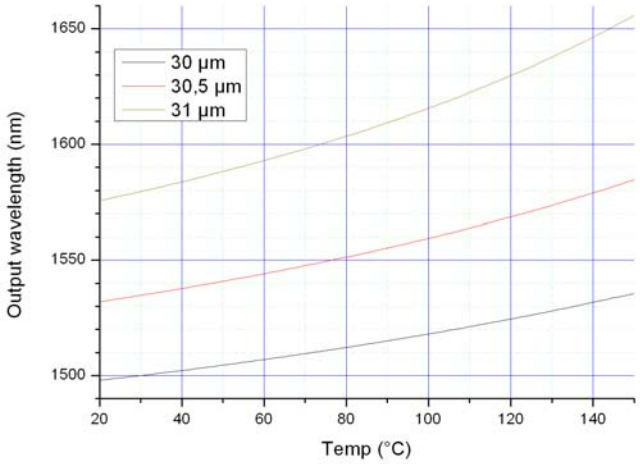

(a) Variation in signal wavelengths with temperature

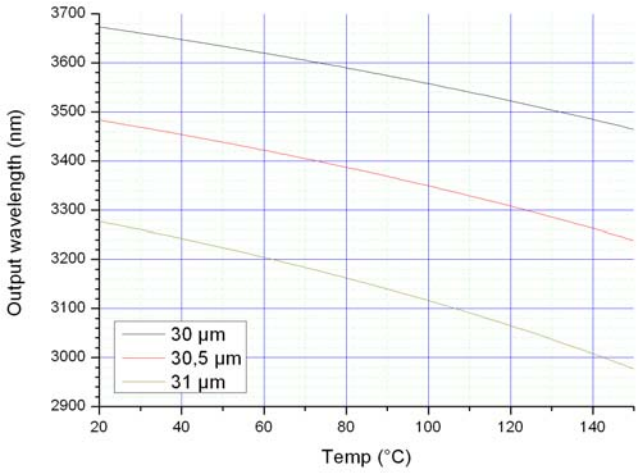

(b) Output idler wavelengths with temperature

Figure 8.3: PPLN crystal output wavelengths and temperature relationship. (Datasheet: Covesion Ltd, UK)

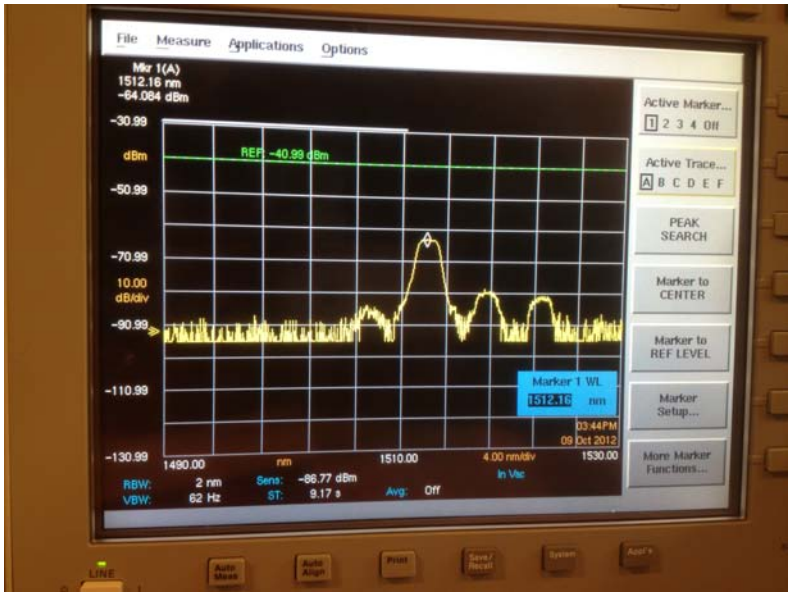

Figure 8.4: Measurement of signal wavelength through an Optical Spectrum Analyzer (OSA), the measured wavelength in this case is 1512.16 nm.

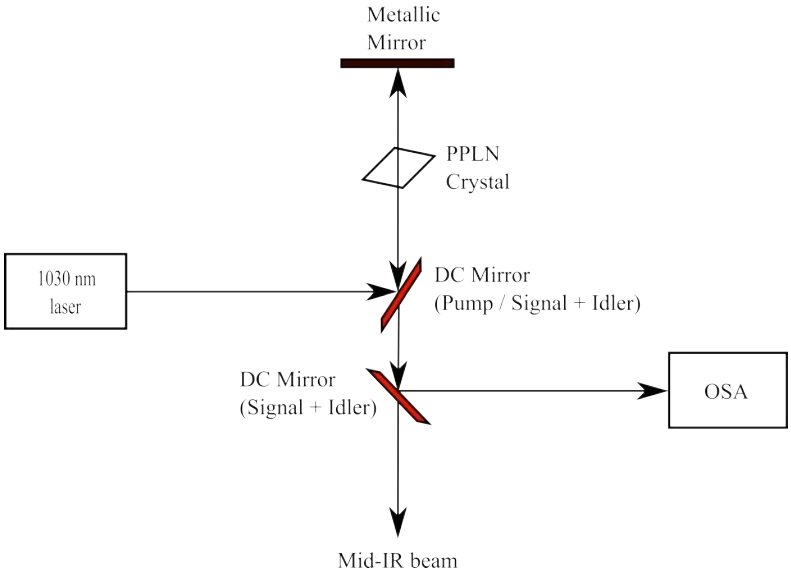

Figure 8.5: Picosecond tunable mid-IR resonant ablation set-up.

8.3.4 Analysis

The investigation and analysis of the samples after experiments were performed with an optical microscope and a non-contact optical profiler (WYKO NT 3300). Scanning electron microscopy (SEM) was used to investigate the surface topography and possible contamination after the ablation experiments. SEM analysis was performed on a JEOL-5600 and a Zeiss Neon 40 instrument. Prior to analysis, the samples were coated with a thin gold layer (roughly 20 nm) via plasma magnetron sputter coating. For elemental surface analysis, energy dispersive X-ray spectroscopy (EDX) was carried out to get spatially highly resolved elemental surface mapping. It turned out that this technique is a very efficient tool to characterize the quality of laser scribes.

8.4 PEDOT:PSS mid-IR selective patterning

In the first part of this investigation, the use of a long wavelength mid-IR nanosecond laser for ablation of PEDOT:PSS thin organic films was evaluated. Various layers of PEDOT:PSS were prepared using the procedure described in the Methodology section earlier. To study the influence of overlap between the absorption of the PEDOT:PSS thin-film and the substrate, both glass and PET foil carriers were selected. The absorption spectra of PEDOT:PSS and PET are shown in Figure 8.6.

From these spectra, it is observed that PEDOT:PSS has two absorption bands around 3.40 µm and 3.50 µm, and a broader absorption band at 3.03 µm. The latter can be ascribed to the O−H stretch of PSS−H. The band around 3.40 µm can be assigned to the asymmetric aliphatic C−H stretch of the PSS units. The other band around 3.50 µm arises from the symmetric aliphatic C−H stretch of PSS. Note that the PEDOT:PSS weight ratio is 1:6 in this case. PET has absorption bands at 2.91 µm, and around 3.37 µm. The band around 2.91 µm arises from the O−H stretch of the PET functional end groups. The band at 3.37 µm can be assigned to the asymmetric C−H stretch of CH_2 moieties. Already now it is clear from the overlap in spectra between PEDOT:PSS and PET, that for selective removal of PEDOT:PSS from PET, the absorption band around 3.40 µm-3.50 µm has to be avoided, because of cross-sensitivity with the PET substrate. On the other hand, a wavelength of 3.03 µm, could be a good candidate.

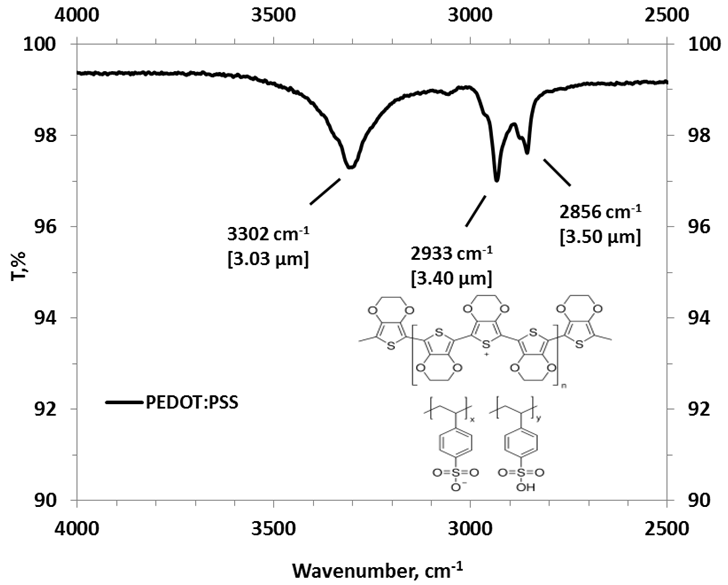

(a) PEDOT:PSS mid-IR spectrum

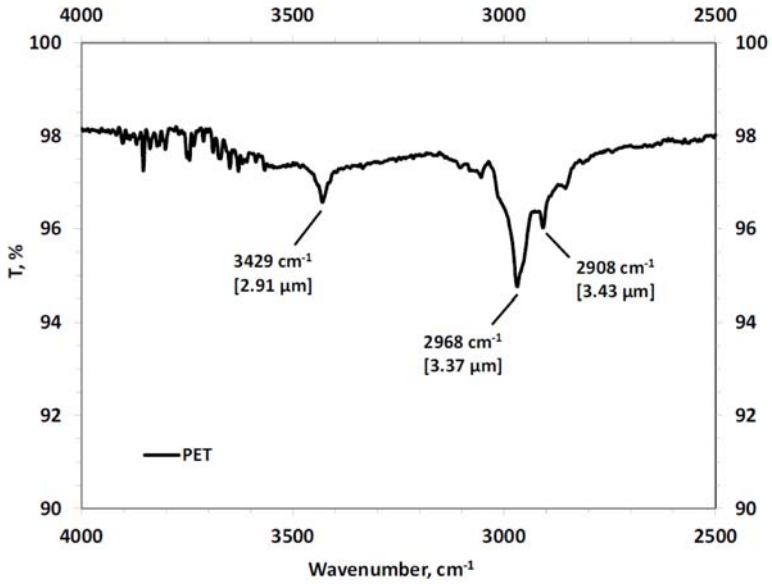

(b) PET mid-IR spectrum

Figure 8.6: Transmission / absorption spectra of PEDOT:PSS and PET in mid-IR wavelength region.

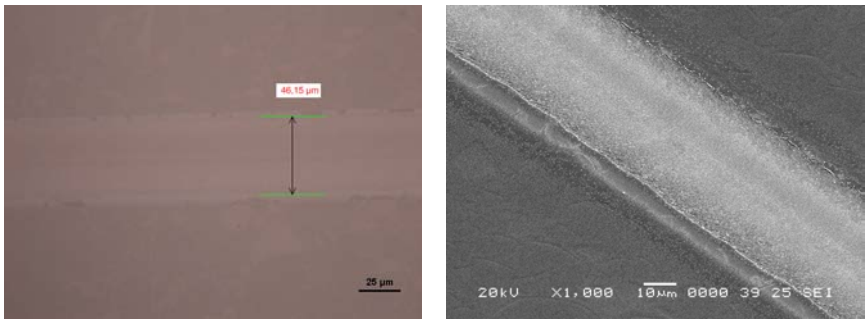

(a) Line width = 46 µm (b) Scale bar = 10 µm

Figure 8.7: Patterning of the PEDOT:PSS thin film with mid-IR nanosecond laser at 3.40 µm wavelength: (a) optical microscopic image (b) SEM micrograph.

The initial goal of these experiments was to prove that a mid-IR laser could be used for removing a thin film of 140 nm in thickness, using a glass carrier. Two wavelengths were investigated: 3.40 µm, corresponding to resonant absorption, and 3.30 µm, corresponding to non-resonant absorption. The (nanosecond) laser parameters used during these experiments are 160 mW of power, 20 kHz pulse repetition rate and various scan speeds. Removal of the PEDOT:PSS film was demonstrated for resonant ablation (3.40 µm), for which the optical microscopic image and SEM micrograph are depicted in Figure 8.7.

In addition to the visual microscopic inspection, the depth profile of the ablated track has been measured using a non-contact optical profiler and the measurements are shown in Figure 8.8. Apart from the fact that the surface roughness of the PEDOT:PSS film seems to be high, the measured depth of the ablated crater is about 120 nm, lower than the specified layer thickness of 140 nm. The spike at the left edge of the ablated groove is attributed to a measurement artifact of the optical profiler. Hence, mid-IR resonant ablation of PEDOT:PSS thin organic film at the absorption peak of 3.40 µm was possible, although the scan speed is very low. In contrast, for similar experimental conditions, but employing a non-resonant wavelength (3.30 µm) no PEDOT:PSS removal was observed.

In order to visualize the influence of the mid-IR wavelength on material removal, a PEDOT:PSS thin film was coated on a PET substrate, and the nanosecond laser wavelength was tuned between

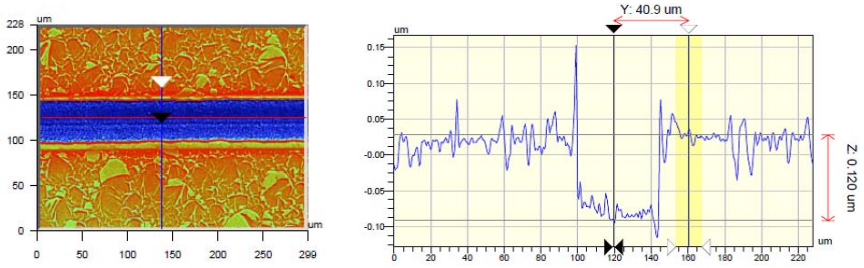

(a) Non-contact optical profile (b) Depth = 120 nm

Figure 8.8: Depth profile measurement after mid-IR nanosecond laser patterning of PEDOT:PSS at 3.40 µm wavelength.

3.41 µm and 3.50 µm. Note that in this case the absorption spectra of PEDOT:PSS and PET have to be taken into account (Figure 8.6). It is clear from the experimental results shown in Figure 8.9, that the influence of changing the wavelength by 100 nm is significant; ablating a few microns compared to a few hundreds of nanometers. The explanation can be found in the much stronger absorption of the PET substrate in the case of 3.41 µm, compared to 3.50 µm.

8.5 Thin films patterning on PET foil

In the first stage of experiments, the PEDOT:PSS thin film removal on a PET substrate with a picosecond laser was performed. The thickness of PEDOT:PSS in this case was 210 nm. In these tests the mid-IR radiation was generated by an OPG configuration delivering about 8 µJ energy per pulse at 3.03 µm. With a repetition rate of 25 kHz and a scanning speed of 90 mm/s, the scribing of the PEDOT:PSS layer could be achieved, and the corresponding results are illustrated in Figure 8.10.

As one can deduce from the previous pictures, the quality of the scribes strongly depends on the beam profile of the mid-IR source. In order to improve the results, the source was changed to an OPG /OPA configuration and the output beam was filtered with a diaphragm before being focused on the sample. In this configuration, the quality of the scribe was better as shown in Figure 8.11 (obtained with pulse energy of 3 µJ at 100 mm/s), although as we do not have a top-hat configuration at this wavelength, the complete removal of the material between two pulses was not possible. Nevertheless, it can

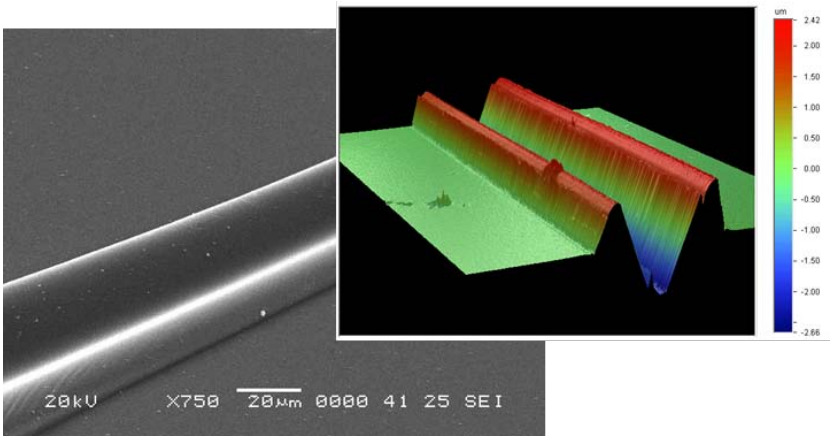

(a) At 3.41 µm wavelength

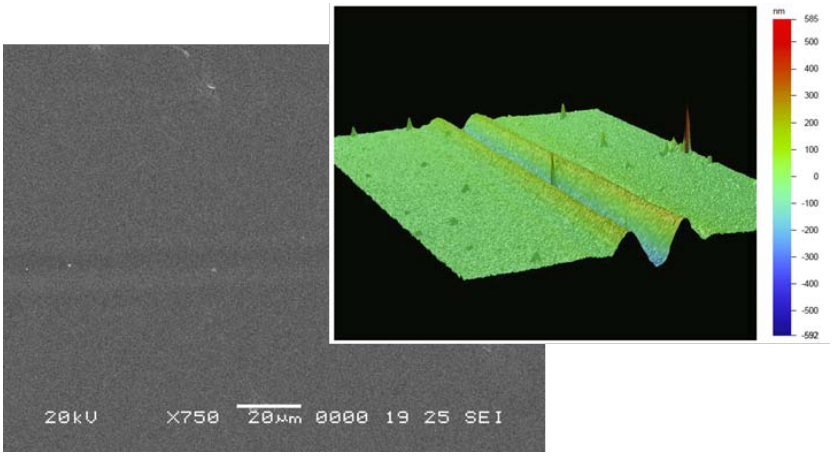

(b) At 3.50 µm wavelength

Figure 8.9: SEM micrographs and wyko optical depth profiles, for identical experimental laser settings (ns, 80 mW, 40 mm/s, 2 µJ), except the wavelengths.

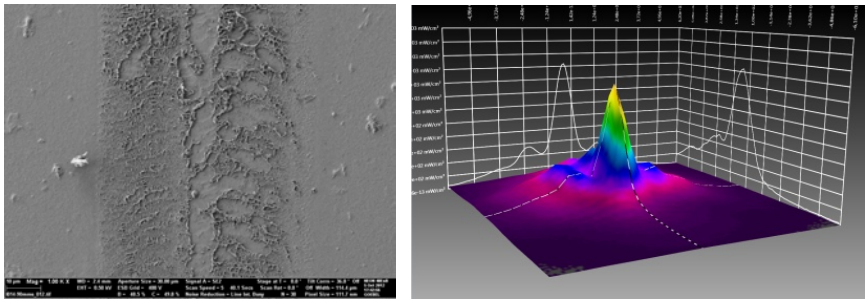

(a) SEM miorograph (b) Beam profile

Figure 8.10: SEM micrograph after mid-IR picosecond laser selective patterning (3.03 µm, 90 mm/s, pulse energy ≈8 µJ) of 210 nm PEDOT:PSS on PET foil and beam profile of the mid-IR source used for this experiment.

be seen from the EDX elemental mapping that a selective removal of PEDOT-PSS on PET was possible at 3.03 µm. It clearly indicates that the organic thin film removal on foil substrate is improved with ultra-short (picosecond) laser pulses compared to nanosecond pulses. The selection of the mid-IR wavelength (3.03 µm) at which the absorption of the PEDOT:PSS thin film is higher and no absorption for PET film was certainly a relevant choice. These results can be further improved with better beam profile (flat-top) and beam quality.

Other thin film materials like DCV4T-Et2 and HDR014 were also investigated in this picosecond pulse regime. First of all, the absorption spectra of these thin films were characterized and are shown in Figure 8.12. Because of the overlap on absorption spectra with PET, it is difficult to find a clear selective absorption band in the accessible wavelengths range of our system. The experiments were carried out at 3.31 µm and 3.37 µm wavelengths. The results obtained for these thin films are illustrated as SEM images in Figure 8.13. A dependence of the ablation threshold on the wavelength absorption coefficient was confirmed with these results. There is a possibility to obtain clean grooves, however at low scanning speeds.

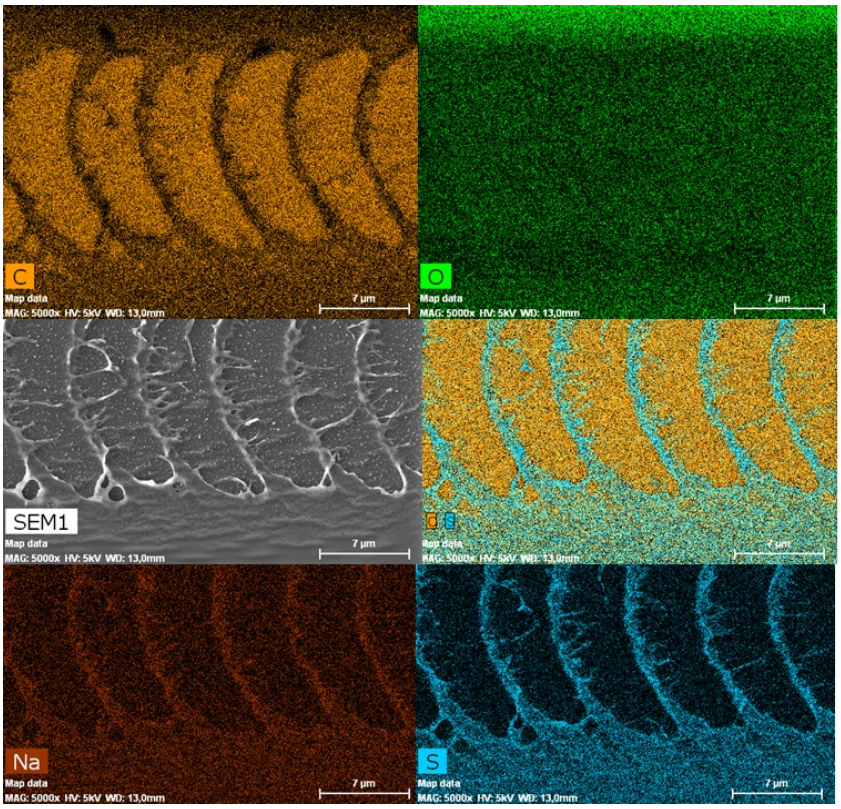

Figure 8.11: SEM micrograph and corresponding EDX elemental maps after picosecond laser ablation (3.03 µm, 100 mm/s, 3 µJ) of 140 nm PEDOT:PSS on PET foil, spot diameter in the focal plane is 12 µm.

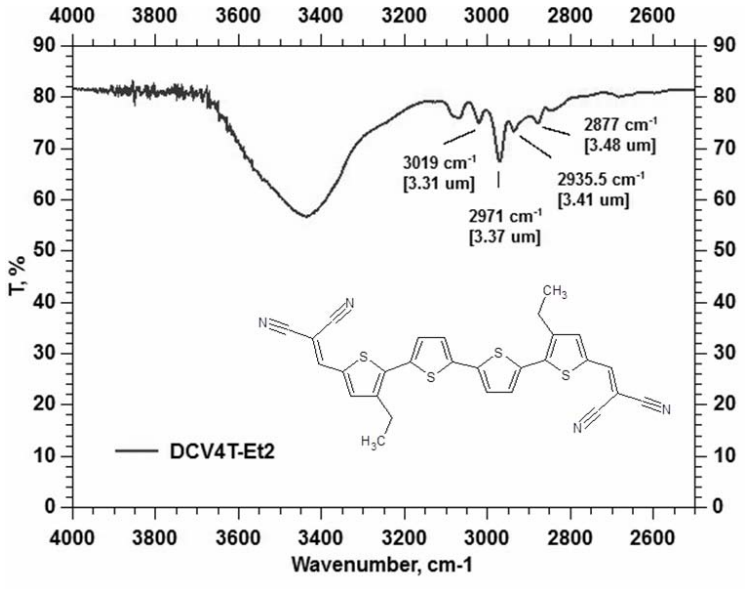

(a) DCV4T-Et2

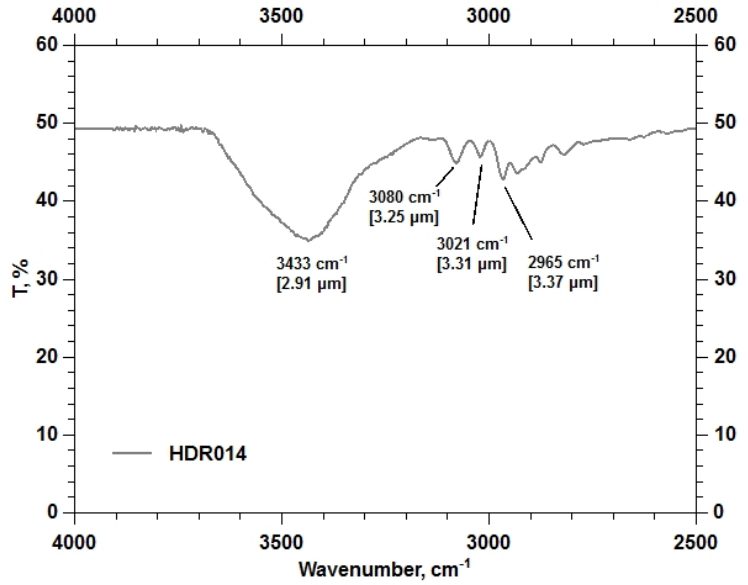

(b) HDR014

Figure 8.12: Absorption spectra of DCV4T-Et2 and HDR014 in the mid-IR region.

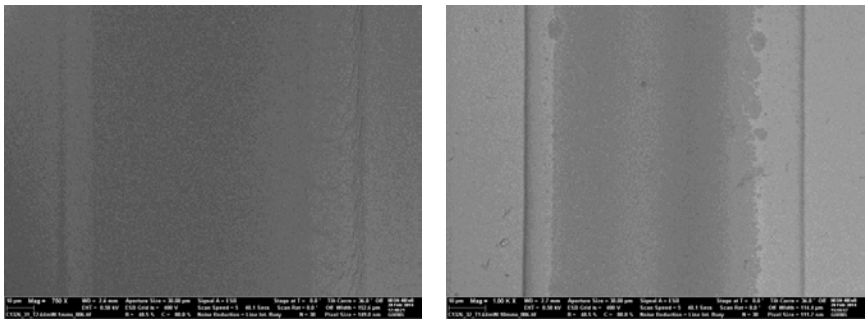

(a) DCV4T-Et2 on PET (b) HDR014 on PET

Figure 8.13: SEM micrographs (a) DCV4T-Et2 on PET at 3.31 µm, ps, 1 mm/s, 3.2 µJ and (b) HDR014 on PET at 3.37 µm, ps, 10 mm/s, 2.5 µJ.

8.6 BPAPF, αNPB and HDR014 mid-IR nanosecond patterning

In a similar fashion, the optical absorption spectra of BPAPF and αNPB were characterized first, which are shown in Figure 8.14. Afterwards, experiments were carried out for 140 nm thick BPAPF on a glass substrate at 3.30 µm (resonant peak) and at 3.40 µm (non-resonant) wavelengths. At 3.30 µm resonant absorption, processing was carried out with 170 mW power, at repetition rate of 20 kHz and different scan speeds. The corresponding results obtained for BPAPF thin films with these experimental conditions are illustrated in Figure 8.15.

These observations show a clean debris-free ablated track at the central part, however at the edges there are pronounced higher rims. The possible reason for this kind of behavior at edges can be the melting of material due to nanosecond laser pulse, which is followed by re-solidification of material. Depth measured at the central part of the ablated groove by a non-contact optical profiler is about 130 nm, which is lesser than the actual film thickness (140 nm). Thereafter, experiments for BPAPF at non-resonant wavelength (3.40 µm) have been carried out with the identical laser processing parameters. Interestingly, there was no laser beam interaction with the thin film of BPAPF as no material removal was observed and the surface topography remained intact.

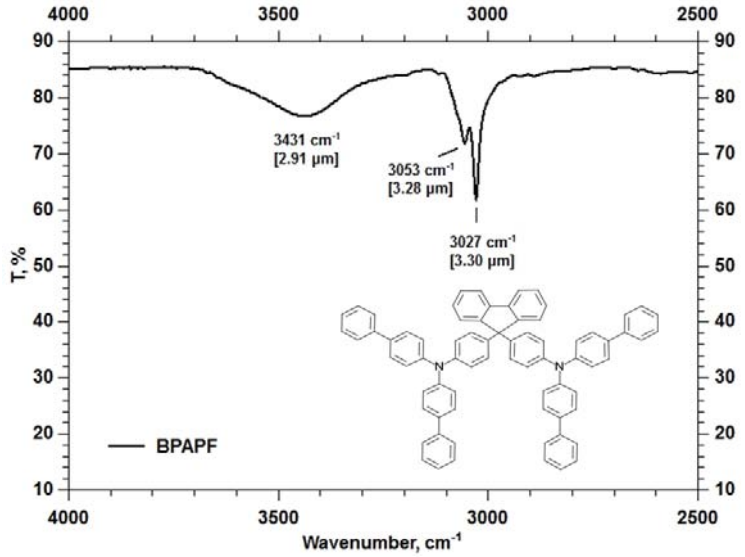

(a) BPAPF

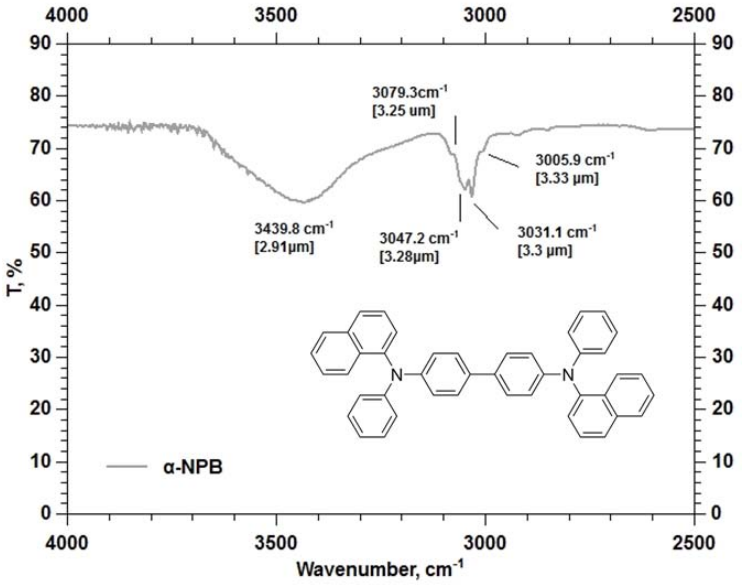

(b) αNPB

Figure 8.14: Mid-IR absorption spectra of BPAPF and αNPB.

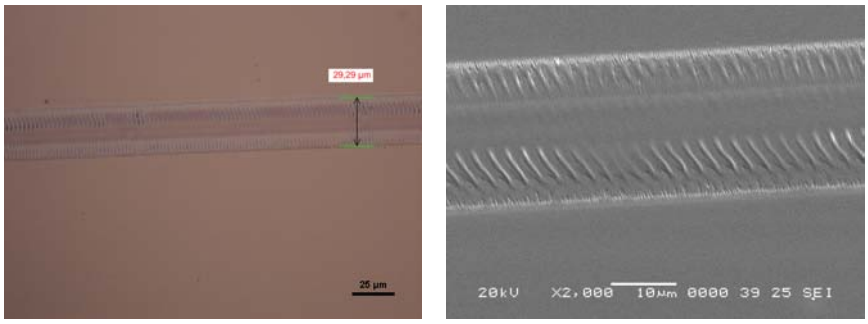

(a) Optical microscopic image (b) SEM micrograph

Figure 8.15: Mid-IR patterning of BPAPF thin film (3.30 µm, ns, 170 mW, 20 kHz).

Nanosecond laser experiments were further continued for thin organic film of αNPB at resonant and non-resonant wavelengths of absorption. As in the previous studies of PEDOT:PSS and BPAPF, a thickness of the 140 nm αNPB thin film on a glass substrate has been investigated. It can be inferred from the absorption spectrum of αNPB (refer Figure 8.14) that there is a peak of absorption at 3.30 µm, which is considered for resonant ablation. These experiments were conducted with 160 mW power, 20 kHz pulse repetition rate and at 3.30 µm wavelength. The results obtained for αNPB patterning on glass are illustrated in Figure 8.16 with the help of a microscopic image and SEM micrograph. If the SEM micrograph is considered, it shows that at the central part of the ablated groove the material has been removed mostly. The incomplete removal at the edges corresponds to partially removed material during the ablation process. At the non-resonant wavelength of 3.40 µm, there has not been any interaction of the laser beam with the thin film of αNPB.

Finally, the experiments were carried out with the nanosecond laser for the thin film of HDR014 on a glass substrate. Investigations were conducted for the identical thickness of 140 nm thin film of HDR014 on a glass substrate. The processing is carried out with a power of 160 mW, 20 kHz pulse repetition rate, different scan speeds, at wavelengths of 3.37 µm(resonant absorption) and 3.30 µm(non-resonant). The optical absorption spectrum for HDR014 is shown earlier in Figure 8.12 (b). The result obtained at the wavelength of resonant absorption for HDR014 are shown in Figure 8.17. It is observed from this figure that HDR014 thin film removal is clean,

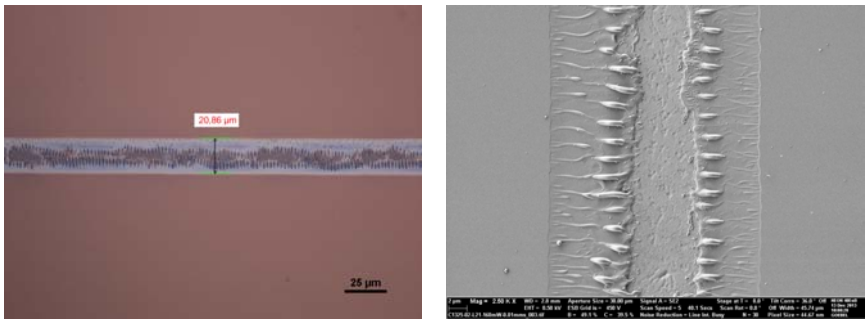

(a) Optical microscopic image (b) SEM micrograph (20.86 µm)

Figure 8.16: Mid-IR patterning of αNPB thin film (160 mW, ns, 20 kHz , 3.30 µm).

however there is some roughness at the edges which is due to flakes after ablation. For more detailed analysis of HDR014 patterned areas, EDS spectra of the ablated areas and non-ablated areas were investigated. The results of EDS analysis are depicted in Figure 8.18. Comparing the EDS spectra of non-ablated material and ablated material, it is observed that the Sulphur (S) peak has disappeared almost completely. This means that the oligothiophene material HDR014 has been removed almost completely from the glass substrate. Also the Carbon (C) content has been reduced widely in the ablated area (bottom) as compared to non-ablated area (top), and the remaining carbon may correspond to impurities. Moreover, precise monolayer investigation can be carried out by using Time-of-Flight Static Secondary Ion Mass Spectroscopy (TOF-S-SIMS) [11], as an analytical method to analyze the outermost molecular surface layer of the ablated area after thin films removal from the substrate.

8.7 Investigations at higher mid-IR wavelengths

So far, all the nanosecond and picosecond laser patterning experiments have been performed using a mid-infrared laser with a wavelength tunable in the 3 µm to 4 µm range. Even with this rather limited tuning range, we have been able to successfully address the absorption bands of typical OPV organic thin-films. However, to develop a layer selective patterning process, it is necessary to avoid cross-overlap of the absorption spectra of the multiple organic layers

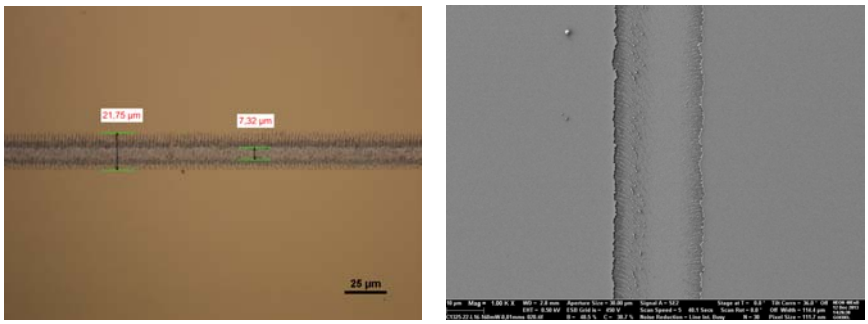

(a) Optical microscopic image (b) SEM micrograph (21.75 µm)

Figure 8.17: Mid-IR patterning of HDR014 thin film (160 mW, ns, 20 kHz , 3.37 µm) .

present in the OPV stack. As an example, nanosecond laser patterning of the OPV donor material HDR014 has been possible for thin films deposited on glass, but for the films on a PET substrate the overlap of both spectra (HDR014 and PET) at 3.37 µm, resulted in a non-selective patterning process.

If we take a closer look at the absorption spectra of typical organic electronic materials, there is a very interesting wavelength region between 6 µm and 7 µm, with strong absorption peaks. As shown in Figure 8.19 , the spectrum for the hole transport layer αNPB is presented for higher wavelengths. There is a moderate absorption peak in the 3.3 µm region, but the absorption peaks at 6.28 µm, 6.72 µm, 7.2 µm, and 7.73 µm are the most promising ones. For the material DCV4T-Et2 (HDG075), the absorption spectrum is presented in Figure 8.20, which clearly indicates the presence of a strong absorption at 4.50 µm. The similar higher absorption bands are noticed for the donor material HDR014, and there is also a stronger peak of absorption at 4.50 µm. This is the main peak of interest for additional studies, since the PET substrate foil does not show a strong absorption at these wavelengths, so potentially a selective laser patterning process can be developed.

The experiments were conducted at Thales Research and Technology (TRT), France at 4.50 µm resonant peak and 4.77 µm non-resonant absorption wavelengths. The laser source used in this study was developed at TRT and the ablation set-up was build at CMST/IMEC. The considered source is a rugged Optical Parametric Oscillator (OPO). Starting from a remote commercial continuous wave

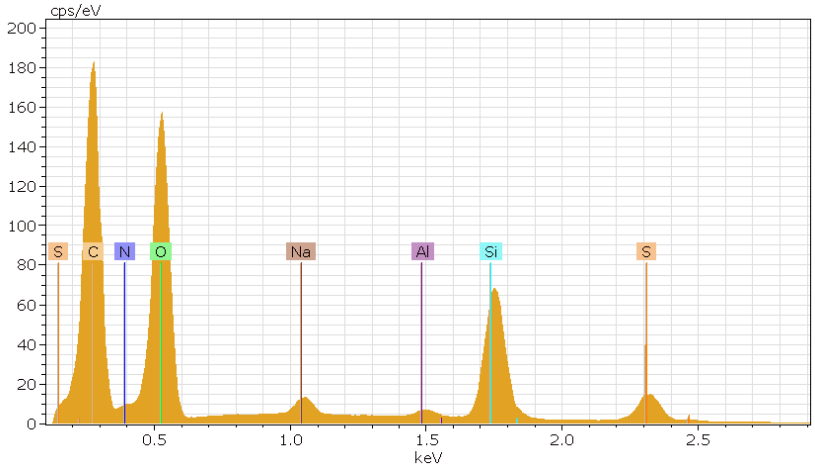

(a) Non-ablated area

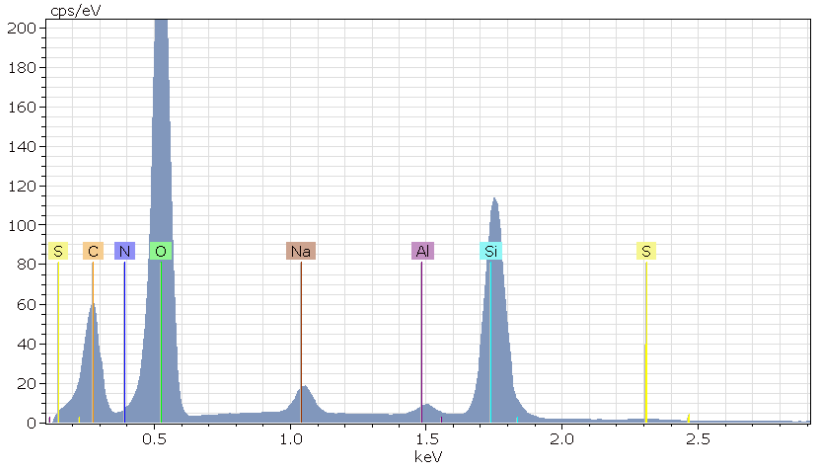

(b) Ablated area

Figure 8.18: EDS spectra of HDR014 patterning on glass substrate with 160 mW, ns, 20 kHz , 3.37 µm.

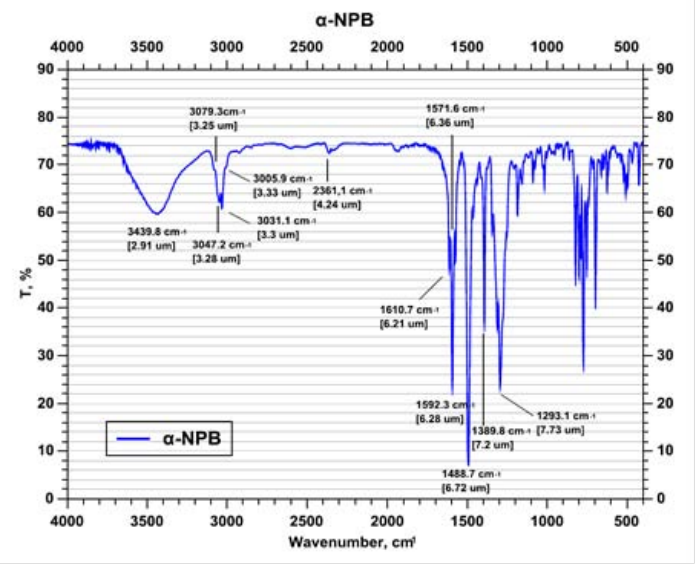

Figure 8.19: Higher absorption bands for αNPB at higher mid-IR wavelengths compared to 3 µm range.

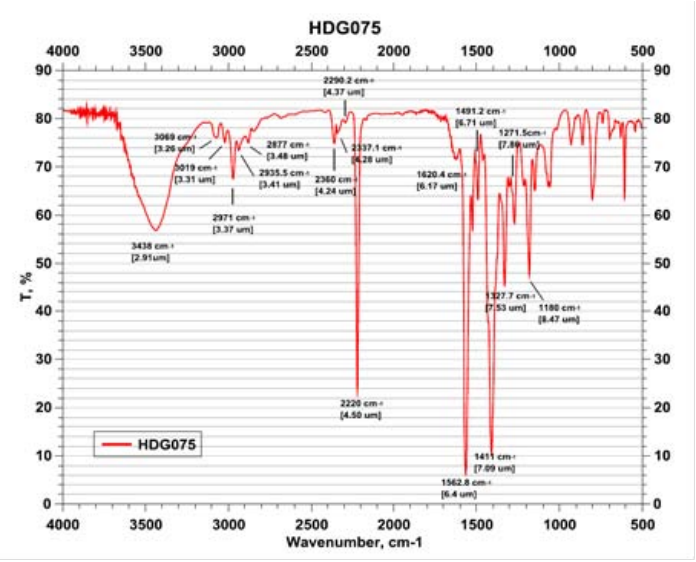

Figure 8.20: Higher absorption bands for DCV4T-Et2 (HDG075) at higher mid-IR wavelengths compared to 3 µm range.

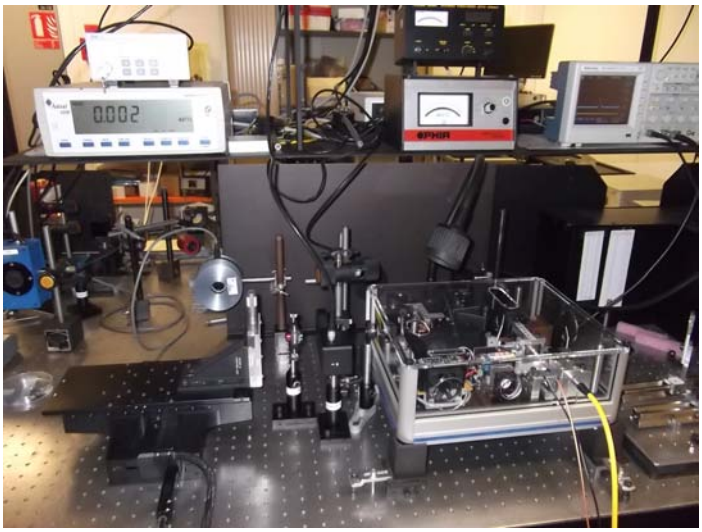

Figure 8.21: Mid-IR nanosecond laser set-up tunable around 4.50 µm at Thales Research and Technology, France.

fiber laser, it is packaged in a compact $25cm \times 30cm \times 6cm$ module integrating a 50 kHz, 40 ns Q-switched Ho:YAG laser at 2.09 µm, a variable attenuator and an OPO based on an OP-GaAs crystal operated at 25 °C. 3 W mid-IR output power is delivered by this OPO in the 3 µm to 5 µm range (signal and idler) with a 53 % conversion efficiency and an excellent beam quality ($M^2 = 1.4$). With the help of Peltier element, it was possible to adapt this module to the RIA requirements of polymer layers strongly absorbing around 4.50 µm. The unconverted pump and the signal were carefully filtered and dedicated beam shaping optics purchased to make this module compatible with the ablation set-up developed at IMEC. After the OPO, a Zinc Selenide microscopic objective and computer controlled shutter were installed, together with the sample translation stage. A detailed view of the ablation set-up is illustrated in Figure 8.21.

Two donor materials, DCV4T-Et2 and HDR014 were investigated at these higher wavelengths. First, the experiments were conducted for DCV4T-Et2 on PET foil using a nanosecond laser at 4.50 µm and 4.77 µm. The other processing parameters such as the power is varied from 160 mW to 600 mW and different scanning speeds from 50 mm/s to 200 mm/s are utilized. At the resonant wavelength (4.50 µm), no surface modification or slight surface roughening was observed at low powers (160 mW to 175 mW). The start of the material removal was

(a) At 4.50 µm (b) At 4.77 µm

Figure 8.22: Patterning investigations of HDR014 thin film at higher wavelengths, track width 12 µm.

observed at 250 mW with surface modification and smooth line edges. However, at higher laser powers (above 300 mW) strong thermal interaction was noticed with bubble and crack formation along with edge bulging. At the non-resonant wavelength (4.77 µm) with the identical processing parameters, there has been stronger interaction between substrate and laser beam; leading to melting, cracks, wavy profile but no modification of the film surface.

In a same fashion, the experiments were conducted for the HDR014 on PET substrate at 4.50 µm and 4.77 µm wavelengths. At 4.50 µm wavelength, no surface modification occurs, however crack formation has been observed even at low laser powers. At higher laser powers; the cracks, edge-bulging and melting of material were noticed. However, at the non-resonant wavelength (4.77 µm), the thermal effects were pronounced such as bubble formation and cracks. On the other hand, for the thin-film patterning on glass substrate, there was a remarkable difference between laser lines exposed to 4.50 µm (on-resonant) and laser lines exposed to 4.77 µm (off-resonant), and the optical microscopic images are shown in Figure 8.22. It seems that the 4.50 µm wavelength has been well absorbed by the organic material, although the film was not removed, and the 4.77 µm wavelength caused roughening of the glass substrate. Therefore, thin-film removal on glass is possible, given that low marking speeds were used.

8.8 Conclusions

We have applied the concept of RIA for selective patterning of the thin organic films. The primary investigations in this chapter were dedicated to the 3 µm to 4 µm wavelength range. The patterning of the PEDOT:PSS thin films on glass as well as on a PET foil, has been successfully demonstrated. The mid-IR selective ablation for DCV4T-Et2 on PET foil has been successful at lower scan speeds with picosecond laser pulses. Moreover, a qualitative method for selective patterning of BPAPF, αNPB and HDR014 thin organic films on glass substrate has been implemented.

The organic thin-film patterning using a mid-infrared source tunable around 4.50 µm was investigated for two donor materials specific to the OPV stack. For the higher ablation speeds, no material removal was observed. For thin-films patterning on foil substrate, at resonant wavelength (4.50 µm) there is an interaction with the top surface layer of material, however too much thermal energy coupled to the substrate foil leads to thermal deformation. In addition to the stronger absorption band around 4.50 µm, it seems the shorter picosecond pulses are must to eliminate the thermal deformation which has been observed using nanosecond pulses. There are promising absorption bands around 6 µm to 7 µm for organic materials, which can also be investigated, but in that case the first requirement is the development of laser source.

A detailed analysis with the help of optical microscopic images, SEM micrographs, depth profiles and EDS spectra has been done. To summarize, it is possible to use RIA as a patterning scheme for thin organic films removal on a glass or foil substrate, however the scan speed has to be optimized for roll-to-roll processing as a final goal.

References

[1] K. Yung and D. Zeng, "Laser ablation of Upilex-S polyimide: influence of laser wavelength on chemical structure and composition in both ablated area and halo", *Surface and Coatings Technology*, vol. 145, no. 1, pp. 186–193, 2001. [Online].

[2] "EU-FP7-IMPROV Porject: Selective laser strcuturing of OPV stacks", 2014. [Online].

[3] M. Duering, R. Haglund, and B. Luther-Davies, "Resonant infrared ablation of polystyrene with single picosecond pulses generated by an optical parametric amplifier", *Applied Physics ASurface and Coatings Technology*, vol. 114, pp. 151–159, 2014. [Online].

[4] S. Naithani, A. Grisard, D. Schaubroeck, E. Lallier, and G. Van Steenberge, "Mid-infrared resonant ablation of PMMA", in *6th International Congress on Laser Advanced Materials Processing (LAMP-2013)*, 2013, pp. 1–5. [Online].

[5] "http://www.heliatek.com", Viewed on December-2014. [Online].

[6] O. Guskova, C. Schunemann, K.-J. Eichhorn, K. Walzer, M. Levichkova, *et al.*, "Light Absorption in Organic Thin Films: The Importance of Oriented Molecules", *The Journal of Physical Chemistry C*, vol. 117, no. 33, pp. 17 285–17 293, 2013. [Online].

[7] D. Wynands, M. Levichkova, M. Riede, M. Pfeiffer, P. Baeuerle, *et al.*, "Correlation between morphology and performance of low bandgap oligothiophene: C60 mixed heterojunctions in organic solar cells", *Journal of Applied Physics*, vol. 107, no. 1, pp. 0 145 171–0 145 176, 2010. [Online].

[8] H. Aziz, Z. D. Popovic, and N.-X. Hu, "Organic light emitting devices with enhanced operational stability at elevated temperatures", *Applied Physics Letters*, vol. 81, no. 2, pp. 370–372, 2002. [Online].

[9] L. E. Myers, W. Bosenberg, R. C. Eckardt, M. M. Fejer, and R. L. Byer, "Multigrating quasi-phase-matched optical parametric oscillator in periodically poled LiNbO3", *Optics Letters*, vol. 21, no. 8, pp. 591–593, 1996. [Online].

[10] P. E. Britton, N. G. R. Broderick, D. J. Richardson, P. G. R. Smith, G. W. Ross, *et al.*, "Wavelength-tunable high-power picosecond pulses from a fiber-pumped diode-seeded high-gain parametric amplifier", *Optics Letters*, vol. 23, no. 20, pp. 1588–1590, 1998. [Online].

[11] S. Naithani, D. Schaubroeck, Y. Vercammen, R. Mandamparambil, I. Yakimets, *et al.*, "Excimer laser patterning of PEDOT:PSS thin-films on flexible barrier foils: A surface analysis study", *Applied Surface Science*, vol. 280, pp. 504–511, 2013. [Online].

9

Conclusions and Future Work

In this work, there has been very fruitful contributions to the patterning technology as well as to organic electronics. The laser patterning has emerged as an alternative technology for patterning thin organic films. The main contributions of this work and the future possibilities will be discussed in this chapter.

9.1 Main Contributions

9.1.1 Multilayered barrier optimization

A barrier foil with better resistance against water or oxygen permeation is necessary for the fabrication of an OLED / OPV device, as this penetration will lead to shortening the life time of the device. In this study, a multilayered barrier consisting of inorganic-organic-inorganic layers has been utilized. Five different kinds of multilayered barrier foils are designed based on their optical absorption properties, for the optimization of laser patterning process. In addition, laser patterning has been further optimized by varying the laser fluence and number of pulses. It has been concluded that the optical absorption of the barrier foil (substrate) plays a significant role in the selective ablation mechanism of thin organic films.

9.1.2 Demonstration of a laser patterned flexible device

After the optimization of the process and the selection of a multilayered barrier foil, the feasibility of the laser process for patterning and structuring of various OLED layers has been investigated. Multipulse laser processes were optimized for the removal of thin organic layers on a flexible substrate containing a multilayer barrier stack. Minimal debris field and no layer delamination are observed in the ablated zone. Finally, a flexible laser processed OLED device has been fabricated and its operation has been demonstrated under environmental conditions.

9.1.3 Proposing TOF-SIMS for monolayer investigation

The characterization of laser patterned areas is generally carried out using depth profiles and scanning electron microscope (SEM) techniques. While the use of a 3D surface profiler or a SEM allows to conclude whether the laser process is layer selective or not, analyzing the chemical surface composition is required to conclude whether the organic film is completely removed or not. In fact, even a monolayer might be responsible for shortening the life time of organic electronics device, since in that case proper sealing and encapsulation can not be provided. In our study, the use of Time-Of-Flight Static Secondary Ion Mass Spectrometry (TOF-S-SIMS) is proposed as an analytical method to analyze the outermost molecular surface layer of the barrier after laser patterning of thin films. Investigation of the laser ablated area with TOF-S-SIMS has allowed the process to be described with unseen chemical composition as opposed to the traditionally used characterization methods. Although, it can not yet be concluded with certainty that the organic layer left after laser ablation treatment is the result of incomplete ablation or re-deposition, it is clear that the use of TOF-S-SIMS yields an interesting approach to obtain substantially refined insight in comparison to the optical and morphological characterization of the craters.

9.1.4 Ultrafast patterning

One chapter has been fully devoted to the ultrafast laser patterning of thin organic films. Different wavelengths, from ultraviolet to near-infrared, are applied to investigate laser patterning of thin organic films. Ablation thresholds are determined and the influence of the wavelength on patterning has been discussed.

9.1.5 Proof-of-concept RIA

The resonant mid-IR laser ablation (RIA) of bulk PMMA has been successfully demonstrated using a recently developed mid-IR tunable source. Higher ablation rates were observed at the resonant wavelength of operation and the ablated crater was free of debris. A proof-of-concept of thin film patterning using RIA has been provided for PMMA.

9.1.6 RIA for OPV layer patterning

As RIA has been implemented successfully for patterning of PMMA, the attention was clearly to use the technique for a more specific application. The focus was on OPV layers such as transparent conductive materials, hole transport materials, and absorber materials. The utilization of RIA for patterning of OPV thin layers has been implemented, the results have been very successful on glass substrates and further optimization is needed in case of a polymeric substrates.

Eventually, the investigations in this dissertation would lead to a robust industrial process for patterning OLED or OPV thin organic films. Laser patterning is a feasible and long term cost-effective solution for the thin films patterning, especially when integrated to a roll-to-roll (R2R) process.

9.2 Outlook and Future Work

This PhD work is a detailed investigation of thin films patterning using different laser systems with broad range of wavelengths (ultraviolet to mid-infrared) and different pulse lengths (nanosecond to picosecond pulses). Moreover, the investigations are carried out for rigid glass substrates as well as flexible polymeric substrates. The work is mainly focused on the thin organic films used in organic electronics devices, in particular OLED and OPV. In this dissertation a lot of investigations are performed by varying different parameters, however there is still some work which can be further carried out.

First, the life time tests can be conducted for a laser patterned OLED device. The fabrication of a laser patterned device including a RIE step after laser processing might result in better encapsulation of the device and hence the improved life time.

Secondly, it would be interesting to demonstrate a laser patterned OPV device using the RIA technique. We observed that the selective

removal of a thin organic film on a polymeric substrate is challenging and the process needs to be optimized very carefully. Some of the processes developed in this study have very a limited working process window, especially in case of polymer substrates. However, by optimizing the laser parameters (wavelength, fluence, pulse length, number of pulses, pulse repetition rate) it is possible to develop a selective and wider process window to pattern thin organic films.